

AD-A062 091

ROCKWELL INTERNATIONAL THOUSAND OAKS CALIF SCIENCE --ETC F/G 20/5  
A CHEMICAL SINGLET MOLECULAR OXYGEN GENERATOR.(U)

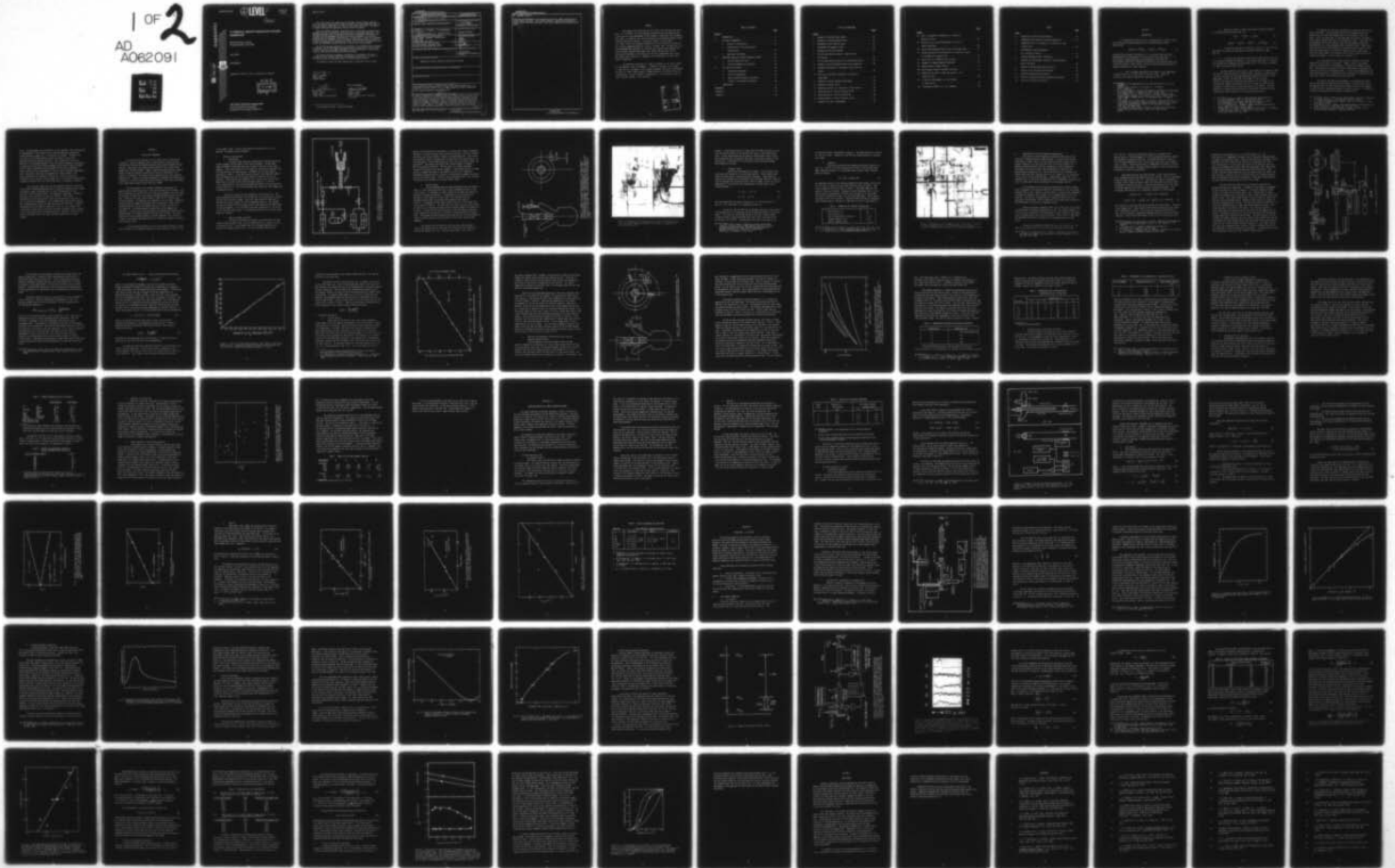
JUL 78 A T PRITT, R D COOMBE, I B GOLDBERG F29601-76-C-0070

UNCLASSIFIED

AFWL-TR-77-265

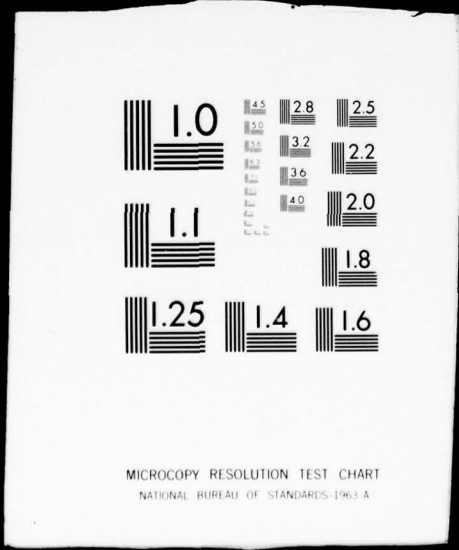
NL

1 OF 2  
AD  
A062091



1 OF 2

AD  
A062091



② LEVEL II  
E

ADL 800192

DDC

AD A062091

# A CHEMICAL SINGLET MOLECULAR OXYGEN GENERATOR

Rockwell Science Center  
Thousand Oaks, CA 91360

July 1978

Final Report

Approved for public release; distribution unlimited

DDC FILE COPY



DDC  
RECEIVED  
DEC 13 1978  
B

AIR FORCE WEAPONS LABORATORY  
Air Force Systems Command  
Kirtland Air Force Base, NM 87117

78 11 20 09

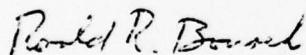
This final report was prepared by the Rockwell Science Center, Thousand Oaks, California, under Contract F29601-76-C-0070, Job Order 33260309, with the Air Force Weapons Laboratory, Kirtland Air Force Base, New Mexico. Maj Ronald R. Bousek (ALC) was the Laboratory Project Officer-in-Charge.

When US Government drawings, specifications, or other data are used for any purpose other than a definitely related Government procurement operation, the Government thereby incurs no responsibility nor any obligation whatsoever, and the fact that the Government may have formulated, furnished, or in any way supplied the said drawings, specifications, or other data, is not to be regarded by implication or otherwise, as in any manner licensing the holder or any other person or corporation, or conveying any rights or permission to manufacture, use, or sell any patented invention that may in any way be related thereto.

This report has been authored by a contractor of the United States Government. Accordingly, the United States Government retains a nonexclusive, royalty-free license to publish or reproduce the material contained herein, or allow others to do so, for the United States Government purposes.

This report has been reviewed by the Office of Information (OI) and is releasable to the National Technical Information Service (NTIS). At NTIS, it will be available to the general public, including foreign nations.

This technical report has been reviewed and is approved for publication.



RONALD R. BOUSEK  
Major, USAF  
Project Officer



DAVID S. OLSON  
Major, USAF  
Chief, Chemical Laser Branch

FOR THE COMMANDER



ARMAND D. MAIO  
Colonel, USAF  
Chief, Advanced Laser Technology  
Division

UNCLASSIFIED

⑩ AFWL, SBIE

SECURITY CLASSIFICATION OF THIS PAGE (When Data Entered)

⑬ REPORT DOCUMENTATION PAGE		READ INSTRUCTIONS BEFORE COMPLETING FORM	
1. REPORT NUMBER AFWL-TR-77-265, AD-E240 192	2. GOVT ACCESSION NO.	3. RECIPIENT'S CATALOG NUMBER	
4. TITLE (and Subtitle) A CHEMICAL SINGLET MOLECULAR OXYGEN GENERATOR.		5. TYPE OF REPORT & PERIOD COVERED ⑨ Final Report.	
		5. PERFORMING ORG. REPORT NUMBER	
7. AUTHOR(s) A. T. Pritt, R. D. Coombe, I. B. Goldberg, and D. Pilipovich R. I. Wagner (Rocketdyne Div., Rockwell Int'l)		8. CONTRACT OR GRANT NUMBER(s) ⑮ F29601-76-C-0070	
9. PERFORMING ORGANIZATION NAME AND ADDRESS Science Center - Rockwell International P O Box 1085 Thousand Oaks, CA 91360		10. PROGRAM ELEMENT, PROJECT, TASK AREA & WORK UNIT NUMBERS 62601F ⑰ 43 33260309 ⑯	
11. CONTROLLING OFFICE NAME AND ADDRESS Air Force Weapons Laboratory (ALC) Kirtland Air Force Base, NM 87117		12. REPORT DATE ⑪ July 1978	
14. MONITORING AGENCY NAME & ADDRESS (if different from Controlling Office) ⑫ 99 P.		13. NUMBER OF PAGES 98	
		15. SECURITY CLASS. (of this report) Unclassified	
		15a. DECLASSIFICATION/DOWNGRADING SCHEDULE	
16. DISTRIBUTION STATEMENT (of this Report)  Approved for public release; distribution unlimited			
17. DISTRIBUTION STATEMENT (of the abstract entered in Block 20, if different from Report)			
18. SUPPLEMENTARY NOTES			
19. KEY WORDS (Continue on reverse side if necessary and identify by block number) Singlet Molecular Oxygen, Chlorine Fluorosulfate, Hydrogen Peroxide, C. W. Population Inversion, Iodine ( $5^2P_{3/2}$ ), Lasers, Quenching, Chemical Reactions, Optical Double Resonance, Fluorescence, ESR. SINGLET			
20. ABSTRACT (Continue on reverse side if necessary and identify by block number) A method of generating a continuous wave (cw) "clean" stream of oxygen containing a large fraction in the ( $a^1\Delta$ ) state has been developed based upon the base catalyzed chemical reaction of chlorine fluorosulfate and hydrogen peroxide. After the addition of molecular iodine a fast energy transfer process between $O_2(a^1\Delta)$ and $I(5^2P_{3/2})$ created a population inversion between the spin-orbit states of atomic iodine. This population inversion was directly observed in an optical double resonance experiment in which the excited spin-orbit state (Over) →			

389 949

8 11 20 00

UNCLASSIFIED

SECURITY CLASSIFICATION OF THIS PAGE(When Data Entered)

20. ABSTRACT (Cont'd)

population was decreased as the transition was driven toward saturation by a pulsed iodine atom laser. The  $O_2(a^1\Delta)$  generator, quantitative diagnostics, optical double resonance experiment, and lasing attempts are described in this report.



UNCLASSIFIED

SECURITY CLASSIFICATION OF THIS PAGE(When Data Entered)

## PREFACE

Many people have contributed to this effort over the past year and a half. R. F. Heidner, III of the Aerospace Corporation was extremely helpful in advising us on the development of the diagnostic techniques used throughout this study. In addition, his fruitful discussion provided much needed insight into the subtleties of the  $O_2^* - I_2$  reaction system. We also thank M. A. Kwok, also of the Aerospace Corporation, for his analytical testing of our intrinsic germanium detector, saving us valuable time. We would also like to acknowledge AFWL personnel, Dr. Bernard, who conceived and developed the optical double resonance experiment, Maj. Bousek, who provided kinetic calculations necessary for the design of the laser experiments, Maj. Olson, Maj. Dymek, Capt. Pchelkin, Lt. Hammond, and Dr. MacKnight, for their many helpful suggestions.

We extend our gratitude to J. Cape, W. Tennant, W. Ho, and A. Harker for the generous loans of equipment. In addition, we would like to thank L. Grant and his colleagues in the Inorganic Synthesis Group at the Rocketdyne Division, for their timely supply of needed chemicals, principally chlorine fluorosulfate. A special thanks is extended to R. K. Horne and G. Lovas for their creative talents in the laboratory.

ACCESSION FOR	
NTIS	Write Section <input checked="" type="checkbox"/>
DDC	DDC Section <input type="checkbox"/>
UNANNOUNCED	<input type="checkbox"/>
JUSTIFICATION	
BY	
DISTRIBUTION AVAILABILITY CODES	
Dist.	AVAIL. ONLY or SPECIAL
A	

## TABLE OF CONTENTS

<u>Section</u>	<u>Page</u>
I. INTRODUCTION . . . . .	7
II. THE $O_2(a^1\Delta)$ GENERATOR . . . . .	11
A. Design of the Generator . . . . .	12
B. Determination of the $O_2^*$ Absolute Concentration . . . . .	20
C. Generator Performance . . . . .	27
III. QUENCHING STUDIES OF SINGLET MOLECULAR OXYGEN . . . . .	43
A. Surface Quenching of $O_2^*$ . . . . .	43
B. Gas Phase Quenching of $O_2(b^1\Sigma^+g)$ . . . . .	46
IV. The $O_2(a^1\Delta)$ - $I_2$ SYSTEM . . . . .	59
A. Experimental Apparatus . . . . .	59
B. Zero Gain Experiments . . . . .	68
C. Optical Double Resonance Experiments . . . . .	72
D. $I(5^2P_{1/2})$ Fluorescence Experiments . . . . .	81
V. CONCLUSIONS . . . . .	87
REFERENCES . . . . .	89
APPENDIX A . . . . .	94
APPENDIX B . . . . .	96

## LIST OF ILLUSTRATIONS

<u>Figure</u>	<u>Page</u>
1 Schematic of Reactant Feed System . . . . .	13
2 Schematic of Cyclone Reactor Vessel . . . . .	15
3 Photograph of Dual Reactor Vessel . . . . .	16
4 Photograph of Cryogenic U-Trap . . . . .	19
5 Schematic for O <sub>2</sub> * Calibrations . . . . .	23
6 Plot of Dimol Emission Rate vs. Square of the O <sub>2</sub> * Pressure . . . . .	26
7 Plot of Dimol Emission Rate of the Two Emission Ports . . . . .	28
8 Schematic of Cyclone Reactor Vessel with Diagnostics . . . . .	30
9 Pressure Distribution in the Reactor Vessel and Flow System . . . . .	32
10 Variation of O <sub>2</sub> * Molar Flow Rate vs. Fraction of Argon Added . . . . .	40
11 Schematic of O <sub>2</sub> ( <sup>1</sup> Σ) Quenching Experiment . . . . .	48
12 Quenching of O <sub>2</sub> ( <sup>1</sup> Σ) by HCl . . . . .	52
13 Quenching of O <sub>2</sub> ( <sup>1</sup> Σ) as a Function of Slide Position . . . . .	53
14 Quenching Rate vs. Partial Pressure of HBr . . . . .	55
15 Quenching Rate vs. Partial Pressure HCl . . . . .	56
16 Quenching Rate vs. Partial Pressure of CFS . . . . .	57
17 Schematic for O <sub>2</sub> *-I <sub>2</sub> Experiments . . . . .	61

<u>Figure</u>	<u>Page</u>
18 I <sub>2</sub> (B → X) Resonant Fluorescence vs. Pressure of Molecular Iodine . . . . .	64
19 Fraction of I <sub>2</sub> in the Flowing Argon vs. That for Static Conditions . . . . .	65
20 Typical Time Resolved Flash for the Iodine Atom Laser . . . . .	67
21 Percent Reflection of Polarization as a Function of Angle of Incidence for a Quartz Flat . . . . .	70
22 Cavity Loss vs. Threshold Time to Lasing . . . . .	71
23 Schematic of Double Resonant Experiment . . . . .	73
24 Energy Levels of Atomic Iodine . . . . .	74
25. Oscilloscope Traces of the 206.2 nm Signal . . . . .	75
26. Normalized Variation in 206.2 nm Signal vs. the Fraction of O <sub>2</sub> * . . . . .	80
27. I* and O <sub>2</sub> * Fluorescence vs. Flow Distance in Laser Cavity . . . . .	83
28. Fluorescence Intensity vs. Iris Diameter . . . . .	85

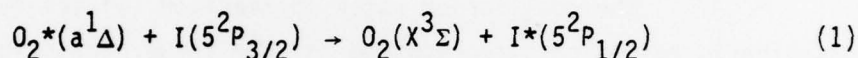
## TABLES

<u>Table</u>	<u>Page</u>
1. Properties of Chlorine Fluorosulfate . . . . .	18
2. Temperature Distribution for Baseline Operation . . . . .	33
3. Temperature Rise in the Reactor as a Function of Time (Typical Run) . . . . .	34
4. Performance of the O <sub>2</sub> * Generator as a Function of Mixing . . . . .	35
5. Average Consumption Rate of Reactants . . . . .	38
6. Greatest O <sub>2</sub> * Percentages Produced at Various Generator Molar Flow Rates . . . . .	38
7. Results of the CFS-H <sub>2</sub> O <sub>2</sub> Product Analysis . . . . .	41
8. Results of the Surface Quenching Study . . . . .	46
9. O <sub>2</sub> (b <sup>1</sup> $\Sigma$ +g) Quenching Rate Constants . . . . .	58
10. Results of the Optical Double Resonance Experiments . . . . .	78
11. Data for the [I*] Time Profiles . . . . .	82

## SECTION I

### INTRODUCTION

In 1970 Derwent and Thrush (Ref. 1) suggested that an atomic iodine laser could be constructed based upon the following energy transfer equilibrium:<sup>a</sup>



The equilibrium constant for process (1) is calculated from statistical thermodynamics and experimentally verified to be 2.9 at 300K (Ref. 2). If equilibrium is established with a  $\text{O}_2^*(a^1\Delta)/\text{O}_2(\chi^3\Sigma)$  concentration<sup>b</sup> ratio greater than 0.174, a population inversion can be produced between the spin-orbit states of atomic iodine. Several interesting features make this concept attractive as a laser candidate:

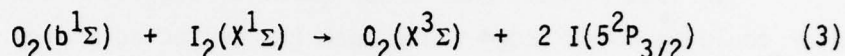
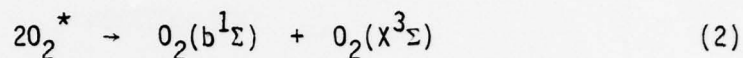
1.  $\text{O}_2^*$  is extremely metastable with respect to both spontaneous radiation (half-life ~ 45 min) (Ref. 3) and collisions. About  $10^6$  collisions are typically required for deactivation (Ref. 4).

<sup>a</sup> A synopsis of the complete model with rate coefficients is given in Appendix A.

<sup>b</sup> Hereafter,  $\text{O}_2^* = \text{O}_2(a^1\Delta)$ ,  $\text{O}_2 = \text{O}_2(\chi^3\Sigma)$ ,  $\text{I}^* = \text{I}(5^2P_{1/2})$ , and  $\text{I} = \text{I}(5^2P_{3/2})$ .

1. R. G. Derwent and B. A. Thrush, "The Radiative Lifetime of the Metastable Iodine Atom  $\text{I}(5^2P_{1/2})$ ," Chem. Phys. Letts. 9, 591 (1971).
2. R. F. Heidner III, J. g. Coffey, and C. E. Gardner, " $\text{O}_2(a^1\Delta)$ -I Atom Energy Transfer Studies: C. W. Inversion on 1.315  $\mu\text{m}$  I-Atom Transition," Interim Report, TR=0078 (3610)-1, The Aerospace Corp., El Segundo, Calif., 1977.
3. R. M. Badger, A. C. Wright, and R. F. Whitlock, "Absolute Intensities of the Discrete and Continuous Absorption Bands of Oxygen Gas at 1.26 and 1.065  $\mu\text{m}$  and the Radiative Lifetime of the  $^1\Delta_g$  State of Oxygen," J. Chem. Phys. 43, 4345 (1965).
4. K. H. Becker, W. Groth, and U. Schurath, "The Quenching of Metastable  $\text{O}_2(^1\Delta_g)$  and  $\text{O}_2(^1\Sigma^+g)$  Molecules," Chem. Phys. Letts. 8, 259 (1971).

2. Molecular iodine is readily dissociated by  $O_2(b^1\Sigma)$  produced in the energy pooling reaction (Ref. 5).



3. The equilibrium rates in reaction (1) are fast. Less than ten gas-kinetic collisions are required for the forward reaction at 300K (Ref. 6).

4. Lasing on the spin-orbit transition of atomic iodine, which was first reported by Kasper and Pimentel, is well established (Ref. 7). Many of its characteristic parameters are understood since it is a serious contender for laser fusion application (Ref.8).

The major problem in developing a laser based on this scheme has been the lack of a suitable source of excited oxygen. Passage of oxygen through a microwave discharge, the technique employed by Derwent and Thrush in their experiments, yields less than 10% of the oxygen in the  $a^1\Delta$  state. Photolysis of ozone could theoretically produce 2/3 of the oxygen in the excited state; however, quenching of  $O_2^*$  by its precursor, ozone, and its co-product, O atoms, places a major constraint on this method. Also the problems of scaleability and the relative inefficiency of photolysis make these physical means impractical for high energy applications.

5. S. J. Arnold and E. A. Ogryzlo, "Some Reactions Forming  $O_2(^1\Sigma_g)$  in the Upper Atmosphere," *Can. J. Phys.* **45**, 2053 (1974).
6. R. G. Derwent and B. A. Thrush, "Excitation of Iodine by Singlet Molecular Oxygen," *Disc. Faraday Soc.* **53**, 162 (1972).
7. J. V. V. Kasper and G. C. Pimentel, "Atomic Iodine Photodissociation Laser," *Appl. Phys. Letts.* **5**, 231 (1964).
8. H. Hohla and K. L. Kompa, "The Photochemical Iodine Laser," in *Handbook of Chemical Lasers*, R. W. F. Gross and J. F. Bott, eds., Wiley-Interscience, New York (1976).

For purposes of scaling to high energies, a chemical source of  $O_2^*$  would be desirable. Base catalyzed reactions of hydrogen peroxide and hypochlorite salts have been demonstrated to yield oxygen in the  $a^1\Delta$  state. Cahill and Taube (Ref. 9) concluded that the evolution of oxygen in these reaction systems were due to an intermediate,  $ClO^-$ . Khan (Ref. 10) has suggested that only the  $O_2(a^1\Delta)$  state could be formed provided the dissociation to  $Cl^-$  and  $O_2$  proceeds along an adiabatic path. These liquid phase reactions hold little promise as a source of  $O_2(a^1\Delta)$  since: (a) the reaction of  $H_2O_2$  and  $ClO^-$  is diffusion controlled in the liquid state, thus limiting the speed of the reaction, and (b) the lifetime of  $O_2^*$  in an aqueous environment, is on the order of  $\mu s$  (see Ref. 11)

It is, therefore, not too surprising that attempts to use these hypochlorite salts were not successful. Common to these liquid phase reactions producing  $O_2^*$  is the presence of a "positively" charged halogen atom. Based upon this rationale, Pilipovich and Goldberg investigated the reaction of chlorine fluorosulphate (CFS), a liquid at room temperature, and basic hydrogen peroxide. Using electron spin resonance (esr) detection they found that  $\sim 40\%$  of the effluent gas was  $O_2^*$  (Ref. 12)

This report describes the development of an  $O_2^*$  generator based upon the CFS- $H_2O_2$  base catalyzed reaction system. The description of the  $O_2^*$  generator which includes reactant feed systems, mixing of the reagents, and elimination of unwanted by-products is given in Section II. In addition, a method of determining the absolute  $O_2^*$  concentration is

9. A. E. Cahill and H. Taube, "Use of Heavy Oxygen in the Study of Reactions of Hydrogen Peroxide," J. Am. Chem. Soc. 74, 2312 (1952).
10. A. U. Khan, "Singlet Molecular Oxygen, A New Kind of Oxygen," J. Phys. Chem. 80, 2219 (1976).
11. P. B. Merkel and D. R. Kearns, "Radiationless Decay of Singlet Molecular Oxygen in Solution, J. Am. Chem. Soc. 94. 7244 (1972 ).
12. I. B. Goldberg, D. Pilipovich, and R. I. Wagner, "A Novel Singlet Molecular Oxygen Generator," patent pending (1977).

given. The performance of the generator is also reported. Key to the success of the generator is the control of all potential quenching processes of singlet molecular oxygen, be it in the  $a^1\Delta$  or  $b^1\Sigma$  states. In Section III the results of gas phase quenching studies of  $O_2(b^1\Sigma)$  and surface quenching studies of  $O_2^*(a^1\Delta)$  are given. The ultimate test of the  $O_2^*$  generator is to determine whether or not this chemical generator has potential in producing a population inversion between the spin-orbit states of atomic iodine. Several experiments were developed to test the  $O_2^*$  generator. These include zero gain experiments, an optical double resonance experiment in which a population inversion was observed, and lasing attempts. The  $O_2^*-I_2$  experiments are reported in Section IV. Finally, the future prospects of utilizing this chemical generator for the purpose of developing a scaleable continuous wave (cw) iodine atom laser is discussed in Section V.

This study has shown that the base catalyzed reaction of chlorine fluorosulfate and 90% hydrogen peroxide is capable of producing clean streams of molecular oxygen with enough  $O_2^*$  to invert the population of the spin-orbit state of atomic iodine. The present  $O_2^*$  generator is capable of producing a calculated gain in excess of  $10^{-5}\text{cm}^{-1}$ . The current configuration of the  $O_2^*$  generator limits the maximum molar flow rate of  $O_2^*$  in high yield; consequently, lasing attempts were unsuccessful implying that integrated gain across the laser cavity was less than  $10^{-2}$ . Although the mechanism for the chemical production of  $O_2^*$  is as yet unknown, the limited molar output rate of high yield  $O_2^*$  does not appear to be a function of the reaction but rather the generator design. Hence the scaling of this reaction to greater molar flow rates could be accomplished via design changes.

## SECTION II

### The $O_2^*(a^1\Delta)$ GENERATOR

Two reactors were employed in the original work of Goldberg and Pilipovich. The first apparatus was of simple design in which chlorine fluorosulfate (CFS) gas was bubbled through a basic (KOH) hydrogen peroxide solution. The second, more sophisticated, method utilized a gas-liquid, commercially available sprayer. Both of these techniques produced a bubbly, frothy mixture with aerosols condensing on the walls downstream of the reactor. Furthermore, the reaction mixture became hot due to the reaction exothermicity. Clearly, from these experiments refinements were necessary to eliminate or at least minimize the aerosol production since such environments could significantly quench singlet molecular oxygen.

The first phase of this contract centered on the design of a generator which would produce  $O_2^*$  in the least detrimental environment. The first attempt was to pre-heat CFS via a glass heat exchanger, pass the heated CFS through a fritted disc, and dropwise add 90% hydrogen peroxide onto the disc. Below the disc was a basin cooled to 196K to aid in trapping the aerosols produced. The generator was attached to a 15 cfm pump. Evidence of singlet molecular oxygen was obtained from this generator. When a basic hydrogen peroxide solution was dropped onto the fritted disc, the disc disintegrated. An improved method of combining the two reagents was necessary. A Kinecs mixer (described below) was attempted and found to be an adequate means of intimately combining the gas-liquid stream. This mixer coupled with a feed system upstream, a cyclone separator, and a series of cryogenic traps downstream comprised the first generator capable of producing clean streams of  $O_2^*$ .

In this section the details of the final generator design is given. Also included are the diagnostic methods for determining the fraction of  $O_2^*$

in the oxygen stream. Finally, the production characteristics of the generator are summarized and presented.

#### A. Design of the Generator

##### 1. Feed System

A pressure feed system was constructed for delivering the two primary reagents, CFS and  $H_2O_2$ , to the reaction chamber. Syringe pumps (Sage Instruments, Model 355) were used to apply 12-14 psig to the liquid reagents. Later this mechanical drive system was replaced by a pneumatic one utilizing helium as the working gas. A schematic of the feed system is presented in Figure 1. Each feed line had a shutoff valve (Whitey SS-OVS-2) and a micrometer metering valve (Nupro SS-2SA) to regulate the flow of chemicals. Teflon packing was necessary on all valves since Viton quickly deteriorates by attack of CFS and the CFS- $H_2O_2$  reaction. A 7 micron filter (Nupro SS-2F-7) was positioned between the shutoff valve and metering valve on the CFS line. This filter prevents small particles from clogging the micrometering valve.

An auxiliary vacuum line was attached to the CFS feed line. This vacuum system kept the CFS feed line dry when not in use and aided in loading the CFS liquid into the syringe. Later this same vacuum line was used to evacuate the delivery vessels for CFS and hydrogen peroxide. The hydrogen peroxide was loaded into the syringes directly and secured to the feed system via Luerlok adaptors. All of the feed lines were constructed of 1/8" Teflon or 1/8" stainless steel tubing. All connections were by 1/8" stainless steel Swage-lok fittings.

##### 2. Reaction Chamber and Mixer

The feed lines between the metering valve and the mixer were warmed by heating tapes to 50C. At this temperature CFS is above its normal boiling point, 45C. It was thought that this increased temperature may enhance the CFS- $H_2O_2$  reaction rate. The liquid hydrogen peroxide and

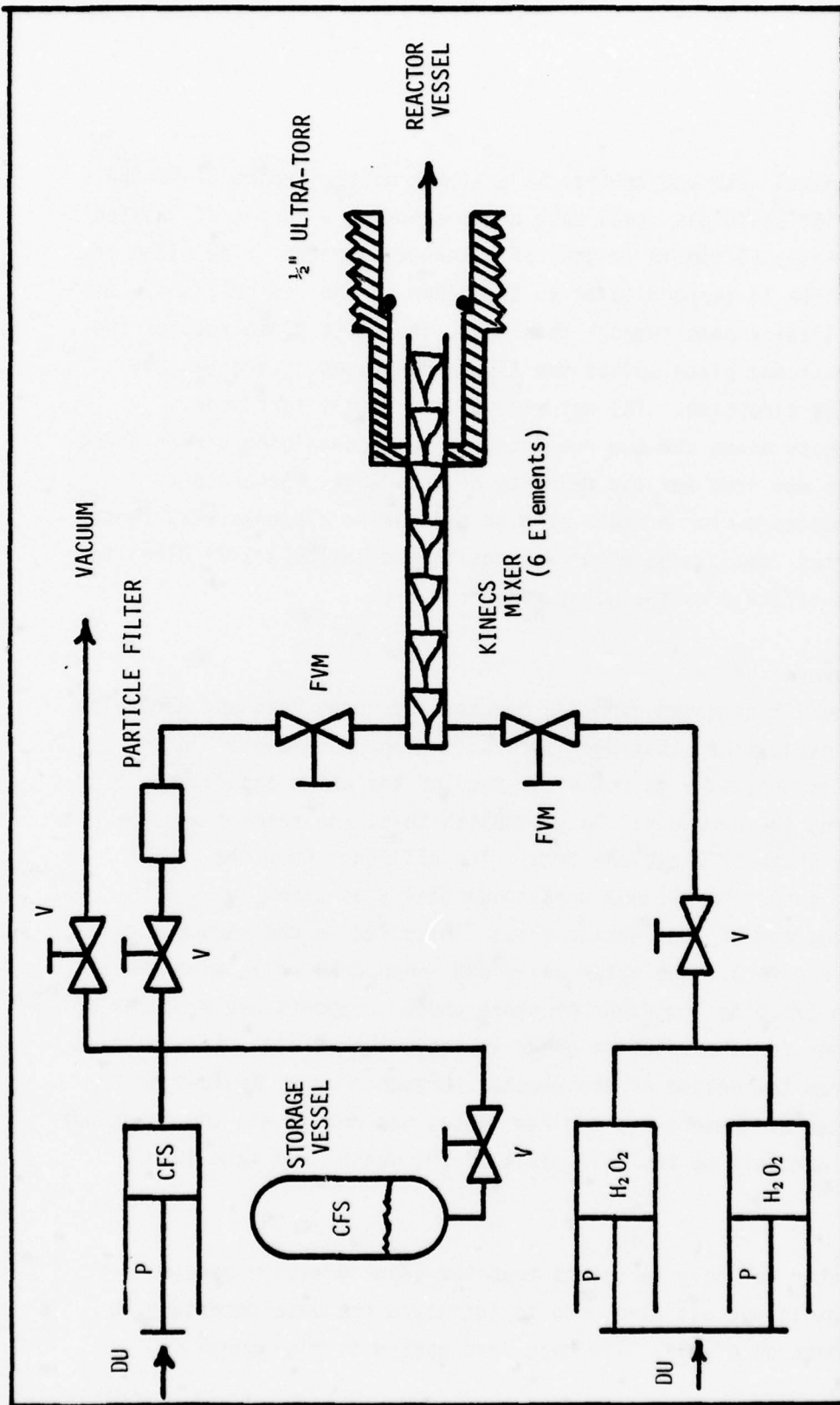


Figure 1. Schematic of the Reagent Feed System and Mixer. DU are the drive units for the plungers P in the syringes. Shut-off valves are designated V and the fine metering valves as FVM.

gaseous CFS were mixed with one another in a static mixer (Kenics 37-03-062). The mixer is a 3/16" stainless steel tube which contains a series of twisted stainless steel plates (0.6cm in length) of alternating pitch. The plane of each successive plate is perpendicular to the plane of the one previous. As the gases and/or liquids pass through this tube, the first plate rotates the mixture 90°. The second plate splits the flow and rotates it another 90° in the opposite direction. The net result is a highly turbulent, disruptive flow which mixes the two reagents. A tube containing six of these plates or elements was used for the majority of this work. Generator performance was monitored for a mixer of nine and twelve elements, and these results are reported later. The mixer was positioned inside a 1/2" Ultra-torr fitting which was attached to the glass reactor vessel.

### 3. Reactor Vessel

The CFS-hydrogen peroxide reaction produces heat and aerosols. Since it is well established that  $O_2^*$  is readily quenched by water in the liquid state, it is necessary to remove as much of the water and liquids as possible, including the aerosols. To accomplish this, the reactor was configured in the shape of a cyclone trap. The effluents from the CFS-H<sub>2</sub>O<sub>2</sub> reaction enter the cyclone trap tangentially as shown in Figure 2. A photograph of the reactor vessel installed in the vacuum flow line is given in Figure 3. The outer walls and inner cone walls were cooled to 196K to aid in trapping low vapor pressure unused reagents and products of reaction. In order for the volatile gases to leave the reactor, they must travel upwards from the bottom of the reactor through another Kenic-type of mixer. The purpose of these twisted glass plates was not to mix the gases but rather to direct aerosols to the cold walls of the vessel and have them condensed.

The reactor not only serves to trap low vapor pressure gases, liquids, and aerosols but was also used to introduce the base necessary to catalyze the production of  $O_2^*$ . The base feed system is also shown in

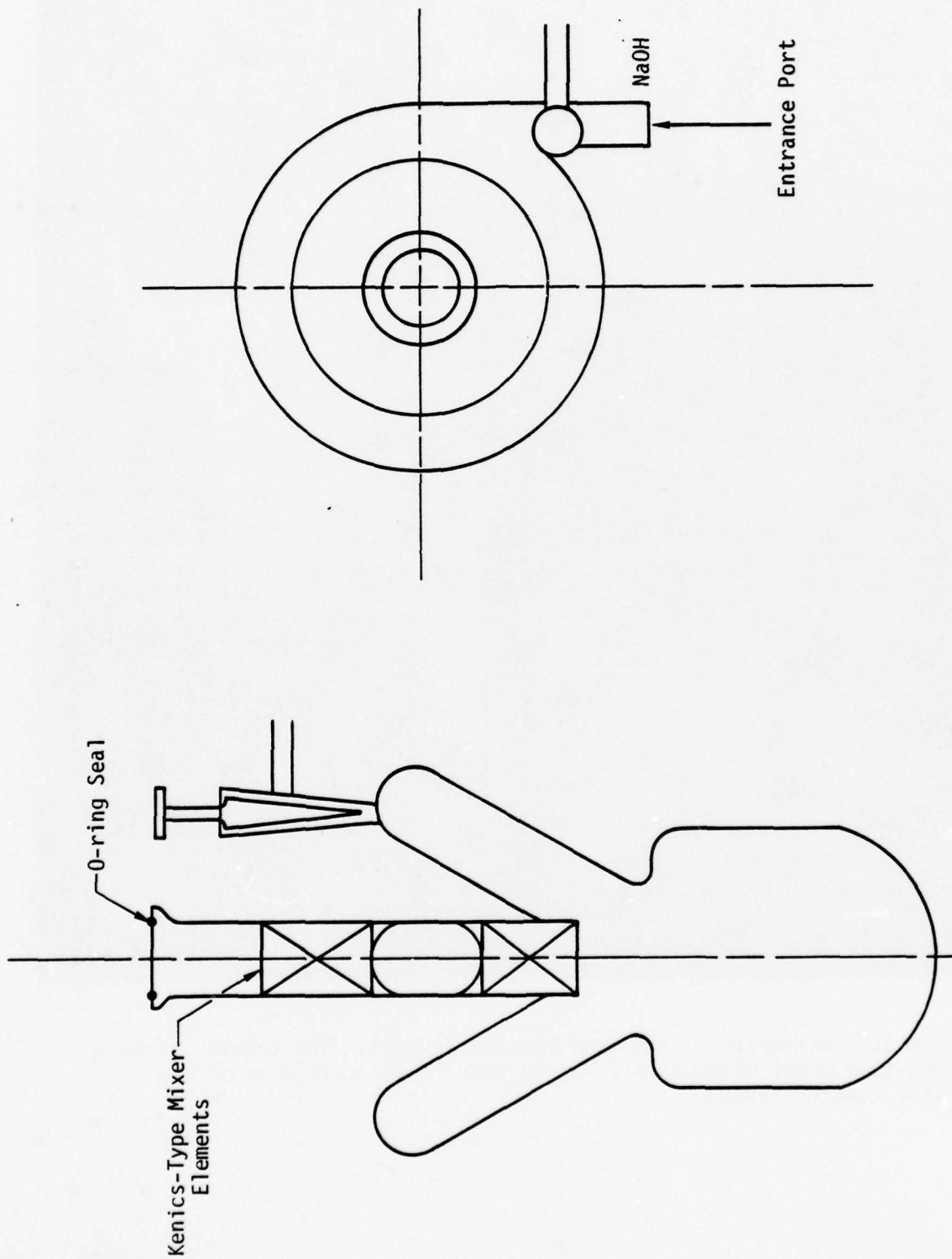


Figure 2. Schematic of Cyclone Reactor Vessel. The total volume of the reactor vessel is  $\sim 103 \text{ cm}^3$ . The entrance port is  $\frac{1}{2}$ " OD. The saturated NaOH enters through a 1.4 mm Fisher-Porter valve. The exit port is a no. 25 glass o-ring joint. During operation the reactor vessel is submerged in a 196K bath. The neck of the reactor is also thermostated at 196K.

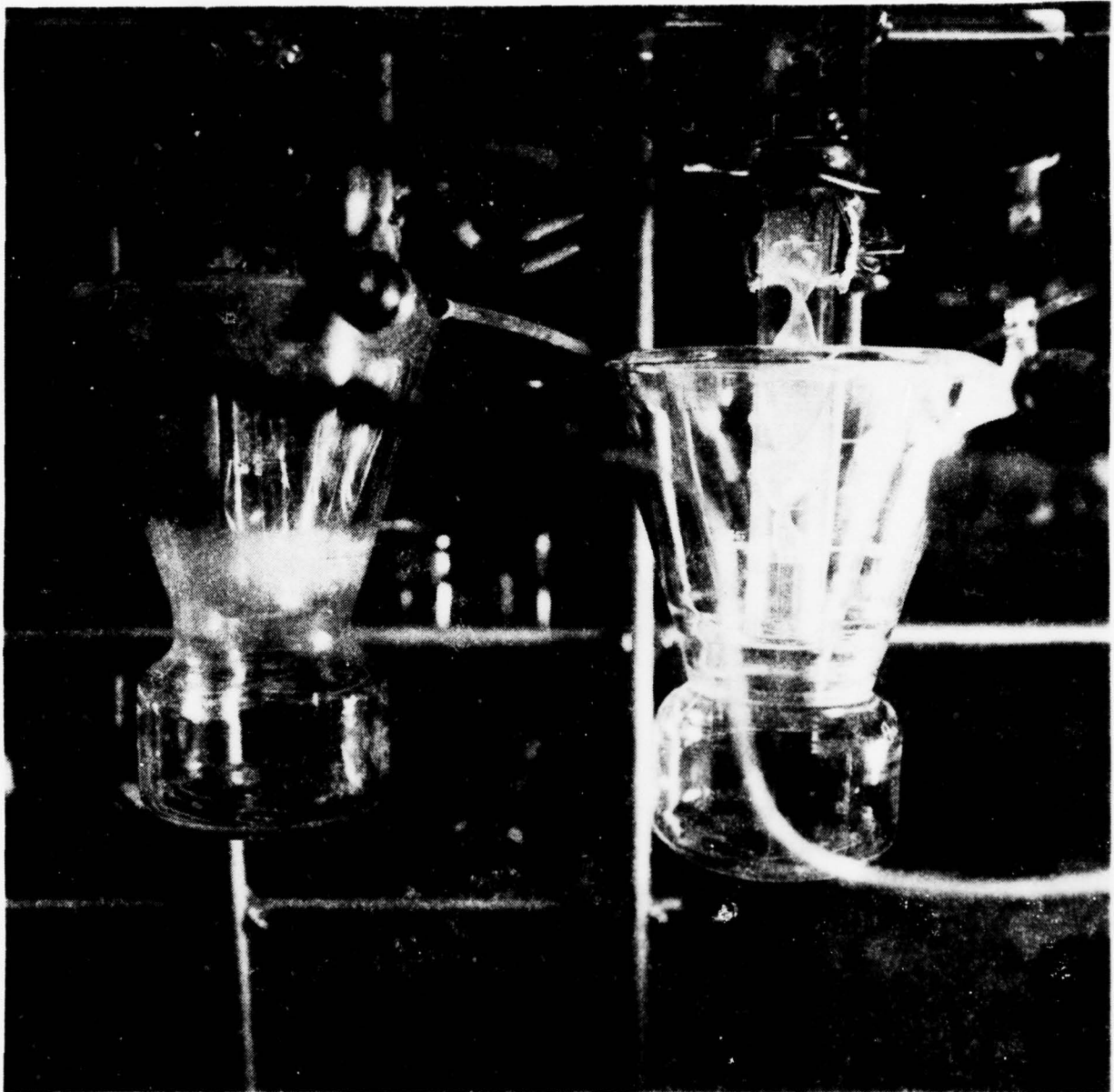
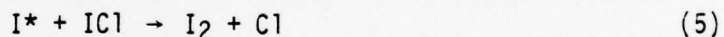
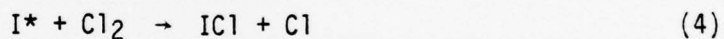


Figure 3. Photograph of the Dual Reactor Vessels. The twisted glass, Kinecs-type mixer elements are easily seen in the exit tube of the cyclone reactor vessel.

Figure 2. A saturated solution of sodium hydroxide (50% by weight) was fed into the reaction vessel at the entrance port via a 1.4 mm Fisher-Porter valve. As the sodium hydroxide was added to the evacuated reactor vessel, water evaporated and salt deposits were made in the annular regions of the cyclone trap. The effluent of the CFS-H<sub>2</sub>O<sub>2</sub> reaction channeled through this wetted salt surface.

#### 4. Cryogenic Traps

Aside from the production of oxygen, it was discovered that other gases were generated in the CFS-H<sub>2</sub>O<sub>2</sub> reaction. These products were identified using typical vacuum analytical techniques. Large amounts of chlorine were produced with trace quantities of hydrogen chloride. Molecular chlorine quenches the excited spin-orbit state of atomic iodine, and just as importantly, it can catalyze the recombination of iodine atoms in the following manner:



The rate coefficients for these reactions are  $2 \times 10^{-13} \text{ cm}^3 \text{ molec}^{-1} \text{ s}^{-1}$  and  $2.4 \times 10^{-11} \text{ cm}^3 \text{ molec}^{-1} \text{ s}^{-1}$ , respectively (Ref. 13).

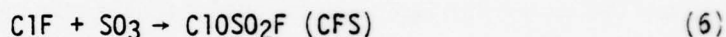
In order to trap the chlorine and hydrogen chloride, a trap cooled to 113K (melting point of iso-pentane) was positioned downstream of the reactor vessel. This trap also had twisted plates to provide a larger trapping surface area and to cause turbulence which would direct the gases to the cooled outer wall surface. A photograph of the 113K U-trap showing the

13. J. J. Deakin and D. Husain, "Electronic Excited Iodine Atoms, I(5<sup>2</sup>P<sub>1/2</sub>): A Kinetic Study of Some Chemical Reactions by Atomic Absorption Spectroscopy Using Time-Resolved Attenuation of Resonant Radiation at  $\lambda = 206.23 \text{ nm}$  I 5p<sup>4</sup>6S(2P<sub>3/2</sub>) 5p<sup>5</sup>(2P<sub>1/2</sub>)," J. Photochem. 1, 353 (1973).

twisted glass plates is presented in Figure 4. The vapor pressure of chlorine at 113K is 0.2 mtorr. Beyond this trap the gas stream essentially contained only oxygen.

#### 5. Chemicals

Chlorine fluorosulfate was prepared according to Schack et al (Ref. 14). Briefly, chlorine monofluoride and sulfur trioxide were mixed under autogenous pressure in a large passivated stainless steel container. When the reaction,



was completed, excess ClF and SO<sub>3</sub> were pumped from the products, and the CFS was distilled in vacuum into passivated stainless steel cylinders. Some of the properties of CFS are given in Table 1. H<sub>2</sub>O<sub>2</sub> (FMC, 90%) was used without further purification. Standard titration techniques (Ref. 15) and specific gravity measurements indicated that the H<sub>2</sub>O<sub>2</sub> was in the 85-90% (by weight) concentration range. The saturated NaOH (Baker, 50% by weight) was used directly from the bottle. Saturated CsOH hydroxide was prepared by adding 100 gm CsOH to a 100 gms of a 50% stock solution of CsOH (ROC/RIC).

TABLE 1. PROPERTIES OF CHLORINE FLUOROSULFATE

Melting Point (C)	84
Boiling Point (C)	45
Heat of Vaporization (kcal/mol)	7.66
Trouton Constant (e.u.)	24.0
Density (gm/cm <sup>3</sup> at 20C)	1.711

14. C. J. Schack and R. D. Wilson, U.S. Patent No. 3, 780, 165, Dec., 1973.
15. I. M. Kolthoff and R. Belcher, Volumetric Analysis Vol III, (trans. by N. H. Furman, New York, Interscience Publishers, 1957) p. 75.

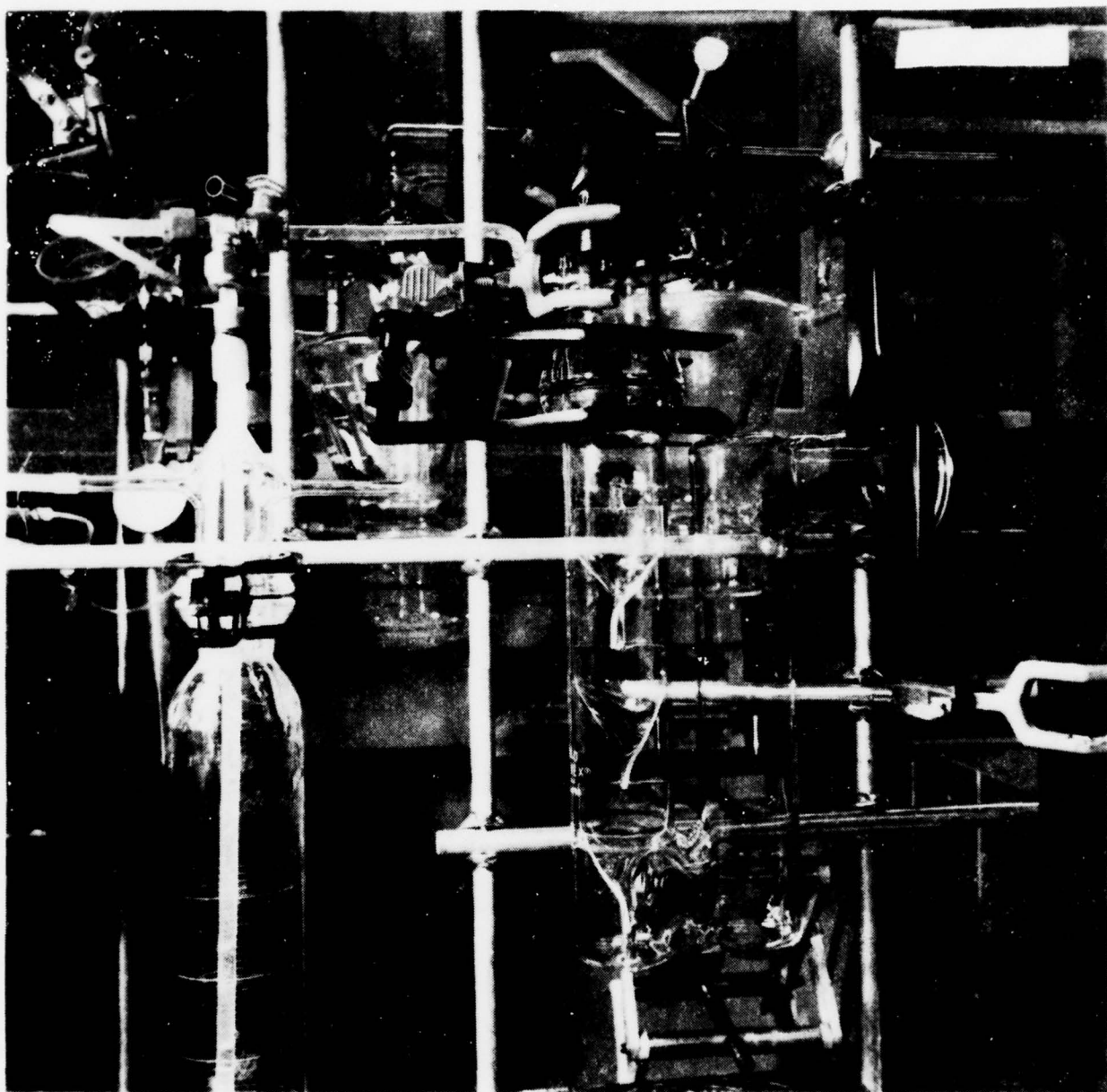


Figure 4. Photograph of the Cryogenic U-Trap. The U-trap is submersed in a 113K isopentane slush bath during operation. At the left is pictured the saturated NaOH storage tank, a converted graduated cylinder.

B. Determination of the  $O_2^*$  Absolute Concentration

The success of the  $O_2^*$  generator program was contingent on the fraction of singlet molecular oxygen produced. To invert the spin-orbit populations of atomic iodine via the resonant electronic energy transfer process (reaction (1)), the fractional yield of  $O_2^*$  must exceed 0.15. A method of determining this fraction, the measure of the  $O_2^*$  generator performance, had to be devised. Many techniques were available for determining the presence of  $O_2^*$ . Due to the nature of this program, the method chosen must have long-term stability with respect to its calibration, sensitivity to low  $O_2^*$  concentrations, a large dynamic range, and a fast response time. In addition, the method had to be independent of pressure and free of interference from the co-products of the CFS- $H_2O_2$  reaction.

Esr techniques yield the absolute concentration directly; however, since the magnetic field must be swept over the absorption line, the system response time is slow. Moreover, the esr signal is significantly broadened as the pressure increases, with an upper limit of approximately 2 torr total pressure. Also the esr instrument which is expensive would have to be dedicated to the program. The esr technique, on the other hand, provides an excellent means of calibrating a secondary source.

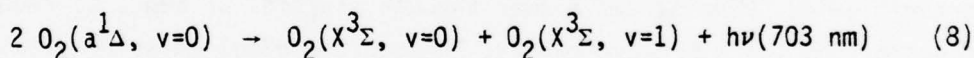
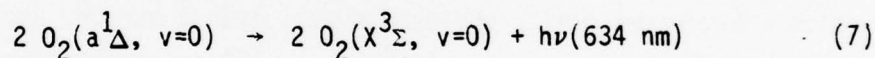
Thermal calorimetry techniques (Ref. 16) also provide a direct means of determining the absolute concentration of  $O_2^*$ . This method, however, is also slow and is susceptible to interferences, primarily those of atom and/or radical recombination on the sensitive surface. Since little is known about the CFS- $H_2O_2$  reaction and its products, this technique would be a poor choice.

The most direct method of detecting  $O_2^*$  is that of emission.  $O_2^*$  emits to the ground state at  $1.27 \mu m$ , but at a radiative rate of only

16. L. Elias, E. A. Ogryzlo, and H. I. Schiff, "The Study of Electrically Discharged  $O_2$  by Means of an Isothermal Calorimetric Detector," Can. J. Chem. 37, 1680 (1959).

$2.6 \times 10^{-4} \text{ s}^{-1}$ . Hence the fluorescence intensity is extremely weak. Recent progress in the development of intrinsic germanium detectors, however, has improved this method of detection. The germanium detector cooled to liquid nitrogen temperatures has a large dynamic range and a fast response time ( $\sim 1 \text{ msec}$ ). The emission process is independent of pressure at the low pressures of this study. The major problem, however is that of maintaining calibration for day to day operation.

Red banded emissions have been observed in both liquid reactions (e.g., hydrogen peroxide and hypochlorite salts, see Ref. 10) and in discharge molecular oxygen studies (Ref. 17). When molecular oxygen is radiated by a microwave source, Bader and Ogryzlo (Ref. 18) noted that two emission bands (one peaked at 634 nm; the other, at 703 nm) were proportional to the square of the heat measured utilizing the thermal calorimetry technique. They attributed these emissions to a cooperative release of a single photon.



The intensity of these two dimol emission peaks were nearly equal. Initially, it was thought that a loosely bound ( $\sim 600 \text{ cal/mol}$ )  $\text{O}_4^*$  molecule was formed which subsequently radiated. This thesis was disproved by Arnold et al. (Ref. 19) who conducted a temperature dependent study on the dimol emission intensity. Since the emission process is strictly a collisional one with a

17. U. K. Kurzweg, A. M. Bass, and H. P. Broida, "Spectra and Afterglows and Discharges from Nitrogen-Oxygen Mixtures," *J. Mol. Spectry.* 1, 184 (1957).
18. L. W. Bader and E. A. Ogryzlo, "Reactions of  $\text{O}_2(^1\Delta_g)$  and  $\text{O}_2(^1\Sigma_g^+)$ ," *Disc. Faraday Soc.* 37, 46 (1964).
19. J. S. Arnold, R. J. Browne, and E. A. Ogryzlo, "The Red Emission Bands of Molecular Oxygen," *Photochem. Photobio.* 4, 963 (1965).

bimolecular rate constant of  $k_d = 5 \times 10^{-22} \text{ cm}^3 \text{ molec}^{-1} \text{ s}^{-1}$ , the dimol emission is independent of pressure until termolecular processes begin to compete with bimolecular ones. These red band emissions, therefore, can be monitored, and their intensities be related to the concentration of  $\text{O}_2^*$ . Since the emission is in the visible red region of the spectrum, sensitive detection by photomultiplier tubes (PMT) can be employed. PMT's when cooled and coupled with photon counting techniques provide large dynamic range ( $\geq 10^6$ ), long term stable operation, and fast response time. As long as the dimol emission is the only one in the 634 nm region, this technique would be free of interference from reaction by-products. Based upon these arguments, the dimol emission technique was utilized in this study.

The dimol emission intensity was calibrated for absolute  $\text{O}_2^*$  concentration using esr techniques. A schematic of experimental arrangement for this calibration is given in Figure 5. A stream of oxygen was passed through a microwave cavity (Evanson type), over a mercury pool to remove O atoms, and through a brine cold bath at  $-10^\circ\text{C}$  to remove elemental mercury and mercuric oxide. The stream flowed through a series of bends to reduce light emission from the microwave cavity, through the dimol emission viewing cell, and finally entered the esr cavity. The Pyrex flow tube was painted black to reduce the background level of light reaching the detection system. Flow velocities were on the order of  $10^3 \text{ cm/sec}$ . Four pressure taps were positioned along the flow path from the viewing cell to the edge of the esr cavity. The pressure inside the esr cavity was determined from the pressure gradient measured at these four pressure taps. The dimol emission from the viewing cell passed a 633 nm filter (full width at half maximum was 5 nm) and was detected by a GaAs photomultiplier tube (RCA C31034) which was biased at -1500 volts by a Keithley Model 246 power supply unit. The signal from the PMT, which was thermoelectrically cooled to  $-20^\circ\text{C}$  by a PR Model TE-102TS-RF, was amplified by a PAR 1120 amplifier-discriminator. The photoelectric pulses were subsequently counted by a PAR 1108 Multi-Mode Processor.

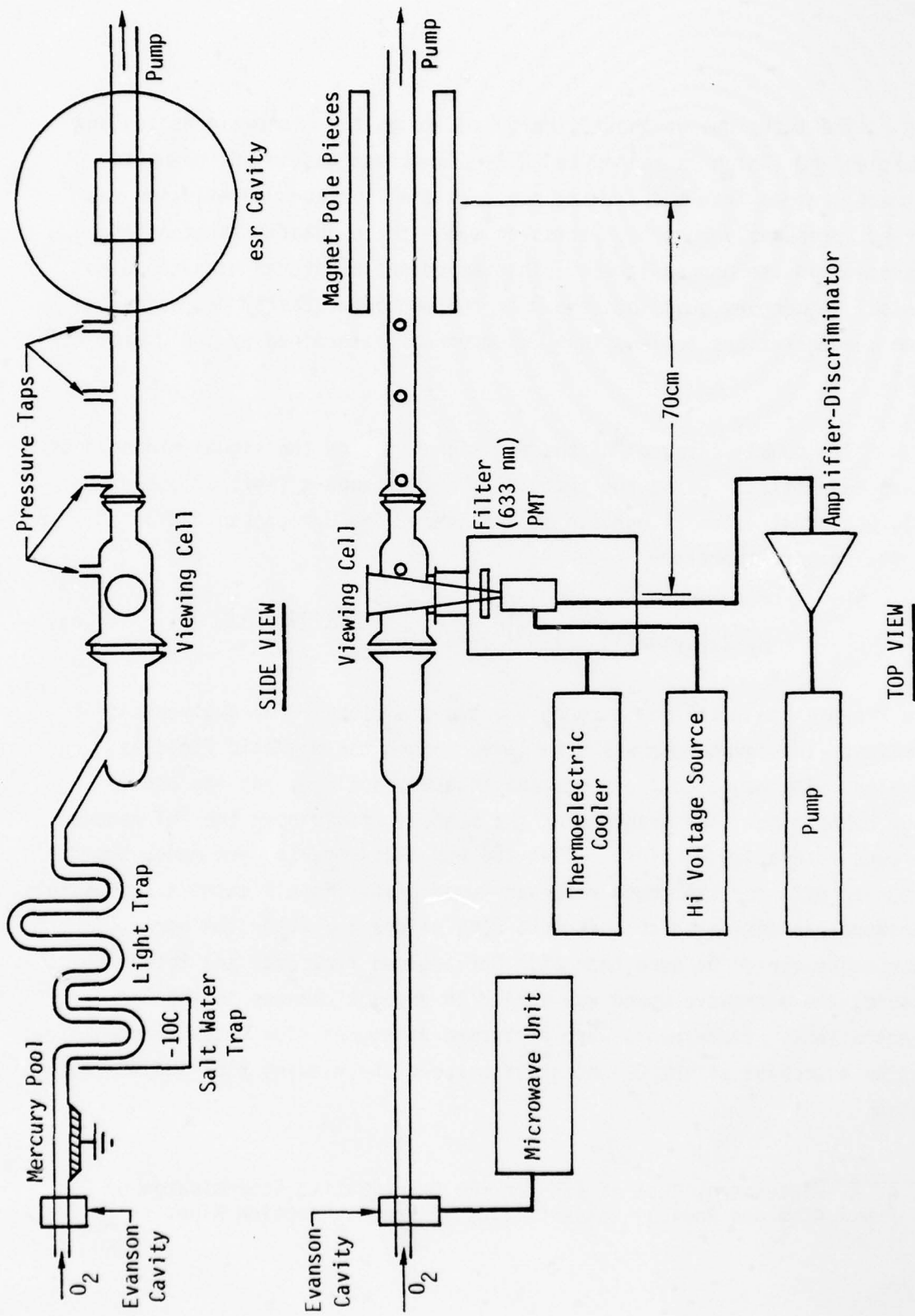


Fig. 5 Schematic for the  $O_2$  ( $\uparrow\Delta$ ) Calibrations

The technique of passing mercury through the microwave region and depositing HgO (which is heated to 120C) downstream was insufficient to eliminate O atoms from the viewing cell. A small background emission was observed, presumably from NO<sub>2</sub>\* emission since trace quantities of nitrogen are present in the oxygen stream. This emission interfered with the dimol emission. A mercury pool downstream of the microwave cavity decreased the O atom concentrations to less than 0.1 mtorr as determined by the O atom esr signal.

The double integral of the esr signal yields the signal strength of the esr transition. Using the techniques of Westenberg (Ref. 20), the absolute concentration of O<sub>2</sub>\* can be obtained. The O<sub>2</sub>\* concentration at the viewing port therefore is

$$[O_2^*]_{\text{viewing cell}} = [O_2^*]_{\text{esr}} \frac{P_{\text{viewing cell}}}{P_{\text{esr}}} \quad (9)$$

where P's are the total pressure at the two positions. For a given set of experiments the count rate was determined before the magnetic field was activated. The magnetic field was subsequently applied, and the esr measurements made. The presence of the magnetic field near the PMT reduced the count rate a few percent. After the esr measurements were made, the field was turned off, and the count rate was remeasured. In all cases a successful experiment was one in which the count rate before and after the esr measurements varied no more than 2%. For a given flow rate and total pressure, the microwave power was varied to produce changes in the O<sub>2</sub>\* concentrations. Experiments were performed at higher flow rates to check that no major quenching of the O<sub>2</sub>\* occurred between the viewing port and the esr cavity.

20. A. A. Westenberg, "Use of ESR for the Quantitative Determination of Gas Phase Atom and Radical Concentrations." *Progr. Reaction Kinetics* 7, 23 (1966).

The dimol emission rate is governed by the following relationship,

$$\frac{d I(634 \text{ nm})}{dt} = G K_d [O_2^*]^2 \quad (10)$$

where G is some unspecified geometric factor which includes the viewing volume, the optical collection efficiency, the transmission of intervening filters and windows, and the quantum efficiency of the detector. Plotting the dimol emission count rate vs. the square of the  $O_2^*$  concentration as determined from the esr signal yielded a linear plot with a zero intercept equal to the background count rate. This plot is presented in Figure 6. The fact that the data for various flow rates and pressures lie on the same plot assures that (1) no quenching had occurred between the viewing cell and the esr cavity, (2) no extraneous residual light was interfacing with the dimol emission, and (3) there was no pressure dependence on the dimol emission. A linear least squares analysis of the data yielded the following relationships

$$C = 2.46 (\pm 0.75) + 7.28(\pm 0.12) [O_2^*]^2 \quad (11)$$

where C is the dimol emission count rate in Hz and  $O_2^*$  is the  $O_2^*$  concentration expressed in room temperature pressure (mtorr). Hence to determine the partial pressure of  $O_2^*$  from the reactor, the following expression was used,

$$[O_2^*] = \left[ \frac{C - \text{BKG}}{7.28} \right]^{\frac{1}{2}} \quad (12)$$

where BKG was the background count rate (typically  $\sim 50\text{Hz}$ ) which varies according to room light condition and room temperature.

The detection system including the viewing cell was installed on the output of the  $O_2^*$  generator. Since the calibration is dependent on the viewing geometry (the G factor in Eq. (10)), all studies had to be done with this viewing cell. Small angle variations between the detection system

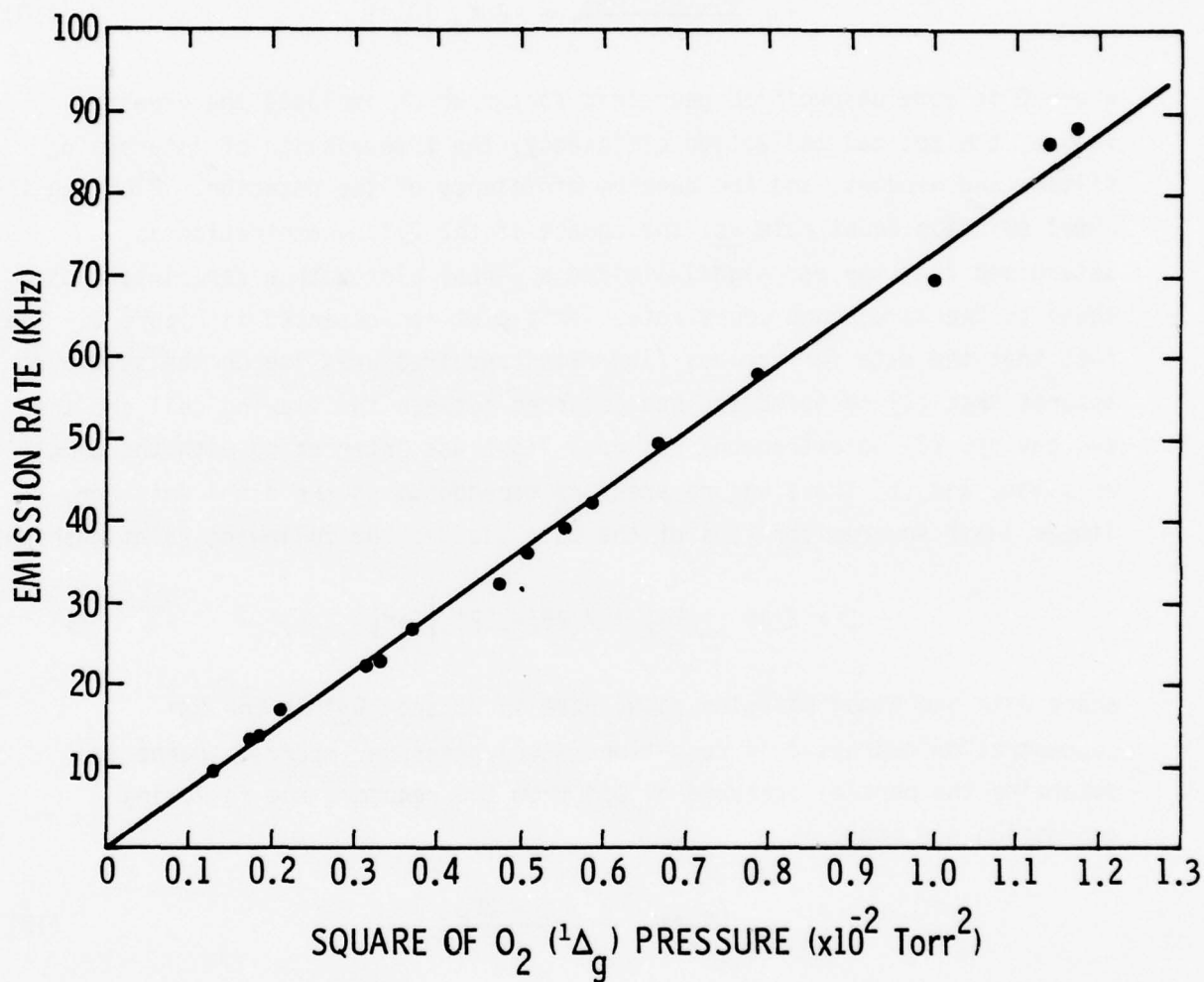


Figure 6. Plot of the Dimol Emission Rate vs. the Square of the Partial Pressure of O<sub>2</sub>\*. These data include flow velocities which varied from 1.0 - 1.5 cm s<sup>-1</sup> and over total pressure range of 1 - 2 torr.

viewing axis and the normal to the viewing window resulted in less than 2% variation in the count rate.

The entrance to the viewing port was 5 cm in diameter, but the exit was only half that size. Later in the program when greater flow velocities were required, the viewing cell had to be redesigned and a calibration made of the new viewing cell. The calibration was accomplished by measuring the fluorescence intensity at each cell while microwaved molecular oxygen flowed through both. A successful measurement was one in which transporting the detection system between these two observation ports reproduced the count rates at each window. A plot of count rates for the new viewing port vs. the original one is given in Figure 7. Hence using the second viewing port the partial pressure of  $O_2^*$  is given by the following expression

$$[O_2^*] = \left[ \frac{C - \text{BKG}}{11.6} \right]^{1/2}$$

### C. Generator Performance

#### 1. Initial Studies

During the initial phase of this work, the  $O_2^*$  generator (feed system, mixer, and reactor) was attached to the dimol emission viewing section and to a 15 cfm pump. The reaction was not base catalyzed in these first experiments. The molar flow rate of CFS typically exceeded that of  $H_2O_2$  producing gases of molar flow rates in the range of 0.1-0.5 mmol/s. Under these flow conditions, the mixer became extremely hot to the touch, and red emissions were occasionally observable to the naked eye in the reactor vessel and in the downstream flow tube. Close examination of the spectral components revealed that the red emission was a broad band continuum and not the dimol emission. The spectrum, though not confirmed, appeared much like that of Cl atom recombination (Ref. 21)<sup>a</sup>. This broad banded red emission

<sup>a</sup> In the analogous nonbase catalyzed bromine fluorosulfate-hydrogen peroxide reaction, a yellow emission was observed.

21. L. W. Bader and E. A. Ogryzlo, "Halogen Atom Reaction. II. Luminescence from the Recombination of Chlorine Atoms," J. Chem. Phys. 41, 2926 (1964).

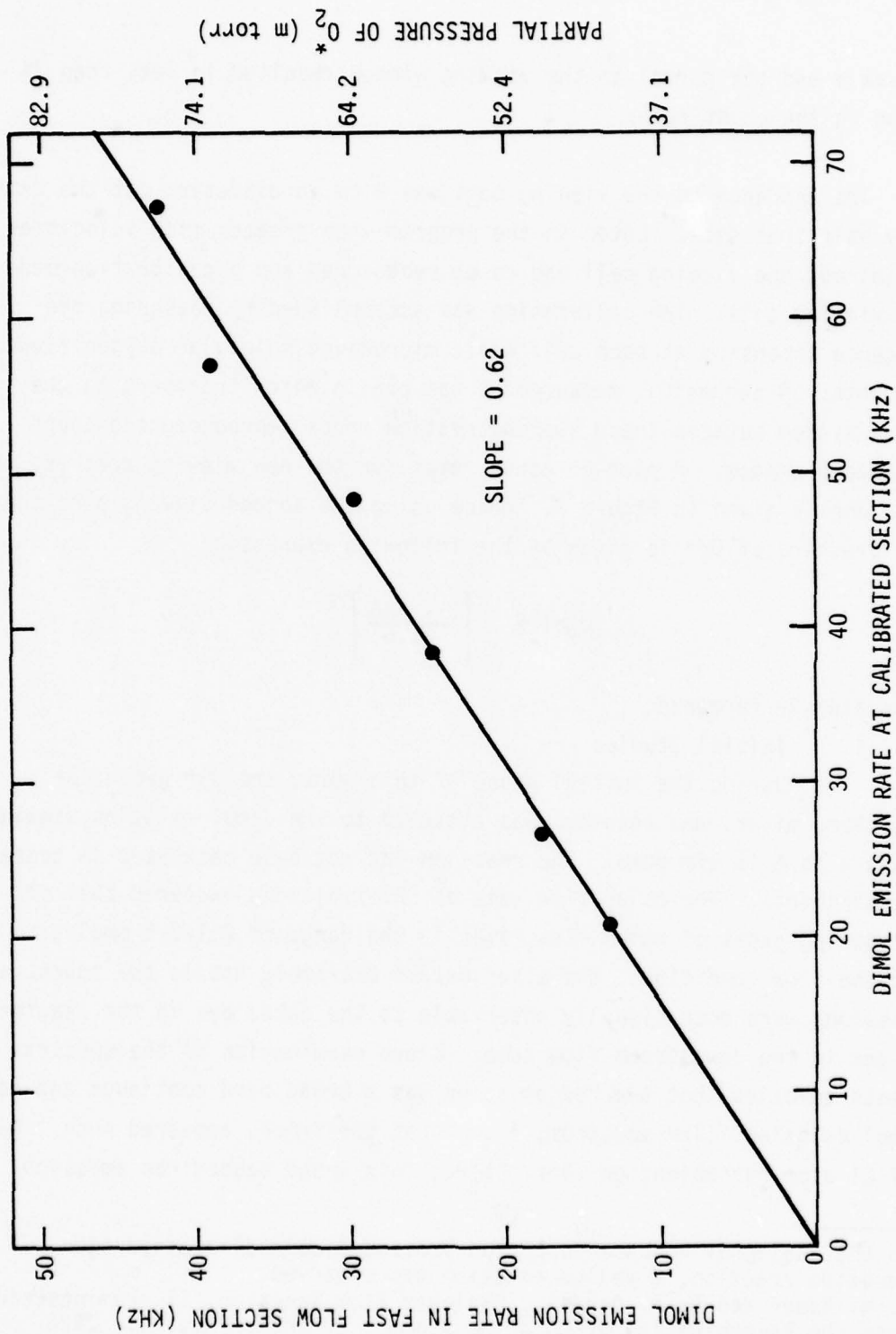


Figure 7. Dimol Emission Rate of the Two Viewing Sections Plotted Against Each Other.

was readily quenched when a cryogenic U-trap (cooled to 131K) was positioned between the reactor vessel and the dimol emission section. There was no evidence of dimol emission indicating that either  $O_2^*$  was also quenched by the U-trap or that no  $O_2^*$  was generated by the reaction. This latter suggestion was proved to be correct later in the program since the 131K trap does not significantly quench  $O_2^*$ .

Addition of saturated NaOH downstream of the mixer resulted in the formation of a red emission also; however, this emission was identified as dimol emission. The emission at 634 nm was accompanied by a strong emission at 762 nm ( $O_2(b^1\Sigma) \rightarrow O_2(X^3\Sigma)$ ). Reducing the temperature in the U-trap from ambient to 131K did not affect the emission intensity. Addition of molecular iodine to the flow downstream of the U-trap produced the familiar B  $\rightarrow$  X transition of molecular iodine as reported by Derwent and Thrush. With the U-trap cooled to 131K, small traces of a yellow residue were found in the liquid nitrogen trap which was positioned downstream of the dimol emission section. This yellow residue was thought to be molecular chlorine. Since molecular chlorine catalyzes the recombination of iodine atoms (see reaction 4 and 5), the U-trap was lowered to 113K. At this temperature  $Cl_2$  has a vapor pressure of only 0.2 mtorr. The conclusion reached at the end of this phase of work was that the based catalyzed reaction of CFS and 90% hydrogen peroxide in the generator produced clean streams of molecular oxygen in which the fractional yield of  $O_2^*$  was in excess of 0.30.

## 2. Pressure and Temperature Distribution Within the $O_2^*$ Generator Reactor Vessel

The  $O_2^*$  generator including cryogenic traps and dimol emission diagnostics was attached to a larger capacity pump, 500 cfm Kinney. For the same molar flow rates, the pressure dropped, establishing a pressure gradient from the mixer through the reactor and subsequent flow lines. Pressure taps were positioned at critical points in the reactor vessel; the position of these pressure ports are depicted in Figure 8. The pressure lines

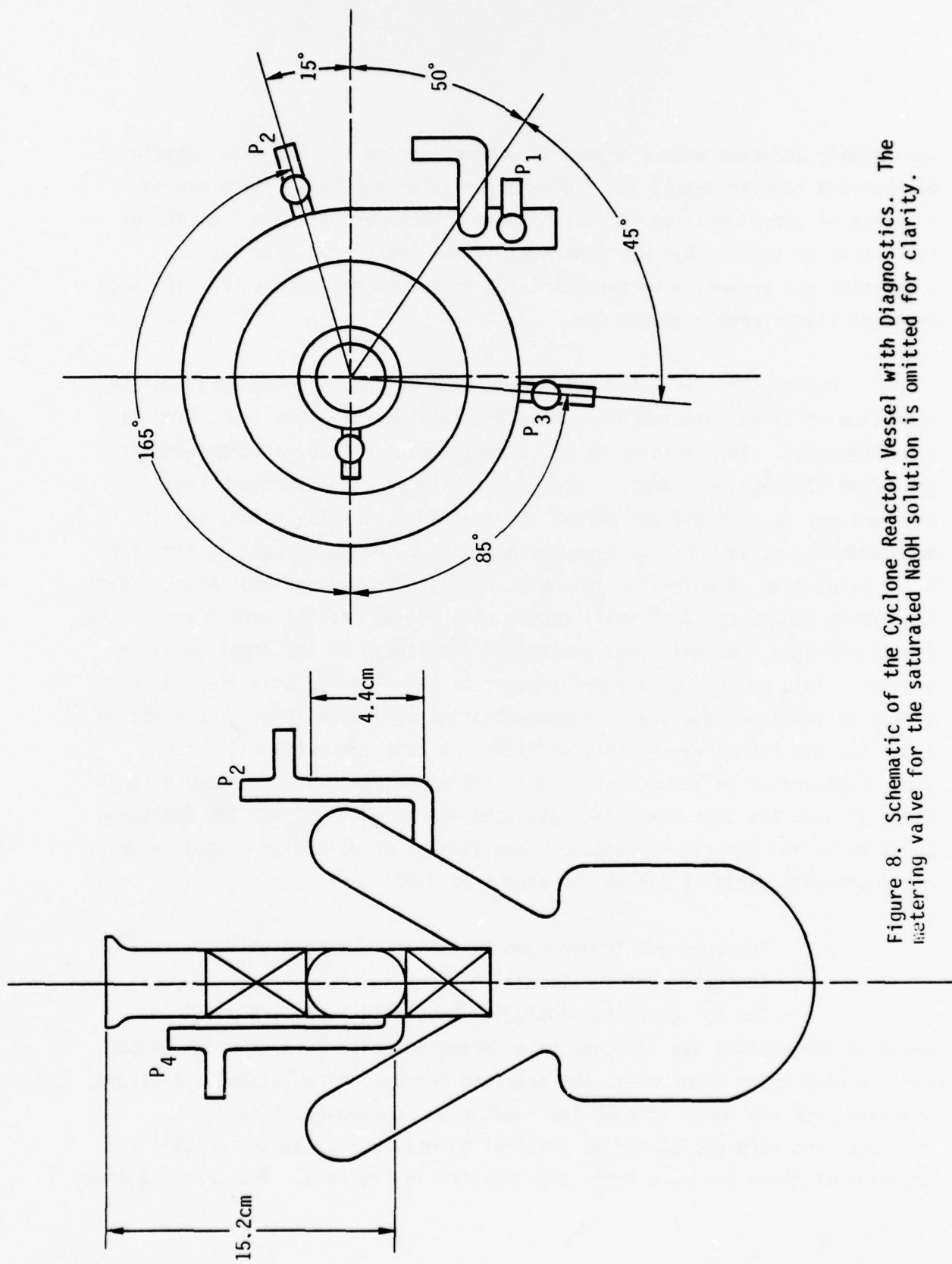


Figure 8. Schematic of the Cyclone Reactor Vessel with Diagnostics. The metering valve for the saturated NaOH solution is omitted for clarity.

were attached to a common manifold with intervening shut-off bellow valves (Hoke, 4611N4M). An MKS capacitance manometer monitored the pressure of whichever valve was open to the pressure taps. Hence to measure all pressure taps each successive port had to be open and shut during the measurement period. For the reactor runs this was only accomplished when steady operation of the generator was achieved. This steady operation was confirmed when the downstream pressure remained constant before and after a measurement of each of the pressure taps.

The pressure gradient for baseline operation (i.e., without the generation of  $O_2^*$ ) was determined. The reactor and U-trap were cooled to 196K and 113K, respectively, while air, a noncondensable gas for these traps, was metered through the reactor vessel. The pressures were measured for each pressure tap as a function of molar flow rate. Plots of these data are presented in Figure 9. Hence, a vertical cut in these plots at a given molar flow rate represents the pressure gradient for this baseline operation.

During the base catalyzed CFS- $H_2O_2$  reaction, salt deposits formed within the annular regions of the reactor vessel (see Figs. 2 and 3). These deposits hinder the flow of gases resulting in an increase in the pressure (hence the pressure gradient) in the reactor vessel for a constant molar flow rate. In addition, any gases which are condensible in either of the traps held at 196K or 113K also increase the pressure gradient. Under typical reactor operation, no resistance to flow occurs past the pressure tap attached to the exit of the reactor vessel (P4 in Figure 8). Hence any difference in the pressure relative to the baseline operation represents the partial pressure of gases which condense in the 113K U-trap. In all experiments in which P4 was monitored, this pressure difference did not exceed 10 mtorr. The flow velocity and distance between P4 on the reactor vessel and the 113K trap was typically 800 cm/s and 70 cm, respectively. The contact time between these gases and molecular oxygen, therefore, is at most 90 msec. To have significant gas phase quenching by these condensible gases, the rate constant

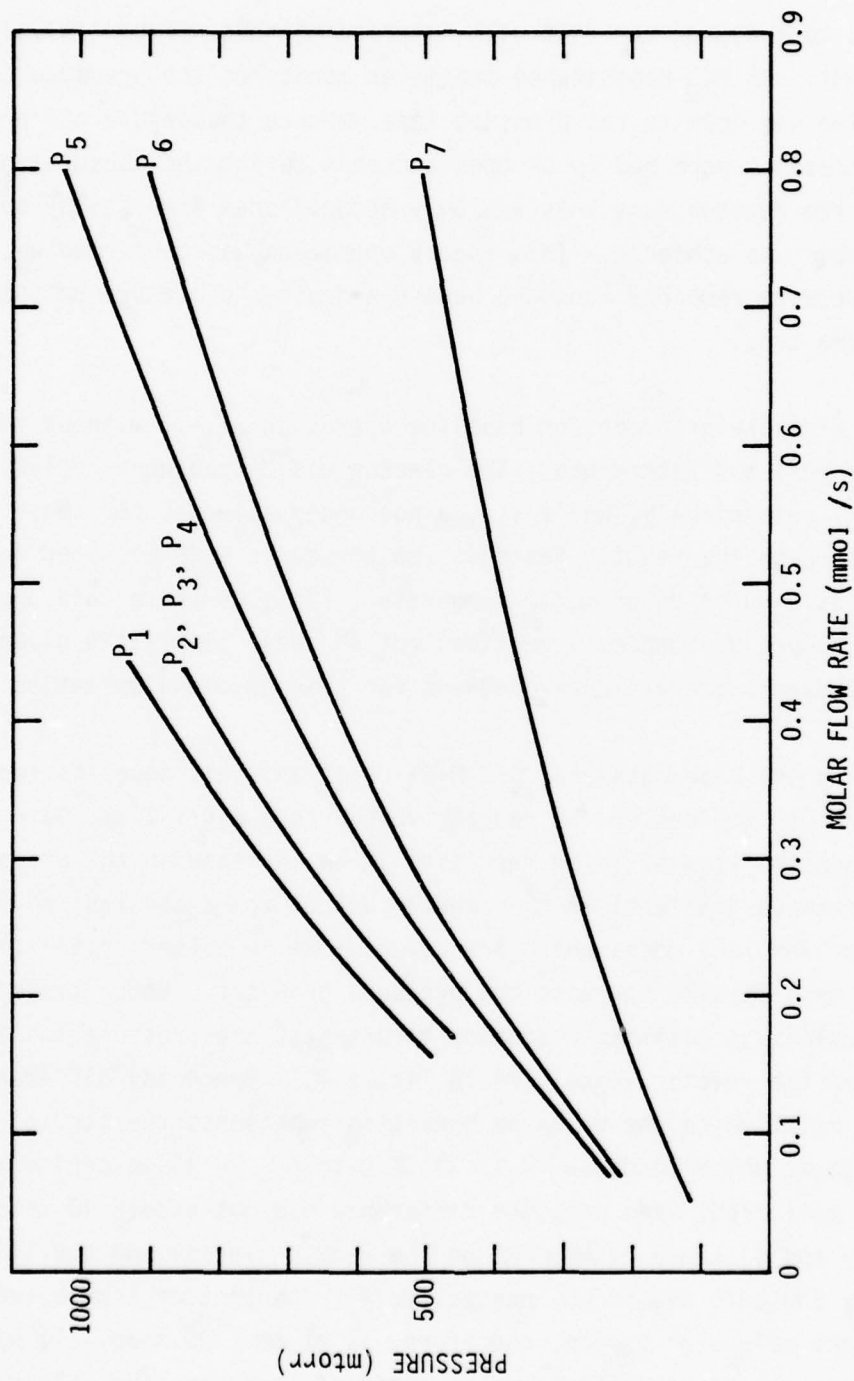


Figure 9. Plots of the Pressure at Each Diagnostic Port vs. Molar Flow Rate in the Reactor Flow Lines. P1 - P4 are the pressure taps designated in Fig. 8. P5 is the pressure tap at the dimol emission viewing section. P6 and P7 are the pressure taps in the downstream  $O_2^*-I_2$  diagnostics described in Section V.

( $k_Q = 1/\text{pt}$ ) would have to be  $\sim 10^3(\text{torr}\cdot\text{s})^{-1}$ . Quenching rate constants of  $\text{O}_2^*$  by  $\text{NO}$ ,  $\text{O}$  atoms and ozone, the fastest known quenchers of  $\text{O}_2^*$ , range from 1-100  $(\text{torr}\cdot\text{s})^{-1}$ . Therefore, quenching of  $\text{O}_2^*$  between the reactor and U-trap would be insignificant and at most 10%.

The  $\text{CFS-H}_2\text{O}_2$  reaction is a vigorous one producing hot gases which flow from the mixer to the reactor vessel. At each of the pressure ports thermocouples were positioned to monitor the variations in the temperature of the gases in the reactor. Type S thermocouples (Pt-Pt(10% Rd)) were used throughout (Ref. 22). The metal junctions were dipped in Halocarbon wax, and the leads were covered with Teflon sleeves. The wires were vacuum sealed with Halocarbon wax. Platinum thermocouples were necessary due to the corrosive nature of the reaction. The temperature gradient within the reactor was determined for a baseline operation, one in which the reactor was immersed in 196K bath while air was metered through the reactor. It was found that the temperature distribution was independent of the molar flow rate in the 0.15-0.40 mmol/s range. The data for baseline operation is given in Table 2.

TABLE 2. TEMPERATURE DISTRIBUTION FOR BASELINE OPERATION

Thermocouple	Temperature (K)
T <sub>1</sub>	293 (room temperature)
T <sub>2</sub>	212
T <sub>3</sub>	212
T <sub>4</sub>	198

During the  $\text{CFS-H}_2\text{O}_2$  reaction, the hot gases left the mixer, travelled past the first thermocouple, and reacted with the incoming saturated

22. R. L. Powell, W. J. Hall, C. H. Hyink, Jr., L. L. Sparks, G. W. Burns, M. G. Scrogee, and H. H. Plumb, "Thermocouple Reference Table Based on the IPTS-68," Nat. Bur. Stand. (US), Monogr. 125, 13 (1974).

NaOH solution. The gaseous effluents from the total reaction heated the surfaces including the salt deposits which were formed. As the reaction progressed in time, the temperature within the reactor vessel continued to increase. Results of a typical run are given in Table 3.

TABLE 3. TEMPERATURE RISE IN THE REACTOR AS  
A FUNCTION OF TIME (TYPICAL RUN)

Time (min)	Temperature (K)			
	T <sub>1</sub>	T <sub>2</sub>	T <sub>3</sub>	T <sub>4</sub>
0	21	-78	-78	-78
2.4	45	- <sup>a</sup>	-45	-68
3.0	51	-	-45	-50
5.8	57	-	-68	-50
8.7	45	-	-68	-49

<sup>a</sup> Ceased functioning properly.

### 3. Fraction Yield as a Function of Mixing

The static Kenics mixer consists of a series of twisted stainless steel plates (elements) of alternating pitch. The twist is a full 90° rotation. This arrangement disrupts the flow of gases and/or liquids for the purpose of enhancing the mixing rate. The performance (i.e., fractional yield of O<sub>2</sub>\*) of the generator was evaluated in terms of the time of mixing. The performance was measured for 6, 9, and 12 elements in the mixing tube. The results are presented in Table 4.

TABLE 4. PERFORMANCE OF O<sub>2</sub>\* GENERATOR AS A FUNCTION OF MIXING

<u>No. of Elements</u>	<u>Fractional Yield of O<sub>2</sub>*</u>	<u>Total Oxygen Pressure</u> (torr)
6	0.82	0.30
9	0.58	0.38
12	0.36	0.48

These data represent over an hour of operation with the maximum fractional yield observed during that time period. As the number of elements were increased the mixing region became noticeably warmer. In the case of the 12 element mixers, cooling with a piece of dry ice improved the generator performance. The value reported in Table 4 is for a cooled 12 element mixer. It is well known that H<sub>2</sub>O<sub>2</sub> undergoes homogeneous decomposition,  $\text{H}_2\text{O}_2 \rightarrow \frac{1}{2}\text{O}_2(^3\Sigma) + \text{H}_2\text{O}$  at temperatures above 400C (Ref. 23). In these experiments, it is unlikely that such high temperatures were encountered. However, heterogeneous decomposition of H<sub>2</sub>O<sub>2</sub> is also strongly temperature dependent. At temperatures above 66C catalytic decomposition can occur (Ref. 24). We have tentatively assumed that thermal heterogeneous decomposition is responsible for the lower yield of O<sub>2</sub>\* with increased temperature. This temperature problem is also encountered when the mass flow rate in the generator is increased. At greater mass flow rate, more heat needs to be dissipated, hence the temperature rises resulting in decomposition of H<sub>2</sub>O<sub>2</sub> and a low O<sub>2</sub>\* output. The current single mixer feed system, therefore, represents an upper limit on the molar flow rate of high yield O<sub>2</sub>\*.

23. C. N. Satterfield and T. W. Stein, "Decomposition of Hydrogen Peroxide Vapor," J. Phys. Chem. 61, 537 (1957).

24. "Hydrogen Peroxide Handbook," Chemical and Material Sciences Department, Research Division, Rocketdyne, Canoga Park, Calif. p. 426 (1974).

#### 4. Fractional Yield as a Function of Base

In the original CFS-H<sub>2</sub>O<sub>2</sub> experiments of Goldberg and Pilipovich, KOH pellets were dissolved in the H<sub>2</sub>O<sub>2</sub> solution. Using esr techniques, they obtained fractional yields from 0.2-0.4. In the current generator design, the base was added after the initial CFS-H<sub>2</sub>O<sub>2</sub> reaction. Saturated NaOH, when added to the effluents from mixer, produced salt deposits within the reactor vessel, restricting the gaseous flow. This constriction produced a dynamically varying pressure gradient within the reactor. Saturated CsOH is known to be more soluble; hence its addition was thought to produce less salt deposits, thus circumventing the variable operation of the generator under NaOH conditions. Operation of the O<sub>2</sub>\* generator when utilizing CsOH resulted in the absence of salt deposition. The pressure gradient in the reactor remained constant for a given molar flow rate.

The fractional yield of O<sub>2</sub>\* in the CsOH catalyzed system was lower than that for the NaOH system. The maximum molar flow rate was the same, however. The surface area provided by the CsOH was much less; only wetting a 5 cm wide strip on the inner sides of the annular region of the reactor vessel from top to bottom. If one considers that a gas-surface heterogeneous reaction is necessary for the production of O<sub>2</sub>\*, the CsOH system would clearly provide only a limited surface area for reaction. A gas-surface reaction mechanism, therefore, appears to have some validity.

#### 5. Consumption Rate of Reactants

The generator performance was not only evaluated in terms of the fractional yield of O<sub>2</sub>\* as determined by the calibrated dimol detection system and the total pressure, but also in terms of the ability of the active molecular oxygen stream to create a population inversion between the spin-orbit states of atomic iodine. The results of these latter experiments are reported in Section IV. Oxygen molar flow rates and reactant consumption rates are summarized here. The average values presented here represent over eight hours of actual O<sub>2</sub>\* generator operation.

During the evaluation of the  $O_2^*$  generator, it was determined that the oxygen molar flow rates were too small to produce a significant inversion density on the spin-orbit states of atomic iodine when utilizing a single reactor. Hence the flow system was modified to incorporate a dual generator configuration. These two generators include a duplicate reactant metering system sharing the same mechanical drive, reactor vessel, and NaOH feed system. The 113K U-trap and flow lines from the reactors were common to both generators but the glass tubing cross-sectional area was doubled.

The average results for the single and dual reactor configurations are reported in Table 5. Note that the average run time for the dual configuration was not halved on the average. The fractional yield of  $O_2^*$  often decreased when attempts were made to run both reactors. Hence the data reported for the dual reactor configuration has single generator operation time included. The yield of oxygen from these generators are only approximate, since addition of argon in the  $O_2^*-I_2$  evaluation test may have altered the  $O_2$  production rate from the generator. More of this phenomena is reported in the next subsection. In general, however, approximately one mole of oxygen was produced for every mole of CFS consumed. These results were also obtained in product analysis experiments which are reported in a following subsection (Section II.7). In all cases, the amount of  $H_2O_2$  used was in excess. The  $H_2O_2$  remained a liquid through the mixer and into the reactor vessel.

TABLE 5. AVERAGE CONSUMPTION RATE OF REACTANTS

		<u>Single Reactor</u>	<u>Dual Reactor</u>
CFS	(ml)	8.0	8.8
	(moles)	0.103	0.113
87% H <sub>2</sub> O <sub>2</sub>	(ml)	100	100
	(moles)	3.52	3.52
NaOH	(ml)	57	67
Time	(min)	17.0	15.4
Q(O <sub>2</sub> ) <sup>a</sup>	mmoles/sec	0.09	0.14
Total O <sub>2</sub>	(moles)	0.09	0.15
Moles O <sub>2</sub> /moles CFS		0.79	1.3
Moles O <sub>2</sub> /moles H <sub>2</sub> O <sub>2</sub>		3 x 10 <sup>-2</sup>	4 x 10 <sup>-2</sup>

- a. These values are rough estimates since the molar flow rates were not monitored continuously; only the total pressure was monitored. During these runs, variable amounts of argon and I<sub>2</sub> were introduced.

The greatest fractional yield of O<sub>2</sub>\* generally occurred at lower molar flow rates, i.e., at lower total oxygen pressure recorded in the dimol emission viewing section. The best values of O<sub>2</sub>\* percentages at various molar flow rates from the generator are summarized in Table 6.

TABLE 6. GREATEST O<sub>2</sub> PERCENTAGES PRODUCED AT VARIOUS GENERATOR MOLAR FLOW RATES

<u>Total O<sub>2</sub> Pressure (mtorr)<sup>a</sup></u>	<u>% O<sub>2</sub>*<sup>b</sup></u>
300	83
360	72
420	41.5
580	53.5
600	31
660	30
720	46
740	22

- a To obtain molar flow rates see curve labeled P<sub>5</sub> in Figure 9.  
 b These percentages are the peak values for a given experiment in which the reported pressure was relatively constant ( $\pm 20\%$ ) during the majority ( $>50\%$ ) of the run.

#### 6. Addition of an Inert Gas

Molecular iodine was introduced to the oxygen stream produced by the  $O_2^*$  generator via argon carrier gas. The addition of this gas changes the pressure distribution throughout the flow system including the reactor vessel and Kenics mixer region. The difference between the total flow rate and the argon flow rate is the flow rate of the oxygen produced by the  $O_2^*$  generator. It was found the molar flow rates of oxygen changed when argon was added to the stream. The oxygen flow rate with argon added relative to its flow rate prior to argon addition is plotted against the mole fraction of argon in the flow stream. This plot is presented in Figure 10. During single generator operation, the addition of argon seemed to enhance the production of oxygen, and hence increased the pressure within the reactor and mixer regions. On the other hand, the opposite effect was generally observed with the dual reactor configuration. It is difficult to assess the significance of this phenomena without knowledge of the mechanism(s) by which oxygen including  $O_2^*$  is made by the generator.

#### 7. Product Analysis of the CFS- $H_2O_2$ Reaction

Liquid phase static reaction studies in the CFS  $H_2O_2$  system were conducted to identify reaction products, to maximize molecular oxygen yield, and to establish overall stoichiometry. The  $H_2O_2$  reagent was assayed by titration with standard  $KMnO_4$  (Ref. 15) and found to range from 85-90%. A vacuum line was calibrated to enable quantitative measurement of gaseous products formed in small scale static experiments, which were conducted in an attached Teflon reactor tube. A weighed quantity of the assayed  $H_2O_2$  was placed in the reactor and a measured volume of CFS was condensed into the evacuated reactor tube at 77K. In the base catalyzed reaction, a weighed quantity of saturated NaOH was placed in the reactor beside the  $H_2O_2$ . Very small quantities were used, hence they formed a small drop inside the reactor. The reaction proceeded as the tube warmed from 77K to room temperature. After the reaction, molecular oxygen was measured by expansion into a known volume of the vacuum line with the reactor cooled to

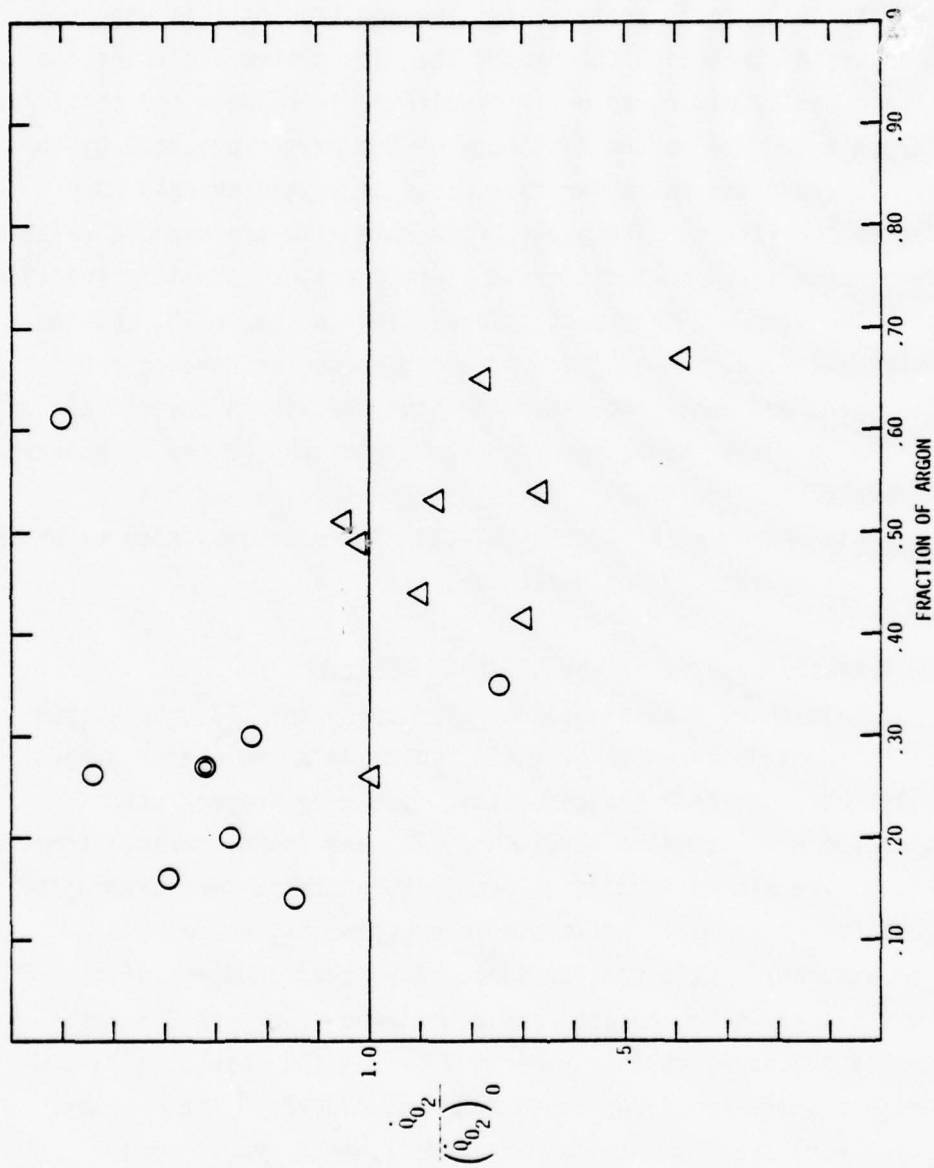


Figure 10. Variation of the  $O_2^*$  Molar Flow Rate vs the Fraction of Argon Gas Added to the Generator Stream. The  $\circ$  symbol refers to the single reactor configuration; the  $\Delta$  symbol to the dual reactor configuration.

77K. The remaining volatile components were separated by fractional condensation and were identified by vapor pressure measurements. For the uncatalyzed reaction, the products were fractionated through four Teflon U-traps cooled to 209, 175, 131 and 77K, respectively. For the base-catalyzed reaction the U-traps were 196, 131, and 77K.

The uncatalyzed reactions were run prior to the knowledge that the base was required to produce  $O_2^*$ . The results are reported here such that one might ascertain possible reaction mechanism on the initial CFS- $H_2O_2$  reaction. The results are presented in Table 7. Since water is carried with the  $H_2O_2$  reactant, a separate run was made with CFS and  $H_2O$  only. In the non-peroxide run, no oxygen was made; however, molecular chlorine was still produced. For the base catalyzed reaction, the reactants were proportioned as they were for optimum performance of the  $O_2^*$  generator, hence the large excess of both  $H_2O_2$  and  $H_2O$ . Note that in the static reaction experiment, very little molecular chlorine is produced. This result might be anticipated since the basic solution within the reactor would tend to react with any molecular chlorine produced. In the  $O_2^*$  generator operation, however, the relative amount of molecular chlorine, which is trapped in the 113K U-trap on the generator flow line, may be greater since the reaction is conducted in dynamic fashion.

TABLE 7. RESULTS OF CFS- $H_2O_2$  PRODUCT ANALYSIS

<u>Mole Ratio</u> <sup>a</sup>	<u>A</u>	<u>B</u>	<u>C</u>	<u>D</u>	<u>E</u> <sup>a</sup>
Reactants:					
CFS	1.00	1.00	1.00	1.00	1.00
$H_2O_2$	0.77	0.36	1.49	-	26.9
$H_2O$	0.27	0.13	0.50	0.31	20.0
NaOH			-	-	5.08
Products:					
$O_2$	0.53	0.16	0.53	-	1.00
$Cl_2$	0.73	0.48	1.18	0.34	.06

<sup>a</sup> Represents average results of two runs.

In all of the experiments trace quantities of other volatile gases were found. In the uncatalyzed reactions, trace quantities of HCl, ClO<sub>2</sub> and HF were tentatively identified. In the base catalyzed reactions, a trace amount of gas was found in the 196K trap. Unfortunately this amount of material was insufficient to make a vapor pressure identification.

## SECTION III

### QUENCHING STUDIES OF SINGLET MOLECULAR OXYGEN

Any major quenching of  $O_2^*(a^1\Delta)$  represents a severe limitation on the yield and hence the potential of the chemical  $O_2^*$  generator. From the discussion in Section C.2 of Section II, it appears that gas phase quenching between the reactor vessel and the 113K U-trap is not a significant problem. Surface quenching by the wetted salt surface in the annular regions of the reactor vessel, however, does represent a potential problem. A reactor dependent surface quenching experiment was done to assess the quenching of  $O_2^*$  by these surfaces.

The probability of gas phase quenching of  $O_2(b^1\Sigma)$  is typically several orders of magnitude greater than that for  $O_2^*(a^1\Delta)$ . Since  $O_2(b^1\Sigma)$  plays an important role in dissociating molecular iodine (reaction (3)) and keeping it dissociated, quenching studies of  $O_2(b^1\Sigma)$  were performed. The quenching rate constants for chlorine fluorosulfate (CFS), hydrogen fluoride, hydrogen chloride, hydrogen bromide, and molecular chlorines were determined.

#### A. Surface Quenching of $O_2^*$

##### 1. Experimental Details

The reactor vessel was modified to accept a constant stream of microwaved oxygen. The oxygen stream was injected into the entrance port of the reactor vessel via an Ultra-Torr "tee" adaptor. With this configuration the microwave oxygen and the  $O_2^*$  generator could be operated concurrently. The pressure at the entrance port was monitored by a Validyne inductance manometer. The oxygen flow rate was monitored by a Matheson rotameter calibrated for oxygen flow.

The fundamental emission of  $O_2^*$  at  $1.27 \mu\text{m}$  was monitored by an intrinsic germanium detector (Applied Detector Technology). Observation of

this emission circumvented the problems of  $\text{NO}_2^*$  emission interference in the dimol emission technique, so little effort was expended in removing oxygen atoms. A HgO ring was deposited downstream of the microwave cavity, but no checks on its effectiveness at removing O atoms were made. The germanium detector cooled to 77K was positioned  $\sim 170$  msec downstream of the 113K U-trap. The  $\text{O}_2^*$  emission was chopped and dispersed by an 1/8 m grating monochromator. The preamplified signal (part of the detector assembly from the manufacturer) was further amplified utilizing phase sensitive techniques. The pressure in the  $\text{O}_2^*$  emission region was monitored by an MKS Baratron capacitance manometer.

The oxygen stream was microwaved and entered the reaction vessel at a specified molar flow rate. This flow rate remained constant throughout the course of this experiment. The  $\text{O}_2^*$  emission signal was recorded. The  $\text{O}_2^*$  generator was operated for a set period of time in which salt deposits were formed in the annular region of the reactor vessel. The base catalyzed CFS- $\text{H}_2\text{O}_2$  reaction was stopped. Once the original downstream pressure was established verifying that no gas was being produced by the  $\text{O}_2^*$  generator, the  $\text{O}_2^*$  emission intensity was recorded. The  $\text{O}_2^*$  generator was then operated again, and the recording of pressures and  $\text{O}_2^*$  emission signals were repeated.

During the course of the experiment, the pressure in the microwave region increased due to the restricted flow in the region where the salt deposits were formed. The fractional yield of  $\text{O}_2^*$  produced by the microwave oxygen is a function of the total pressure in the microwave cavity. Hence a second experiment had to be conducted to factor out the fractional yield variations due to this pressure effect. In this second experiment the reactor vessel was replaced by a large bore (10 mm) stopcock. Variation in the opening of this stopcock changed the total pressure in the microwave cavity at a constant oxygen molar flow rate. The same flow rate was utilized for both quenching and pressure variation experiments.

## 2. Results

The results of the quenching experiment are presented in Table 8. For this experiment the molar flow rate of the microwaved oxygen was 0.4 mmol/s. The time reported in column one is not the real time but the accumulated O<sub>2</sub>\* generator "on" time. While the O<sub>2</sub>\* generator was operated, the O<sub>2</sub>\* emission signal increased due to the O<sub>2</sub>\* produced by the based catalyzed CFS-H<sub>2</sub>O<sub>2</sub> reaction. Although the fractional yield of the O<sub>2</sub>\* generator during this experiment was not absolutely determined, the results clearly indicated that the relative fractional yield of O<sub>2</sub>\* with the generator operating exceeded that of the microwaved oxygen alone. Thus the O<sub>2</sub>\* generator's performance is demonstrated to exceed that of the microwave methods.

In these experiments the reactor vessel was cooled to 196K. The O<sub>2</sub>\* emission signal decreased ~ 2% when the reactor was cooled. The U-trap was pre-cooled to 77K during which time the O<sub>2</sub>\* emission was totally quenched. When the 113K bath was positioned and the trap warmed to the new temperature, the O<sub>2</sub>\* emission increased. The signal strength, however, only returned to 60% of the original value. There appears to be a quenching effect of the 113K trap alone. (This quenching effect should be studied in greater detail.) Variations in the temperature of the 113K U-trap caused scatter in these experiments. Note that the value of the O<sub>2</sub>\* emission for the quenching experiment after 7 minutes of operation (see Table 8) exceeds the value that would be expected if no surface quenching occurred. This phenomena is attributed to the temperature fluctuations within the U-trap. It might be noted that during the O<sub>2</sub>\* generator operation, the isopentane slush bath (113K) was reconditioned periodically by additions of liquid nitrogen.

TABLE 8. RESULTS OF THE SURFACE QUENCHING

Time <sup>a</sup> (min)	Pressure at Entrance Port (torr)	O <sub>2</sub> * Signal Strength Relative Units	
		s <sup>b</sup>	s <sup>c</sup>
0	1.12	15.9	15.9
1	2.35	11.9	13.8
7	7.11	7.3	5.8
11	6.20	6.1	7.3

<sup>a</sup> The time reported is the accumulated time of the O<sub>2</sub>\* generator operation.

<sup>b</sup> The O<sub>2</sub>\* signal strength monitored during the quenching experiment.

<sup>c</sup> The O<sub>2</sub>\* signal strength without surface quenching normalized to the data presented in column 3.

The results of the surface quenching studies indicate that the salt surface, which is apparently necessary for the production of O<sub>2</sub>\*, is not a serious quencher of O<sub>2</sub>\*. After 11 mins of operation when the maximum amount of NaOH had been added, the percent quenched was ~ 17%. Although surface quenching is not serious, a study should be pursued to understand the role of this salt surface in producing O<sub>2</sub>\*. Clearly greater yields would be realized if the salt surface area were controlled to maximize production and minimize quenching of O<sub>2</sub>\*.

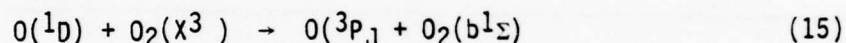
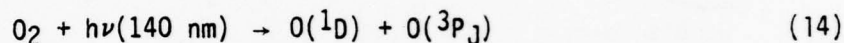
## B. Gas Phase Quenching of O<sub>2</sub>(b<sup>1</sup>Σ)

### 1. Experimental Apparatus

A flow tube technique was used to measure the quenching rate of O<sub>2</sub>(b<sup>1</sup>Σ). The O<sub>2</sub>(b<sup>1</sup>Σ) was prepared at some fixed position upstream and the b<sup>1</sup>Σ → x<sup>3</sup>Σ emission at 762 nm was monitored downstream. A quenching gas is added at various positions along the flow path and the decrease in the

$O_2(b^1\Sigma)$  emission was measured as a function of quenching gas concentration and distance travelled to the viewing port.

A flow tube similar in design to Izod and Wayne (Ref. 25) was constructed (see Figure 11). The major modification was the use of a slide tube to vary the injection point of the quenching gas. The vacuum uv photolysis of oxygen generates  $O_2(b^1\Sigma)$  in the following manner:



$O_2(a^1\Delta)$  is not produced in this fashion, and therefore the pooling reaction does not represent an additional factor which must be accounted for in the data analysis.

The low concentrations of  $O_2(b^1\Sigma)$  generated (typically  $\sim 10^8$  molecules/cm<sup>3</sup>), and the long lifetime of  $O_2(b^1\Sigma)$  (see Appendix B) required sensitive detection methods. The emission from the viewing region was dispersed by a 1/8 meter Oriel monochromator (f/3.7) and was focussed on to the sensitive element in a GaAs photomultiplier tube. Photon counting was employed as described in Section II.

Flow rates of the oxygen and quenching gas were calibrated using the pressure rise technique. The quenching gas flow rate was set by recording the pressure rise in the flowing  $O_2$  stream. The  $O_2$  flow was stopped, and the residual quenching gas flow was calibrated. Plots of the quenching gas pressure rise vs. the actual partial pressure (calculated by the ratioing of the respective flow rates and multiplying by the total pressure monitored by

25. T. P. J. Izod and R. P. Wayne, "The Formation Reaction, and Deactivation of  $O_2(^1 +g)$ ," Proc. Roy. Soc. A308, 81 (1978).

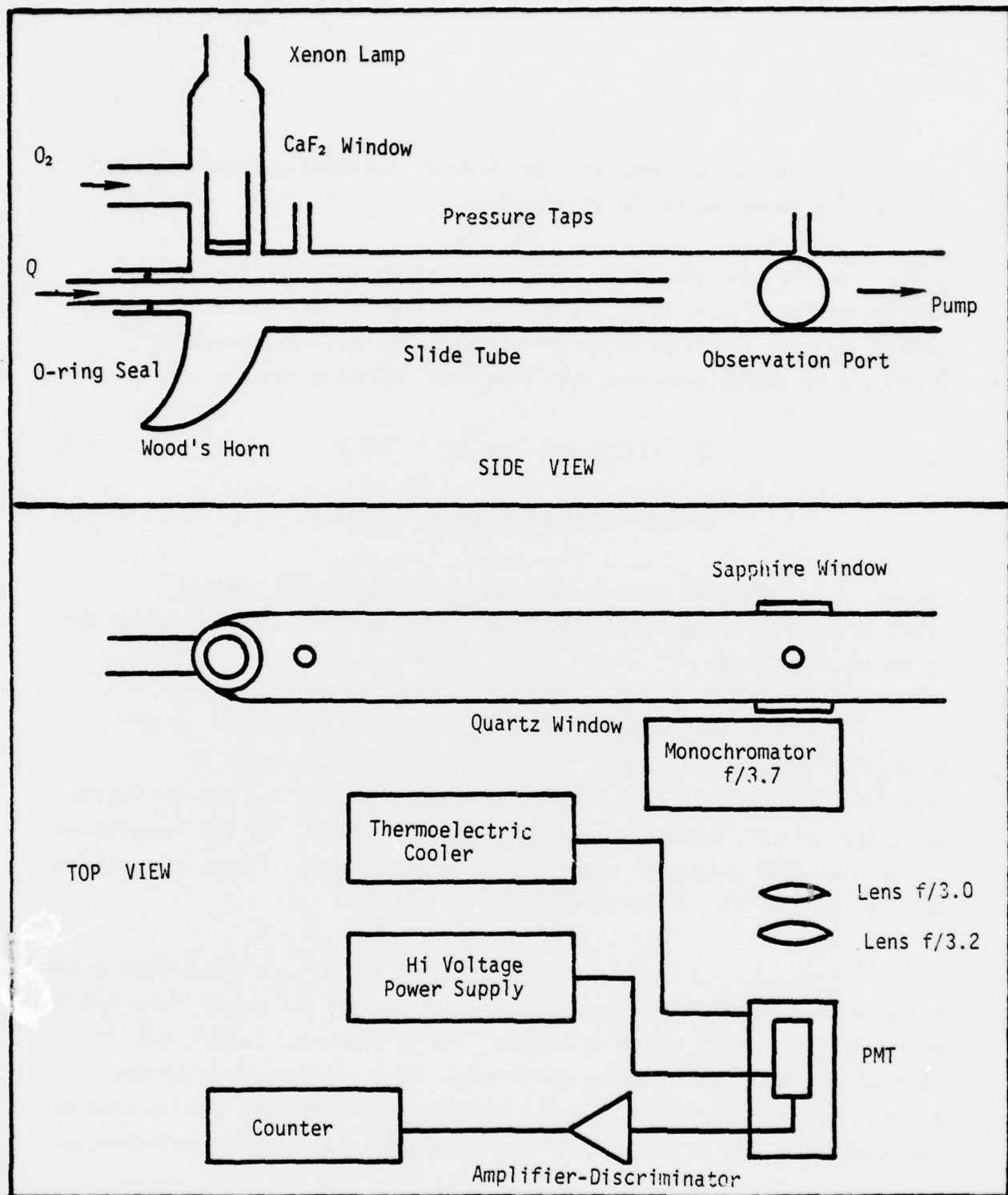


Figure 11. Schematic of the  $O_2(^1\Sigma)$  Quenching Experiments. Q is the quenching gas. PMT is the RCA 31034 GaAs photomultiplier tube. The photon counting system is the same as that employed in the  $O_2^*(a^1\Delta)$  monitor.

an MKS Baratron capacitance manometer) were determined. Hence for a given pressure rise the partial pressure of the quenching gas was known. This method works only for a constant  $O_2$  flow rate and total pressure. The partial pressure of the quenching gas was always less than 4% of the total pressure. The wall quenching phenomena for  $O_2(^1\Sigma)$  was probably diffusion controlled since nearly identical conditions were employed as those of Izod and Wayne. The pressure rise, therefore, did not significantly change the diffusion rate to the walls in the flow tube.

Oxygen (UHP, Matheson, 99.9999%) and  $Cl_2$  (Matheson) were used without further purification. Commercial anhydrous HF (Matheson) was dried by fluorination at 100 psi and distilled in vacuo into a passivated stainless steel cylinder. HBr (Matheson, 99.8%) was purified by fractional condensation in a flowing line and collected in a stainless steel cylinder. Chlorine fluorosulfate was prepared in the same manner described in Section II. Electronic grade HCl (Matheson, 99.99%) was transferred under vacuum to a stainless steel cylinder.

## 2. Data Analysis

The following analysis has been applied to the quenching of  $O_2(^1\Sigma)$ . The initial production of  $O_2(^1\Sigma)$  at a given flow rate of  $O_2$  and microwave lamp power was found to be constant. The  $O_2(^1\Sigma)$  at the viewing port is related to that initially produced as follows,

$$[O_2(^1\Sigma)] = [O_2(^1\Sigma)_0] e^{-k'(\ell-s)/v} e^{-ks/v} \quad (16)$$

where  $\ell$  is the distance between the lamp and the viewing port, and  $s$  is the distance between the end of the slide tube and the viewing port. The quenching rates are defined as follows,

$$k' = k_w' + k_{O_2} [O_2] + \sum k_T [T] \quad (17)$$

$$k = k_w + k_{O_2} [O_2] + \sum k_T [T] + k_Q [Q] \quad (18)$$

where  $k'_w$  and  $k_w$  are the wall deactivation rates in the slide tube region and the nonslide tube region, respectively.  $k_{O_2}$ ,  $k_T$ , and  $k_Q$  are the quenching rate constants for  $O_2$ , trace impurity gas, and the specific quenching gas. The flow velocity,  $v$ , is assumed constant down the entire flow tube. The pressure was constant to within 10% along the length of the flow path.

Taking the logarithm of equation (6) we obtain the following relationship,

$$\ln [O_2(^1\Sigma)] = A - (k-k')s/v \quad (19)$$

Hence a plot of  $\ln O_2(^1\Sigma)$  vs.  $s/v$  yields a linear relationship with a negative slope of  $(k-k')$ . Note, that

$$\kappa = (k-k') = (k_w - k'_w) + k_Q [Q] \quad (20)$$

Plots of  $\kappa$  vs.  $[Q]$  yield a slope equal to the quenching rate constant,  $k_Q$ .

The wall quenching effect of the variable positioned slide tube was not constant from one run to the next. For each data run, therefore, the wall quenching efficiency of the slide tube had to be measured. The following procedure was employed in taking the data:

1. Background count rates ( $\sim 120$  Hz) were obtained with no  $O_2$  flowing pass the photolysis zone.
2. The  $O_2$  flow was established (4 liter/min,  $2 \times 10^3$  cm/sec at a pressure of 5 torr) and the intensity of  $O_2(^1\Sigma)$  measured. The count rates were typically  $\sim 1000$  Hz.
3. The quenching gas was added with the slide tube fully inside the flow tube, and the pressure rise due to the presence of the quenching gas recorded.

4. The slide tube was sequentially moved back away from the viewing port, and the count rate determined at a minimum of 3 points along an 18 cm length.

5. The quenching gas was then turned off, and the count rate determined again. This count rate reflects the absence of both the slide tube and quenching gas.

6. The  $O_2$  flow was stopped and the background count rate was checked against the original determination (in all cases the difference was less than 20%).

The count rate for each data point was adjusted for the background and the  $\ln(O_2(1\Sigma)$  intensity) vs. the slide tube position was plotted. A typical data run is presented in Figure 12. The two data points taken without the presence of the quenching gas determine the quenching effect of the slide tube, and the rest include both the effects of the slide tube and quenching gas. Hence,

$$\kappa = \text{slope of slide tube only} - \text{slope of slide tube and quenching gas} \quad (21)$$

All data were multiplied by the linear flow velocity to convert quenching data from  $\text{cm}^{-1}$  to  $\text{sec}^{-1}$ .

Several runs were made with no quenching gas to determine the linearity of the quenching due to the slide tube. In all cases the plot of  $\ln(\text{Emission Intensity})$  vs. slide tube position (with no quenching gas) was linear, thus confirming the first order effect of the slide tube. A representative plot is given in Figure 13. Another check on the data analysis is to determine the  $O_2(1\Sigma)$  count rate under identical conditions for each experiment. When the slide tube is fully pulled back and no quenching gases are present, the count rate was nearly constant ( $\sim 2.9\text{KHz}$ ).

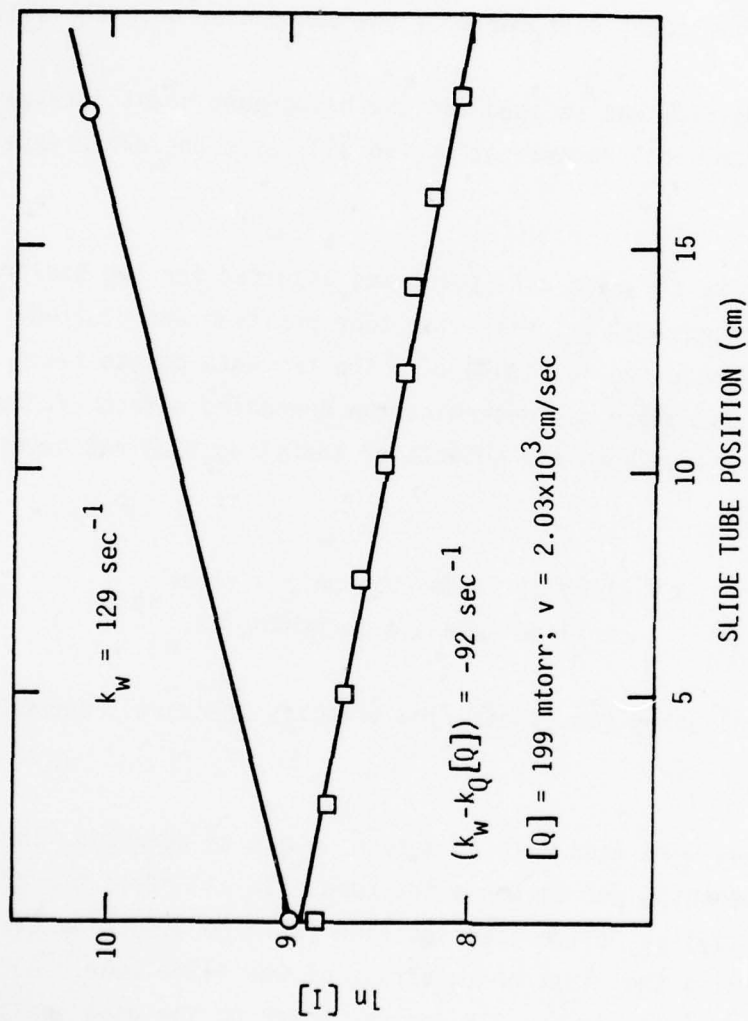


Fig. 12  $\ln[I]$  vs. Slide Position for the Quenching of  $O_2(^1\Sigma)$  by 199 mtorr of HCl. (□) is the data obtained in the presence of HCl. (O) is the data obtained without the presence of HCl, hence showing the effect of the slide tube.

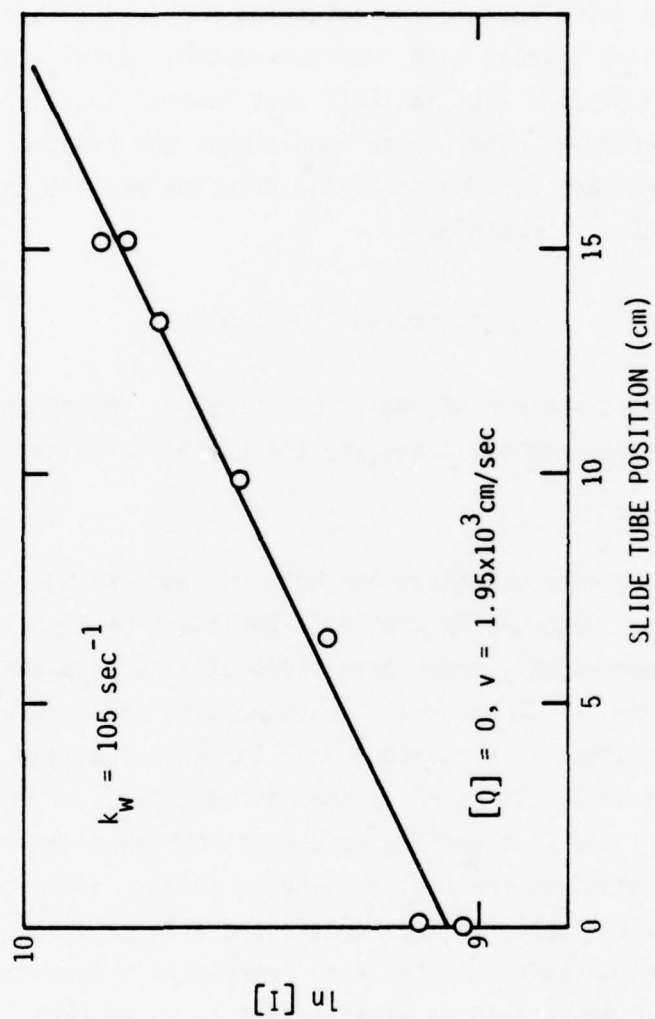


Fig. 13 Typical Plot of  $\ln[I]$  vs. Slide Tube Position without any Quenching Gas.

### 3. Results

These decay rates,  $K_Q[Q]$ , are plotted against the partial pressure of the quenching gas (see Figures 14, 15 and 16). The slopes of these plots yield the value  $K_Q$ , and the intercept should intersect zero since the wall quenching effects have been subtracted. A calculation of the Reynolds number ( $Re = Dvp/\mu < 250$ ) indicate that laminar flow is fully developed in our apparatus. Under these conditions, the kinetic rate constant must be adjusted to account for the parabolic velocity profile across the flow tube diameter (Ref. 26). Therefore,

$$k_q \text{ (corrected)} = 1.6 k_Q \quad (22)$$

The quenching rate constants for HF, HBr, HCl, ClO<sub>2</sub>F, and chlorine are given in Table 9. These rate constants are the corrected values for laminar flow.

The quenching rate constants for both HCl and HBr agree well with the literature values. Chlorine is the least efficient of all the quenchers. The quenching was observed only under conditions of slow flow and relatively large Cl<sub>2</sub> concentrations (~300 mtorr). Hence no plot of reciprocal decay times vs. Cl<sub>2</sub> concentration is presented; only the rate constant at 300 mtorr. Quenching of O<sub>2</sub>(<sup>1</sup>Σ) by HF is the most efficient of the quenchers. To measure the HF quenching rate constant, very small amounts of HF (~20 mtorr) were added to the fast flowing O<sub>2</sub> stream. Unfortunately, the HF partial pressure fluctuated and represented a large error in the data. The HF quenching rate constant reported here represents a lower bound to the value. In general, HF appears to be as efficient as water (Ref. 27),  
 $k_{H_2O} = 2 \times 10^{-12} \text{ cm}^3 \text{ molec}^{-1} \text{ sec}^{-1}$ .

26. C. L. Lin and F. Kaufman, "Reactions of Metastable Nitrogen Atoms," J. Chem. Phys. 55, 3760 (1971).  
27. S. J. Arnold, M. Kulo, and E. A. Ogryzlo, Advan. Chem. Ser. 77, 133 (1969).

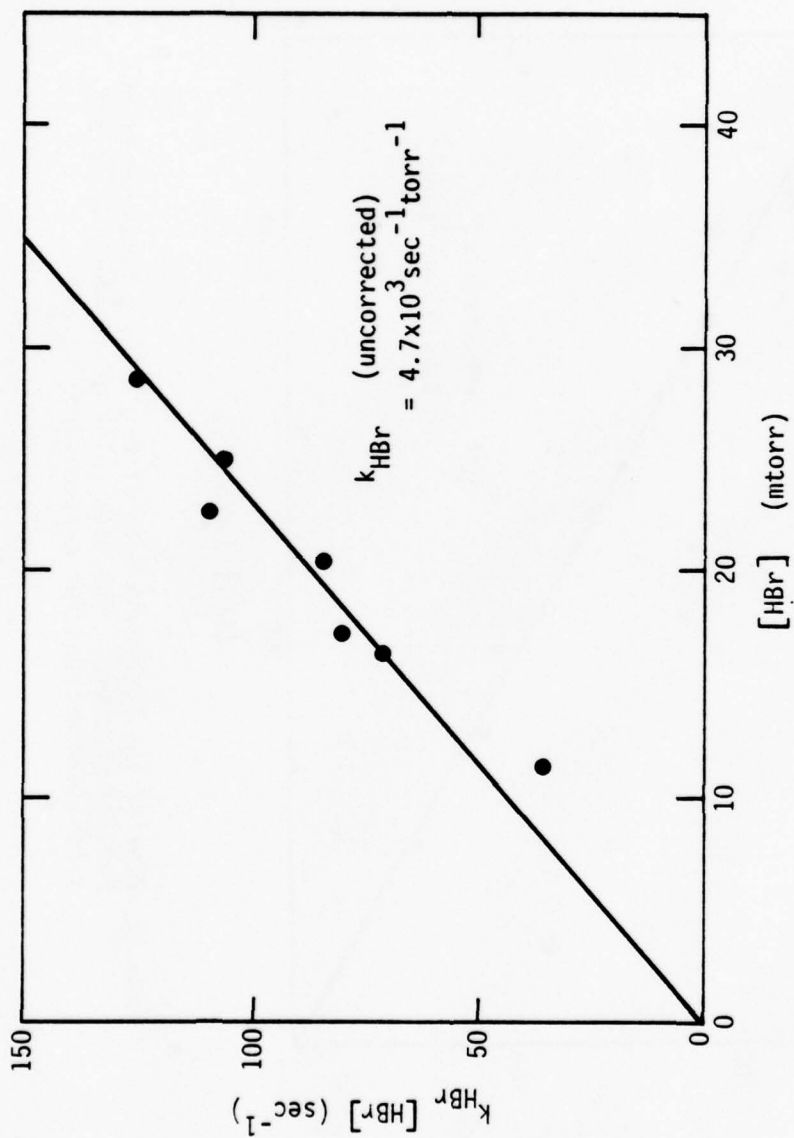


Fig. 14 Plot of the Quenching Rate of  $\text{O}_2(^1\Sigma)$  as a Function of HBr Partial Pressure.

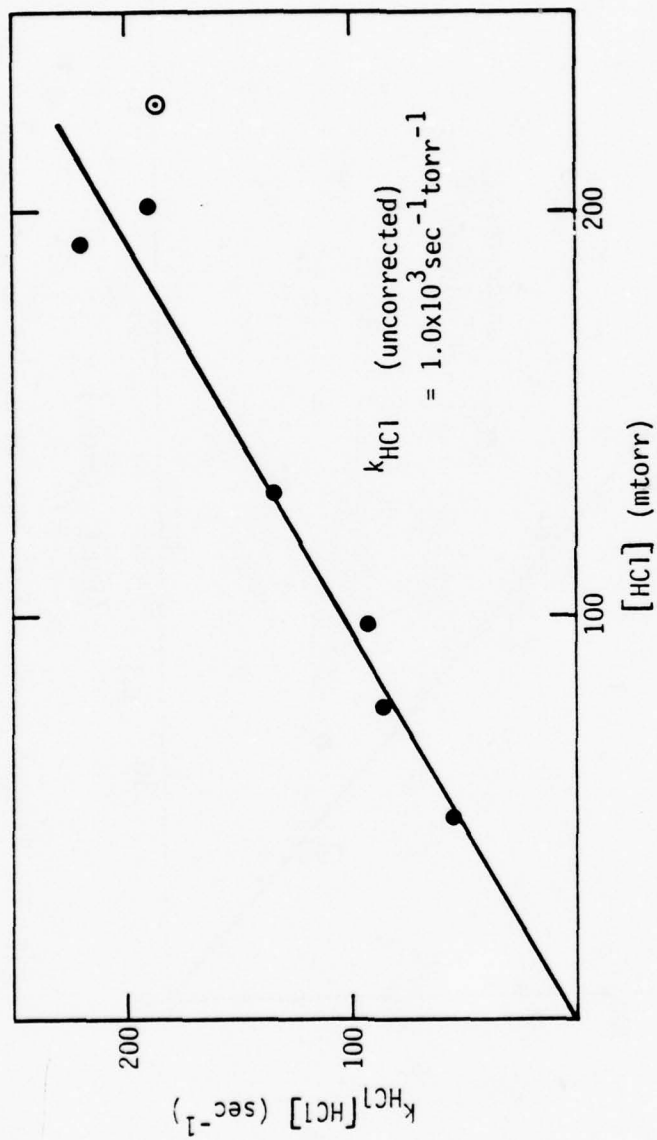


Fig. 15 Plot of the Quenching Rate of  $\text{O}_2(\Sigma)$  as a Function of HCl Partial Pressure. The data point designated ( $\theta$ ) is not taken into account for determining,  $k_{\text{HCl}}$ .

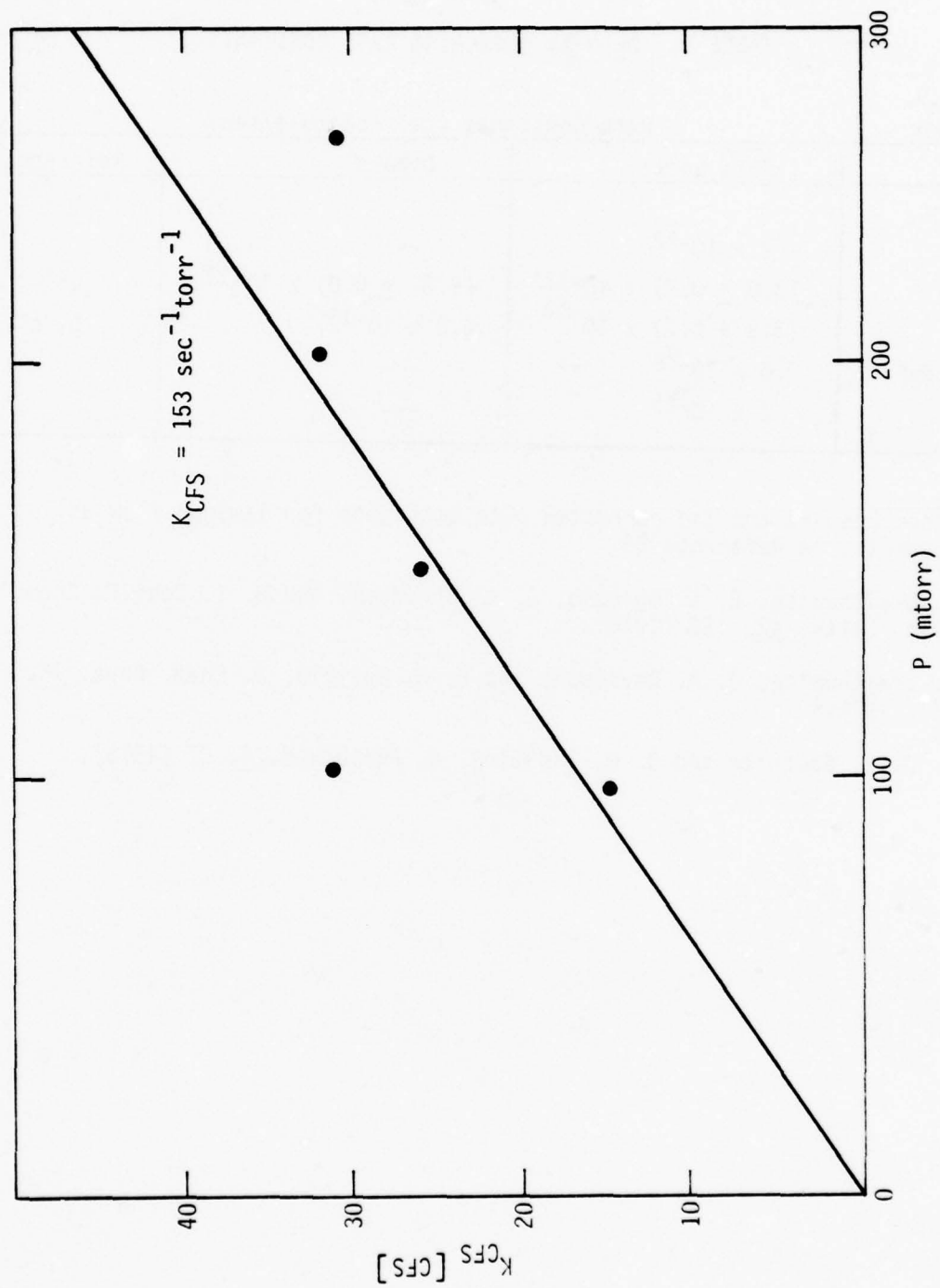


Figure 16. Plot of the Quenching Rate of  $O_2(^1\Sigma)$  as a Function of the Chlorine Fluorosulfate Partial Pressure.

TABLE 9.  $O_2(b^1\Sigma)$  QUENCHING RATE CONSTANTS

Quencher	Rate Constants ( $cm^3/molecule/sec$ )		
	This work*	Others	Reference
HF	$2 \times 10^{-12}$	---	
HBr	$(3.0 \pm 0.7) \times 10^{-13}$	$(3.8 \pm 0.8) \times 10^{-13}$	a
HCl	$(5.3 \pm 0.7) \times 10^{-14}$	$4.2 \times 10^{-13}$	b, c
$ClOSO_2F$	$7.6 \times 10^{-15}$	---	
$Cl_2$	$2 \times 10^{-15}$	---	

\* These results are the corrected rate constants for laminar flow as suggested in Reference 29.

- a. M. Braithwaite, E. A. Ogryzlo, J. A. Davidson, and H. I. Schiff, Chem. Phys. Letts. 42, 158 (1976).
- b. M. Braithwaite, J. A. Davidson, and E. A. Ogryzlo, J. Chem. Phys. 75, 771 (1976.)
- c. M. J. E. Gauthier and D. R. Snelling, J. Photochem. 4, 27 (1975).

## SECTION IV

### THE $O_2(a^1\Delta)$ - $I_2$ SYSTEM

The  $O_2^*(a^1\Delta)$  generator was evaluated in terms of creating a population inversion between the spin-orbit states of atomic iodine. Typically, the fraction of  $O_2^*$  produced by the chemical generator was 30-50%. Only 15% is required to produce a zero population inversion, i.e., threshold. Whether or not an atomic iodine laser can be constructed with this generator depends on several factors. The rate of production of the oxygen stream and its absolute concentration of  $O_2^*$  must be sufficient not only to create a population inversion but also to establish a significant inversion density and maintain that inversion density for a long enough period to establish enough gain to overcome the optical losses of a mirrored cavity.

Three techniques were developed to evaluate the  $O_2^*-I_2$  system. They were:

1. Zero Gain Experiments. The object of this experiment was to measure the gain (loss) over a length of the  $O_2-I_2$  flow.
2. Optical Double Resonance Experiments. The goal of this experiment was to confirm the creation of a population inversion and to evaluate the population inversion density.
3. Laser Tests. In these experiments an optical cavity was positioned around the suspected gain region, and evidence of lasing was sought.

#### A. Experimental Apparatus

##### 1. Flow System

Molecular iodine was injected into the oxygen stream from the  $O_2^*$  generator via a moveable slide tube. The mixture of  $O_2^*$  ( $O_2$ ) and  $I_2$  then entered a test cell which was within an optical cavity. The

length of flow within the optical cavity was 65 cm from entrance port to exit port. The pressure was measured at these two ports to determine the pressure gradient along this section of flow. The pressure gradient vs. molar flow rate is presented in Figure 9 (P6 and P7 refer to these two pressure taps). A schematic of the apparatus is shown in Figure 17. The flow section within the optical cavity was initially made of square Pyrex tubing which was replaced by square quartz tubing for the optical double resonance experiments described later. The inner walls of the flow tube from the 113K trap to the exit port of the test cell were coated with Halocarbon wax to reduce atomic iodine recombination at the walls (Ref. 28).

The ends of the square tubing were mounted in Jriel optical mounts via Ultra-Torr fittings. This o-ring fitting permitted small angle tuning without stressing the tubing. The fitting also had an O-ring seal at the ends to attach a combination of either dielectrically coated mirror or optical flats depending upon which experiment was conducted. Argon purge gas was flowed through these end fittings to protect the coating from chemical attack and sweep out any "dead" gas from the  $O_2^*-I_2$  reaction system. The Ar purge flow represented less than ten percent of the total flow rate. The flow velocities were typically 500 cm/sec in the iodine injection region and 2000 cm/sec along the square flow tube.

## 2. Calibration of the Absolute $I_2$ Concentration

Molecular iodine was injected into the products of the  $O_2^*$  generator via an argon carrier gas. The flow rate of argon was monitored by a Matheson rotameter which was calibrated for the argon flow. The argon was metered into a bed of  $I_2$  crystals. The pressure of argon in the  $I_2$  bed was monitored by a Validyne inductance manometer. The argon- $I_2$  flow was

28. R. B. Badachlape, P. Mamarchik, A. P. Convoy, G. P. Glass, and J. L. Margrove, "Preparation of Nonreactive Surfaces for Reaction-Rate Studies," *Int. J. Chem. Kinetics* 8, 23 (1976).

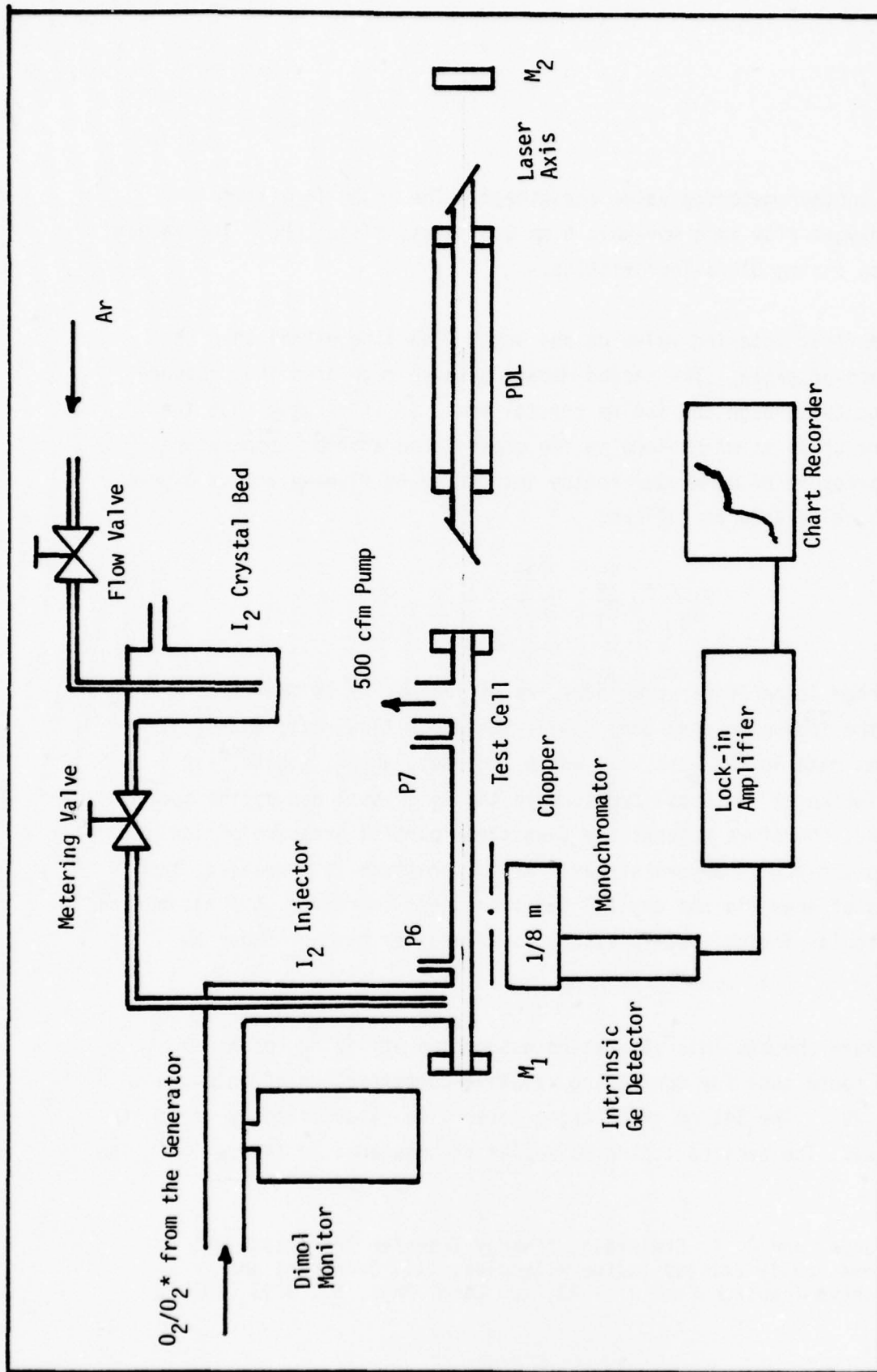


Figure 17. Schematic for  $O_2^*-I_2$  Experiments. The PDL is a pulsed discharge photodissociation  $I^*$  laser. P6 and P7 are pressure monitoring ports; the pressure vs. molar flow rate data are given in fig. 9.  $M_1$  and  $M_2$  are dielectrically coated mirrors (maximum reflectivity at  $1.32 \mu m$ ) and form the laser optical cavity. The chopper, monochromator, and germanium detector are mounted on a moveable platform; thus the fluorescence can be monitored along the test cell.

regulated by another metering valve downstream. The argon-I<sub>2</sub> mixture entered the oxygen flow in a moveable 6 mm O.D. glass slide tube. The vacuum seal was by an o-ring Ultra-Torr fitting.

The first metering valve on the argon flow line established the total flow rate of argon. The second metering valve regulated the pressure and flow velocity through the iodine crystal bed. If it assumed that the vapor pressure of I<sub>2</sub> is maintained in the crystal bed at room temperature, the partial pressure of molecular iodine introduced to flowing active oxygen stream can be calculated as follows:

$$P_{I_2} = \frac{P_v}{P_T} \frac{F_{Ar}}{F_T} \quad (23)$$

where  $P_v$  is room temperature vapor pressure of iodine,  $P_T$  is the total pressure in the iodine crystal bed,  $F_{Ar}$  is the argon flow rate, and  $F_T$  is the total flow rate in the test cell which includes, argon, iodine, and oxygen. Variation of the total pressure in the I<sub>2</sub> crystal bed by the second metering valve, therefore adjusts the downstream partial pressure of iodine injected into the active oxygen stream. As the pressure is decreased, the flow velocity of argon in the crystal bed increases; therefore, the assumption that the molecular iodine vapor pressure is maintained may no longer be valid.

We have checked this saturation assumption utilizing resonance fluorescence techniques for monitoring relative concentration of molecular iodine (Ref. 29). The 541 nm green argon laser line is absorbed by molecular iodine ( $B \leftarrow X$ ). The excited iodine molecules fluorescence in the yellow. The

29. R. B. Kurzel and J. I. Steinfeld, "Energy Transfer Processes in Monochromatically Excited Iodine Molecules, III. Quenching and Multiquantum Transfer from  $v' = 43$ ," J. Chem. Phys. 53, 3293 (1970).

intensity of this yellow emission increases as the concentration of molecular iodine increases. Using this principle, we have determined the concentration of molecular iodine when flowing with the argon carrier gas.

A resonant fluorescence cell was positioned downstream of the second metering valve. A 541 nm line of a cw argon laser was beamed into the cell. The yellow fluorescence was viewed at right angles by a 1P28 photomultiplier tube (PMT). Between the cell and the PMT was a filter (Oriel, 7-772-5400). Attached to the fluorescence cell was a side arm containing a few crystals of iodine.

Two experiments were conducted. The first monitored the resonance fluorescence signal in the closed evacuated fluorescence cell as the iodine pressure was varied by thermostating the side arm from 0C to 19C. A plot of the relative fluorescence signal vs. the partial pressure of molecular iodine, as determined by temperature dependent vapor pressure data (Ref. 30), is given in Figure 18. Note that a linear relationship is not observed due to significant effects of self-absorption (Ref. 29). The argon beam was approximately 1 cm from the viewing window. In the second experiment, the side arm was closed and the cell was attached to the injector tube on the large capacity flow line. Argon was flowed through the iodine crystal bed, through the second metering valve, and through the fluorescence cell. The relative fluorescence signal was monitored as a function of the total pressure in the iodine crystal bed. The fraction of molecular iodine in the flowing argon stream was compared against the fraction that would be found by applying Eq. (23). These two fractions plotted against each other are presented in Figure 19. Only at the fastest flow velocities encountered in this study does the fraction of molecular iodine significantly fall below the saturating values. The maximum deviation being ~17% less. For most flow velocities, the assumption that molecular iodine is saturating the argon flow is valid.

30. L. GiltEspie and L. Fraser, "The Normal Vapor Pressure of Crystalline Iodine," J. Am. Chem. Soc. 58, 2260 (1936).

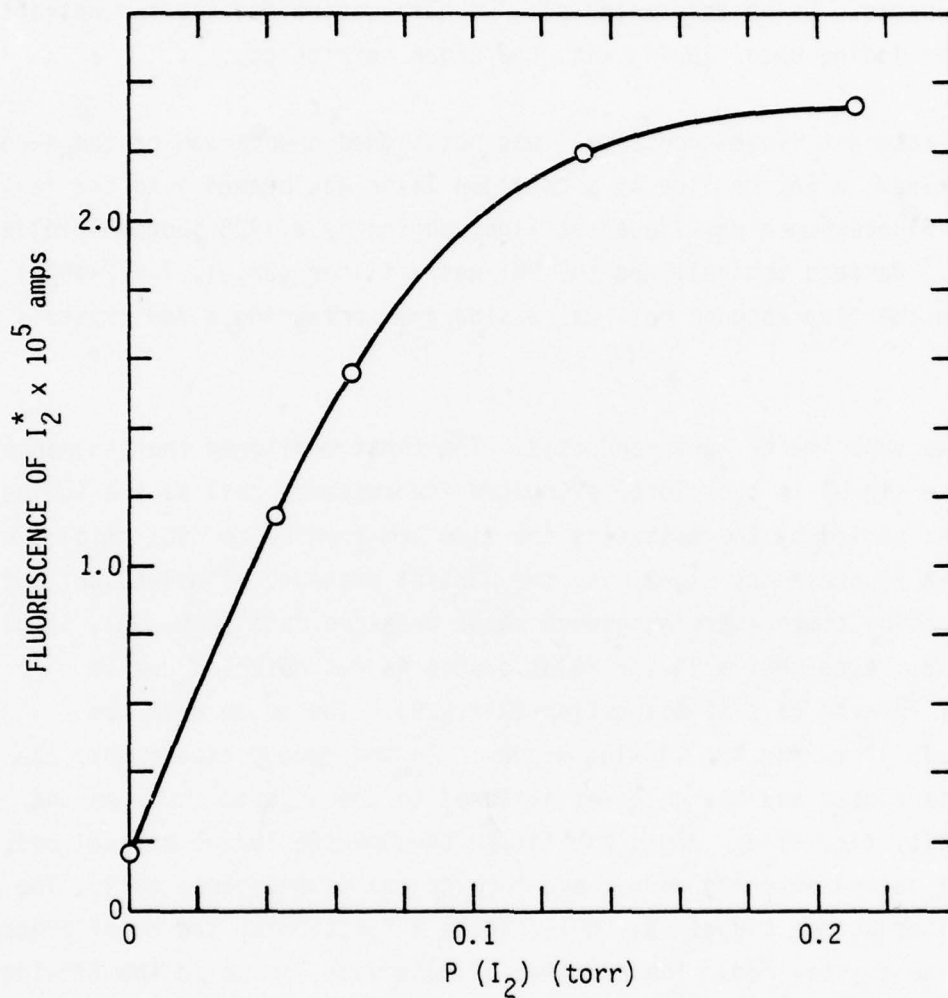


Figure 18. I<sub>2</sub> Resonant Fluorescence ( $B^3\Pi_0+ \rightarrow X^1\Sigma^+$ ) Signal Strength vs. Pressure of Molecular Iodine. The deviation from linearity is due to self-absorption.

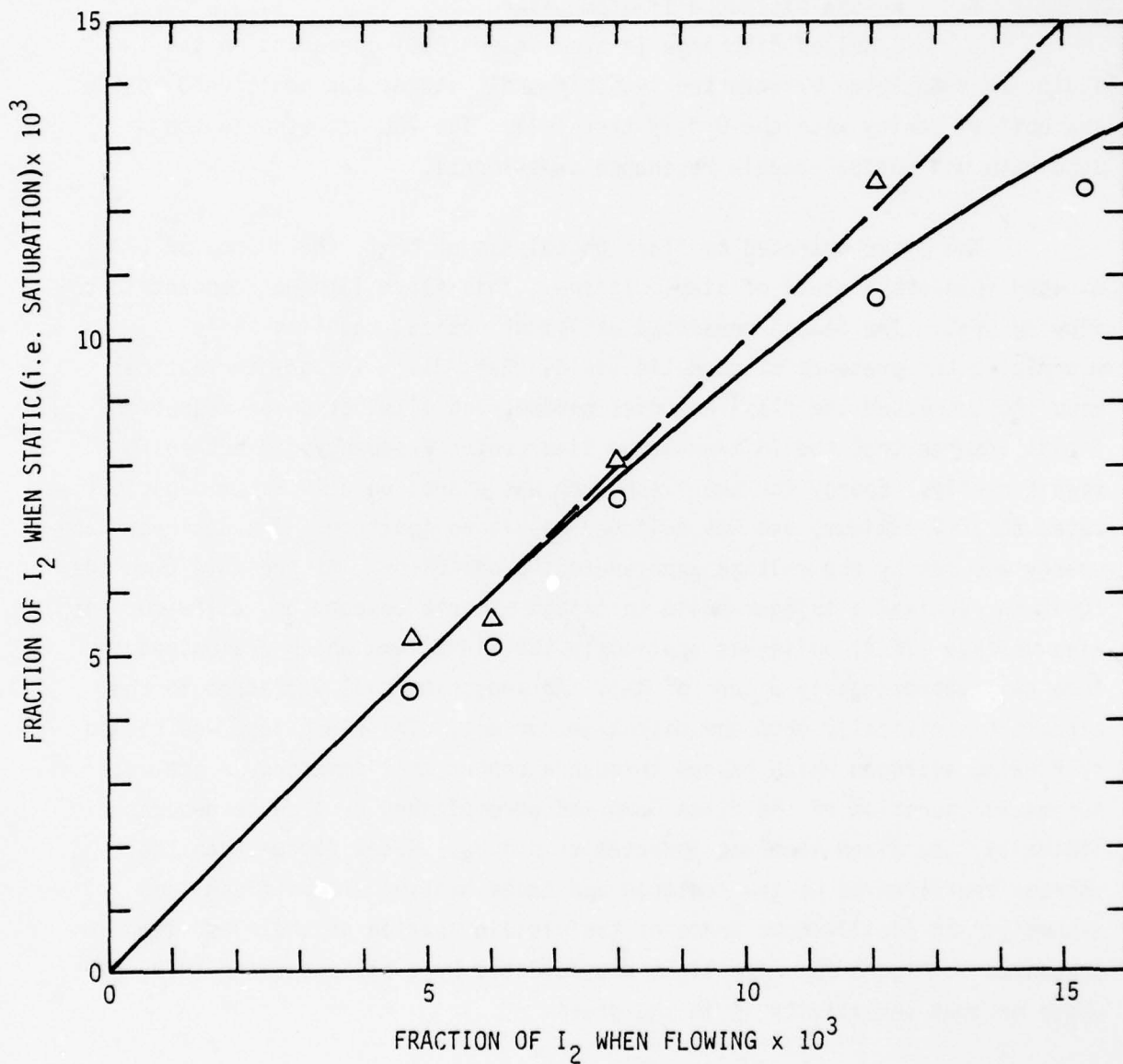


Figure 19. Fraction of I<sub>2</sub> in the Flowing Argon Carrier Gas vs. That for Static Conditions. The two symbols refer to data taken on separate days.

### 3. Pulsed Discharge I\*-atom Laser

A pulsed discharge I\* atom laser (PDL) operating on the 1.315  $\mu\text{m}$  transition between the two spin-orbit states was positioned inside the optical cavity with the  $\text{O}_2^*\text{-I}_2$  test cell. The PDL was used in the zero gain and optical double resonance experiments.

The laser operated by flash photolysis of  $\text{CF}_3\text{I}$ , the source of (PDL) excited spin-orbit state of atomic iodine. This flash lamp was concentric to flowing  $\text{CF}_3\text{I}$ . The design permitted efficient optical coupling while minimizing the presence of magnetic fields (Ref. 31). The greater optical coupling decreased the flash energies needed, and elimination of magnetic fields insured that the I\* transition line center frequency did not shift significantly. Energy for the flash lamp was stored on a 14.2  $\mu\text{f}$  capacitor rated at 20KV maximum, and was switched on via an ignitron. The desired flash energy was set by the voltage applied to the capacitor. At the same time the ignitron received a trigger pulse to switch it into conduction, a low current high-voltage (77KV) pulse was applied to the flash lamp which preionized the lamp gas (approximately 8 torr of Xe). An induction coil was added to the circuit to critically damp the discharge current. The flash lamp was cooled by flowing nitrogen which passed through a copper coil immersed in ice water. Automatic operation of the flash lamp was accomplished by a pulse generator. Typically, the flash lamp was operated at 0.1 Hz. Rates faster than these shorten the lifetime of the ignitron and cause heating of the flash lamp assembly. An oscilloscope trace of the visible portion of the flash lamp is presented in Figure 20. The light was detected by a silicon wafer (UTD, PIN5) whose maximum sensitivity is in the green.

The cavity of the pulsed laser was formed by two 99.8% reflecting dielectric mirrors; one was a 1" dia. flat, the other a 1" dia. with a 2m

31. W. C. Hwang and J. V. Kasper, "Zeeman Effects in the Hyperfine Structure of Atomic Iodine Photodissociation Laser Emission," Chem. Phys. Letts. 13, 507 (1972).

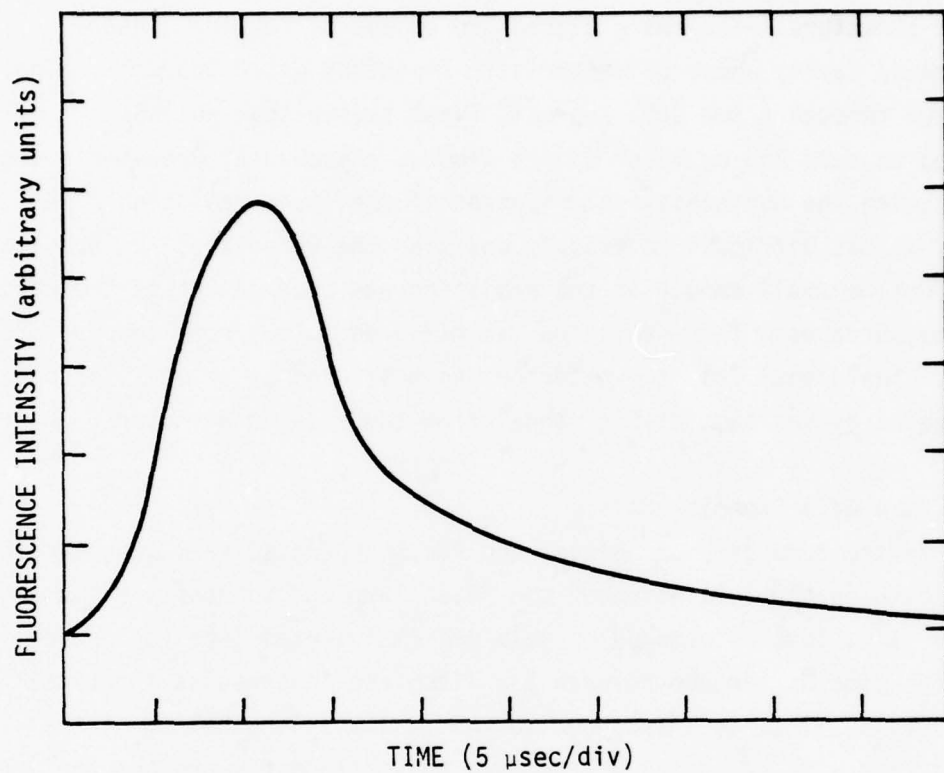


Fig. 20 Reproduction of Oscilloscope Trace of the Visible Portion of the Flashlamp. The stored energy was 500 joules. The detector was a silicon wafer (UTD, PIN5) whose maximum sensitivity is in the green.

radius of curvature. They were placed 160 cm apart, forming a near hemispherical cavity whose characteristic frequency was  $0.003 \text{ cm}^{-1}$ . The  $\text{CF}_3\text{I}$  flowed through a 9mm O.D. Suprasil fused silica tube which was terminated at each end by fused silica windows attached at Brewster's angle, hence favoring the horizontal polarization of the laser radiation. In practice, it was difficult to exactly position the windows at the Brewster angle. Thus, a small amount of the radiation was coupled out of the cavity at the window surfaces. This radiation was mirrored into a room temperature InSb detector. The signal from the detector was monitored by an oscilloscope which was triggered by the fast rising signal from the silicon detector.

#### B. Zero Gain Experiments

In the zero gain technique, the PDL is operated very near threshold. The time between the initiation of the flash lamp and the onset of lasing is measured. If a loss is removed or gain medium inserted into the optical cavity, the time difference between the flash and laser pulse shortens. Conversely, if a loss is introduced to the cavity a lengthening of the threshold time will be observed. We used this method for probing the length of the  $\text{O}_2^* \text{I}_2$  test cell. This technique tested the integrated gain (or loss) along the length of flow.

The sensitivity of this technique relied upon the time stability of the PDL. Approximately 2.5 torr of  $\text{CF}_3\text{I}$  and 100-200 torr of argon were photolyzed by the flash lamp whose stored energy was 450-600 joules (i.e.,  $7.5\text{-}10 \text{ joules cm}^{-1}$ ). The addition of the argon prevented the  $\text{CF}_3\text{I}$  from pyrolyzing and broadened the spin-orbit transition line width. There were eleven translational modes which are between the half maximum points of the broadened transition line width.

The zero gain technique was calibrated by inserting a known loss within the optical cavity of the PDL. This known loss was a thin quartz plate (infrasil) placed in an Oriel optical mount which itself sat on a rotation

stage. The Brewster windows on the PDL favors lasing on the horizontal polarization. The rotation of this optical flat from normal incidence of the laser beam to Brewsters angle at  $55.56^\circ$  reduces the single surface reflection loss from 4% to 0%. A plot of the horizontal polarization reflection loss per surface of quartz for  $1.315 \mu\text{m}$  radiation vs. the angle of incidence is given in Figure 21. The PDL was operated near threshold by varying the energy deposited into the flash lamps. A plot of threshold times to lasing vs. the round trip cavity losses due to the insertion of the quartz flat is presented in Figure 22. From this plot the zero gain technique is sensitive to approximately 1% variation in the round trip pass of the laser.

Zero gain experiments were conducted for both single and dual reactor configurations (see Section III). As molecular iodine was added to the flow system utilizing the single generator, losses were always detected once the concentration of molecular iodine exceeded  $\sim 2.5$  mtorr. However, when the dual reactor configuration was utilized, several runs in which the performance of the reactors were optimized equivalent amounts of added molecular iodine did not show any losses in the cavity. On the other hand, no observation of gain over the full length of the test cell was found. Based upon the calibration work the gain did not exceed 1%. These results were later confirmed by employing the optical double resonance experiment reported in the next section.

The line width of atomic iodine for the  $1.315 \mu\text{m}$  transition in the  $\text{O}_2^*-\text{I}_2$  test cell was governed by its Doppler width of  $0.086 \text{ cm}^{-1}$  (FWHM). Since the PDL laser transition was pressure broadened to enhance stable operation, some of the laser lines may not overlap significantly with the narrower Doppler line exhibited in the test cell. The net result would be a decrease in the sensitivity of the zero-gain technique.

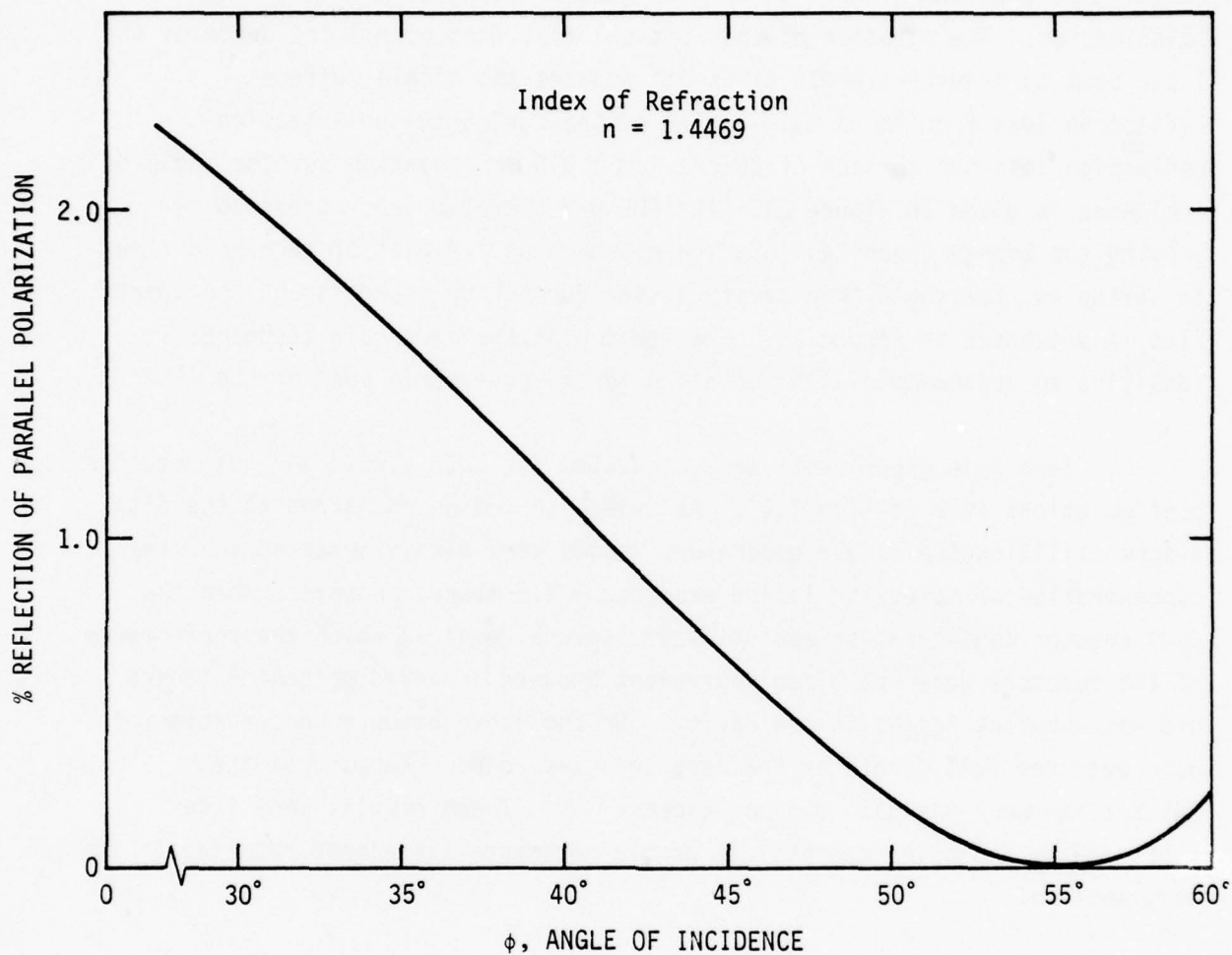


Fig. 21 Parallel Polarization Reflection Losses at the Window Surface (index of refraction = 1.4469) vs. Angle of Incidence. Brewster's Angle is 55.65°.

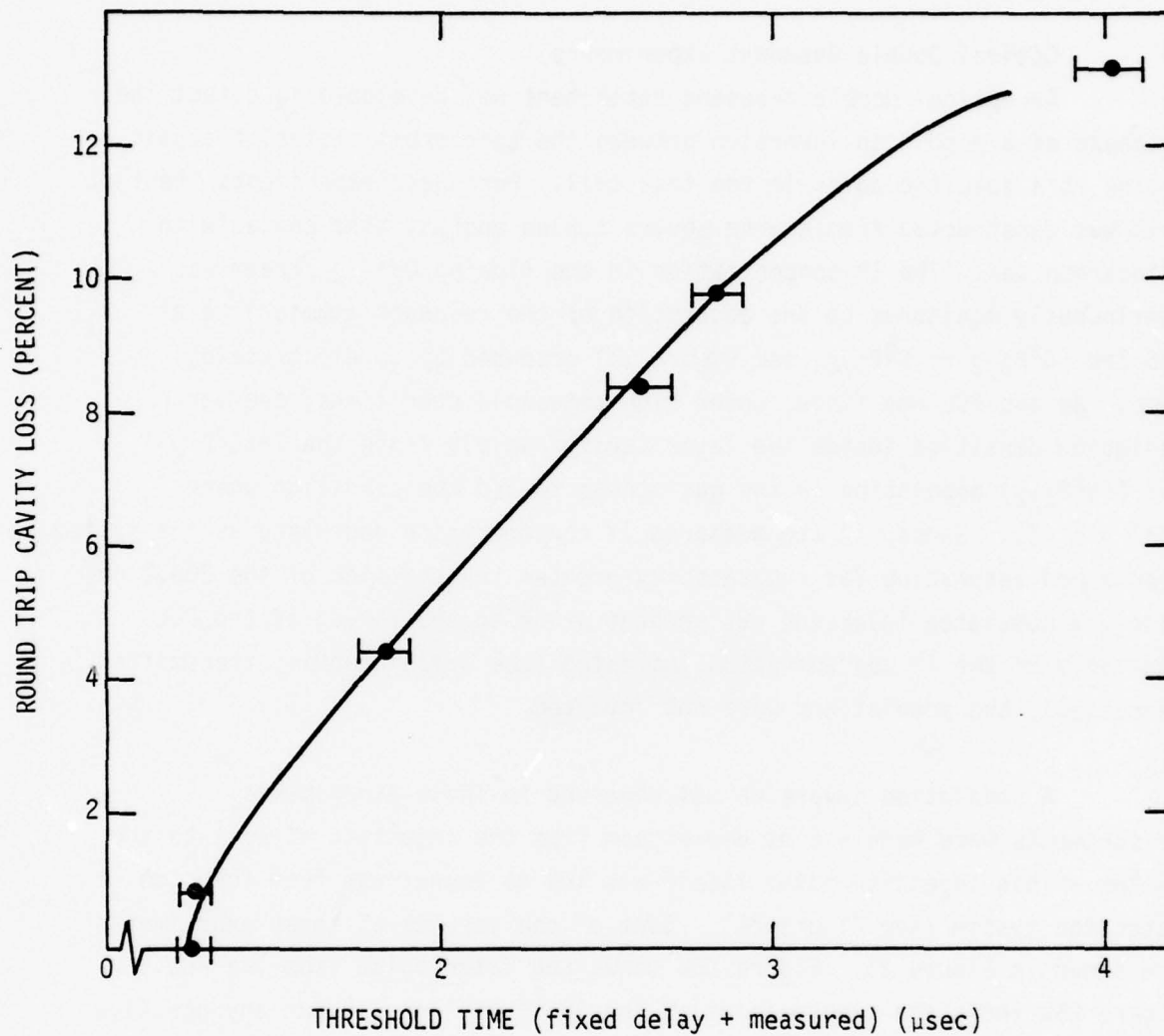


Fig. 22 Plot of Percent Loss vs. Threshold Time to Laser. A flash energy of 710 joules over an active length of 60cm was used. The lasing medium consisted of 229 torr argon and  $\sim 7$  torr  $\text{CF}_3\text{I}$ .

### C. Optical Double Resonant Experiments

An optical double resonant experiment was developed to detect the presence of a population inversion between the spin-orbit states of atomic iodine at a specific point in the test cell. For these experiments the test cell was constructed from quartz square tubing and was also coated with Halocarbon wax. The  $I^*$  concentration in the flowing  $O_2^*-I_2$  stream was continuously monitored by the absorption of the resonant atomic line at 206.2nm ( $6^2P_{3/2} - 5^2P_{1/2}$ , see Figure 23) produced by an electrodeless lamp. As the PDL was fired, under high threshold conditions, the large radiation densities inside the laser cavity rapidly drove the  $I^*(5^2P_{1/2})$  and  $I(5^2P_{3/2})$  population in the gas stream toward the condition where  $[I^*] = \frac{1}{2} [I]$ . Hence, if the measured  $I^*$  concentration decreased as the system approached saturation (as indicated by greater transmission of the 206.2 nm line), a population inversion was present prior to the firing of the PDL. Similarly if the  $I^*$  concentration increased (the lamp intensity transmitted decreased), the populations were not inverted.

A population inversion was observed in these experiments. Measurements were made  $\sim 5$  ms downstream from the injection of  $I_2$  into the system. This injection point itself was 100 ms downstream from the dimol detection system (see Figure 24). Some of the results of these experiments are shown in Figure 25. Figure 25a shows the laser pulse from the PDL. Figure 25b shows the transmission of the 206.2 nm line without any gas flow while Figures 25c-e show the transmission of the 206.2 nm line for different partial pressures of  $O_2^*$  and  $I_2$  in the gas stream (the total pressure remained constant). The data show a progression from a subinversion condition to a population inversion as indicated in Figure 25e. For the data shown, the total pressure in the system was  $\sim 380$  mtorr (212 mtorr of oxygen) with a partial pressure of iodine atoms (assuming total dissociation) of  $\sim 1.6$  mtorr. We note that the data indicate a subinversion condition when the  $O_2^*/O_2$  ratio was measured to be 0.30, i.e., where equilibrium kinetics would predict an inversion. It is possible either that some  $O_2^*$  loss

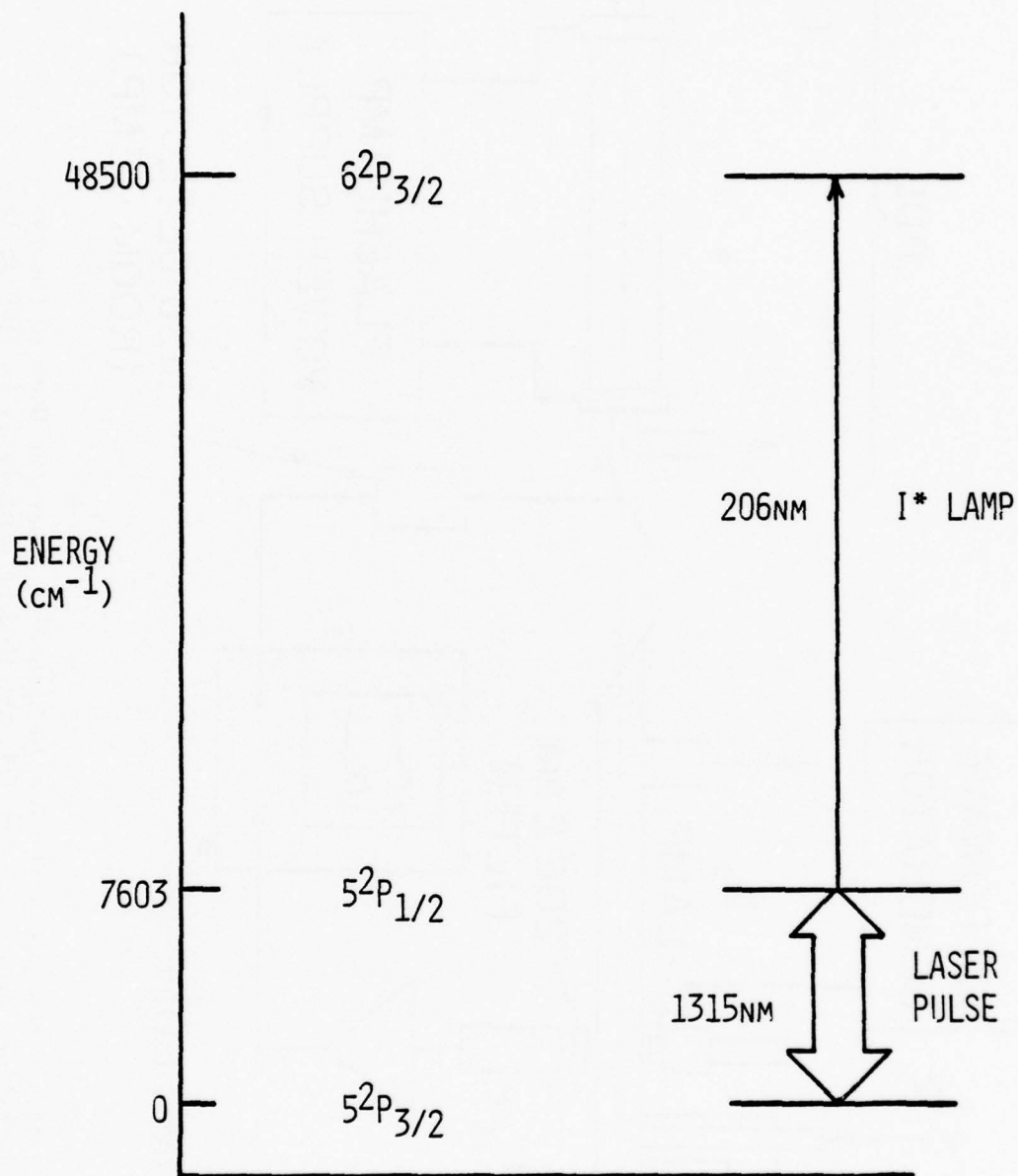


Figure 23. Energy Level Diagram of Atomic Iodine.

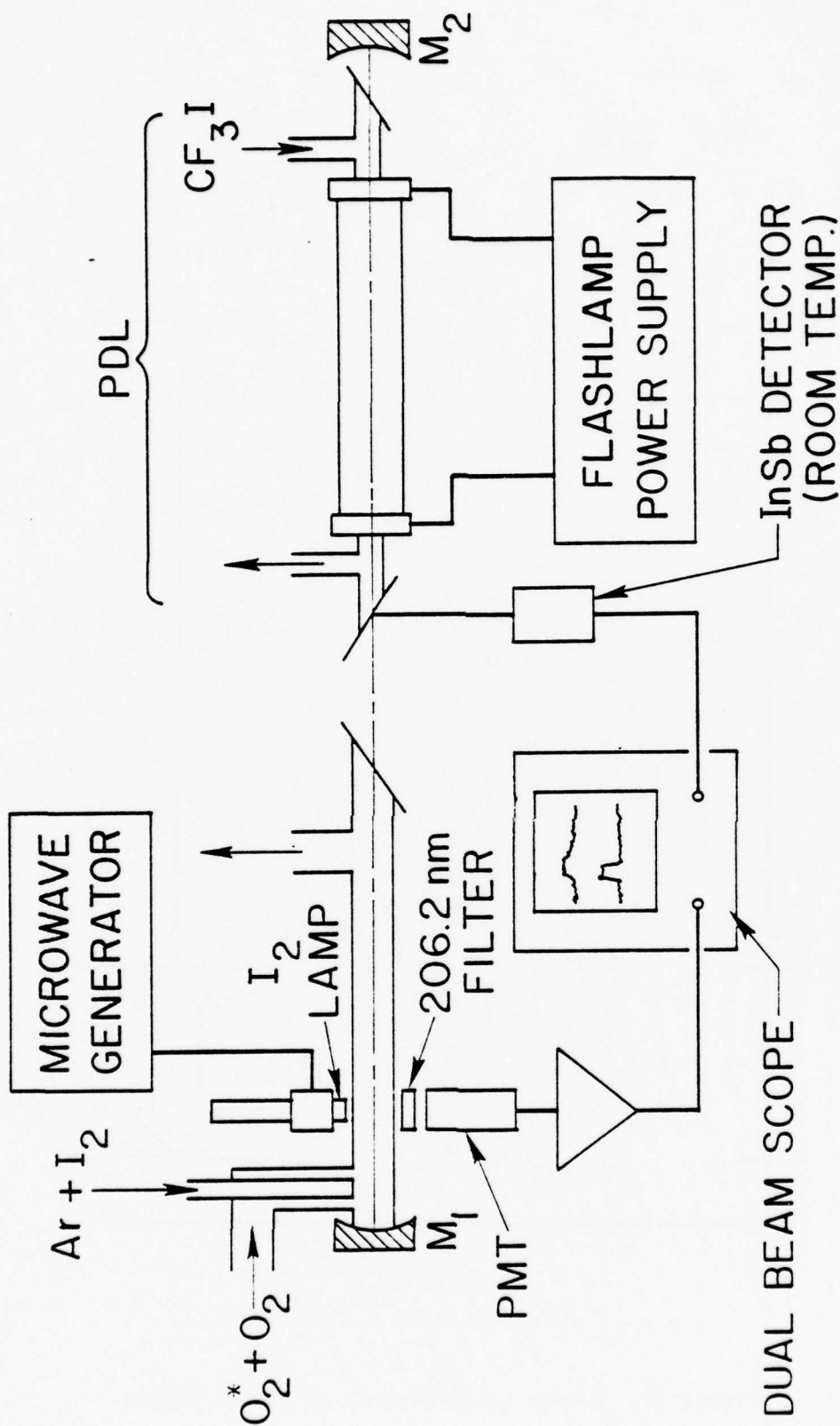


Figure 24. Schematic of the Double Resonance Apparatus Used to Observe the Population Inversion. The PDL operated by photolysis ( $\sim 1100$  joule flash) of  $\sim 15$  torr of  $CF_3I$  over a length of 40 cm. The optical cavity of the laser was formed by mirrors  $M_1$  and  $M_2$  which were coated for high reflectivity at  $1.315\mu m$ . The internal mirror  $M_1$  was protected by a purge of Ar (not shown in figure).

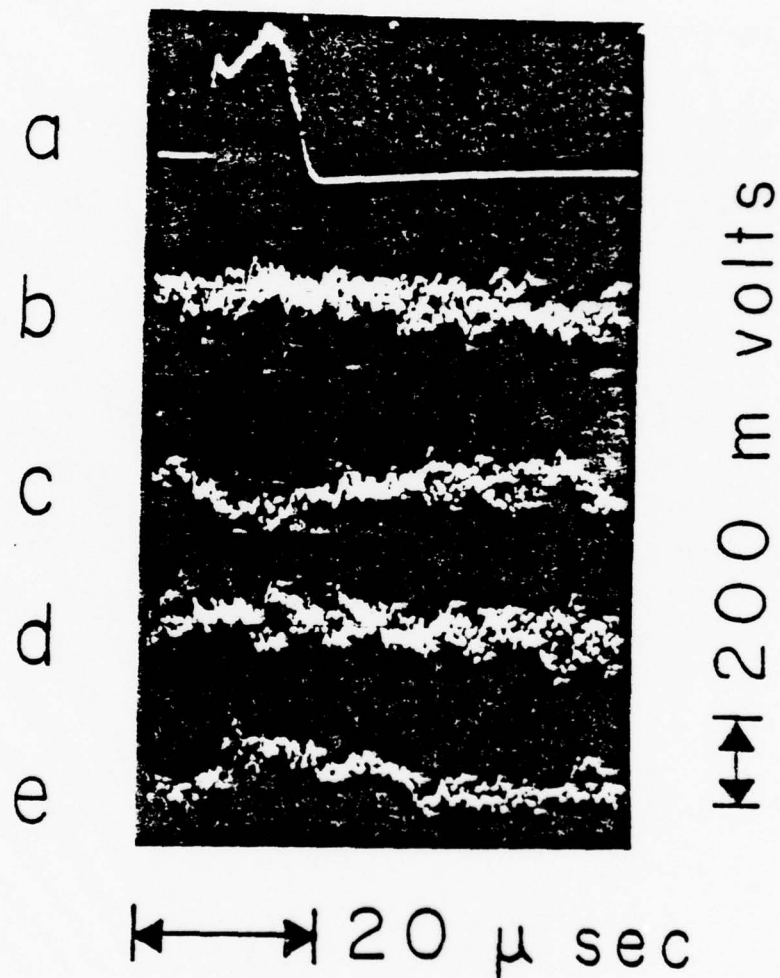


Figure 25. Optical Double Resonance Data Taken 0.5 ms Downstream of the Point of Injection of  $I_2$  into the  $O_2$  Stream. a) Output laser pulse from the PDL. b) Transmission of the 206.2 nm lamp with no  $I_2$  and  $O_2$  flowing. c) Transmission of the lamp with 212 mtorr of  $O_2$  and 1.5 mtorr of  $I$  atoms (presuming total dissociation of  $I_2$ ) at the point of measurement:  $O_2^*/O_2(\text{total}) = 0.27$ . d) Transmission of the lamp with partial pressures as in (c);  $O_2^*/O_2(\text{total}) = 0.32$ . e) Transmission of the lamp with partial pressures as in (c);  $O_2^*/O_2(\text{total}) = 0.63$ .

process occurs in the 100 ms interval between the dimol and inversion measurements, or that the calibration of the dimol detection system changed during the course of the experiments. This discrepancy does not affect the fact that a population inversion was observed.

If we make assumptions that saturation of the medium by the PDL occurs instantaneously and that the  $I^*$  absorption experiment obeys Beer's Law, a quantitative estimate of the gain of the iodine atom medium can be derived from the data shown in Figure 2e. Presuming Beer's Law for small absorptions,

$$V = V_0 (1 - \epsilon [I^*] \ell) \quad (24)$$

where  $V_0$  is the measured voltage corresponding to the original transmitted intensity of the 206.2 nm lamp with no  $I^*$  present and  $V$  is the voltage measured with absorption by  $I^*$  across the pathlength  $\ell$ . The length  $\ell$  is the width of the region saturated by the PDL, i.e., the diameter of the PDL lasing mode. The quantity  $\epsilon$  is the absorption cross section for the  $6^2P_{1/2} \leftarrow 5^2P_{1/2}$  transition. Hence,

$$\frac{V_0 - V}{V_0} = \epsilon [I^*] \ell \quad (25)$$

When the PDL is fired, causing saturation of the  $5^2P_{1/2} \rightarrow 5^2P_{3/2}$  transition, we obtain

$$\frac{V_0 - V'}{V_0} = \epsilon [I^*]_s \ell \quad (26)$$

where  $V'$  corresponds to the intensity of the lamp transmitted through the saturated medium. The quantity  $[I^*]_s$  represents the saturated concentration of  $I^*$ . Subtracting (7) from (6) we obtain

$$\frac{\Delta V}{V_0} = \epsilon \ell ([I^*] - [I^*]_s) \quad (27)$$

The population inversion prior to saturation,  $\Delta N$ , is just  $3/2([I^*] - [I^*]_s)$ . Hence,

$$\Delta N = \frac{3\Delta V}{2V_0\epsilon\ell} \quad (28)$$

The gain per unit length is equal to  $\sigma\Delta N$  where  $\sigma$  is the stimulated emission cross section for the highest component in the spin-orbit transition of atomic iodine when including the hyperfine levels. The transition of interest, therefore, is  $5^2P_{1/2}, F = 3 \rightarrow 5^2P_{3/2}, F = 4$ , where  $F$  is the hyperfine level (Ref. 31). The gain ( $\alpha$ ) is therefore given by

$$\alpha = \frac{3\Delta V\sigma(3-4)}{2V_0\epsilon\ell} \quad (29)$$

$V_0$  and  $\Delta V$  are quantities measured from the experiment. Given values (Refs. 32, 33) of  $\epsilon = 2 \times 10^{-14} \text{ cm}^2$  and  $\sigma(3-4) = 5 \times 10^{-18} \text{ cm}^2$ , we obtain a gain of  $\geq 10^{-5}$  per cm for the population inversion shown in Figure 2d.

We note that the assumptions made in quantifying the experiment are not completely valid. Saturation by the PDL is not instantaneous. Since optical saturation competes with rapid collision processes tending to restore the  $I^*$  and  $I$  atom concentrations to their original value (reaction (1)), noninstantaneous saturation results in a low value of  $\Delta V$  and hence a lower calculated gain or inversion. Similarly, self-reversal of the 206.2 nm absorption line (a phenomenon which is surely occurring in our experiments) would result in a nonlinear underestimation of the  $I^*$  concentrations, hence a lower calculated gain or inversion. We therefore feel that the value of  $10^{-5}$  per cm is a lower limit to the true gain.

31. W. C. Hwang and J. V. Kasper, "Zeeman Effects in the Hyperfine Structure of Atomic Iodine Photodissociation Laser Emission," *Chem. Phys. Letts.* **13**, 507 (1972).
32. C. Dymek and A. K. MacKnight, unpublished results (1975).
33. T. D. Padrick and R. E. Palmer, "Pressure Broadening of the Atomic Iodine  $5^2P_{1/2} - 5^2P_{3/2}$  Transition," *J. Chem. Phys.* **62**, 3350 (1975).

The variation of the 206.2 nm photoelectric signal was observed for a number of conditions of generator output and total I<sub>2</sub> concentration injected. A summary of these data is presented in Table 10. The inversion

TABLE 10. RESULTS OF THE OPTICAL DOUBLE RESONANCE EXPERIMENTS

% O <sub>2</sub> *	Partial Pressure (mtorr)		Voltage Diff. ΔV (volts)
	O <sub>2</sub> (total)	I <sub>2</sub>	
20	470	2.0	-0.2
44	470	2.0	0.0
59	470	0.77	0.05
62	470	0.77	0.1
44	470	0.77	0.0
66	420	1.4	0.1
54	420	1.4	0.0
38	477	1.1	0.0
46	470	1.1	0.0
27	417	0.80	-0.1
32	417	0.80	0.0
63	417	0.80	0.1

density,  $\Delta N = [I^*] - \frac{1}{2}[I]$ , can be related to these two parameters assuming total dissociation of the molecular iodine and assuming the equilibrium between the excited and ground states of oxygen and atomic iodine is established. Starting with the equilibrium condition that

$$[I^*] = K_{eq} \frac{[O_2^*]}{[O_2]} [I] \quad (30)$$

and assuming complete dissociation,

$$[I] + [I^*] = 2 [I_2]_0 \quad (31)$$

where  $[I_2]_0$  is the initial concentration of molecular iodine. Hence  $\Delta N = 3/2[I^*] - [I_2]_0$  substituting Eq. (30) into (31) and rearranging,

$$\Delta N = \left\{ \frac{2 K_{eq} r - 1}{K_{eq} r + 1} \right\} [I_2]_0 \quad (32)$$

where  $r$  is the ratio  $[O_2^*]/[O_2]$ . At the point where the dimol emission measurement was made, the total oxygen concentration was measured, hence converting Eq. (32) in terms of the  $O_2^*$  fraction,  $f$ , in the total oxygen streams, the following expression is obtained,

$$\Delta N = \frac{\left[ (2 K_{eq} + 1) f \quad 1 \right]}{\left[ (K_{eq} - 1) f + 1 \right]} I_2 o \quad (33)$$

In these studies fractional yields of  $O_2^*$  exceeding 0.30, as determined by the calibrated dimol emission signal, were necessary to produce a zero population inversion on the spin-orbit states of atomic iodine. Yet the theoretical fractional yield of  $O_2^*$  necessary is only 0.15. Since the determination of the fractional yield was made over 100 ms upstream of the point where the test for population inversion was made, an alternative method for determining  $O_2^*$  yields was devised. The variation in the lamp intensity,  $\Delta V$ , when the PDL is fired is proportional to the inversion density (Eq.(33)). As long as the introduction of  $I_2$  does not significantly perturb the proportions of  $O_2^*$  within 5 ms (the time from the  $I_2$  injector to the optical double resonant experiment), the fractional yield,  $f$ , of  $O_2^*$  is proportional to the ratio of square root of the dimol emission rate,  $D$ , to the total pressure  $P_T$  as measured in the dimol viewing section. Note that the argon- $I_2$  mixture is added downstream of the dimol emission viewing section. Hence a plot of  $\Delta V [I_2]_0^{-1}$  vs.  $D^{1/2} P^{-1}$  should have the same relationship given by Eq. (33). This plot is given in Figure 26. The solid line represents a fit of the data to the following expression,

$$\frac{\Delta V}{[I_2]_0} = \frac{a \left[ (2 K_{eq} + 1) b D^{1/2} P^{-1} - 1 \right]}{\left[ (K_{eq} - 1) b D^{1/2} P^{-1} + 1 \right]} \quad (34)$$

where  $a$  is the proportionality constant relating  $\Delta N$  to  $\Delta V$ , and  $b$  is the proportionality constant relating  $D^{1/2} P^{-1}$  to the fractional yield,  $f$ .

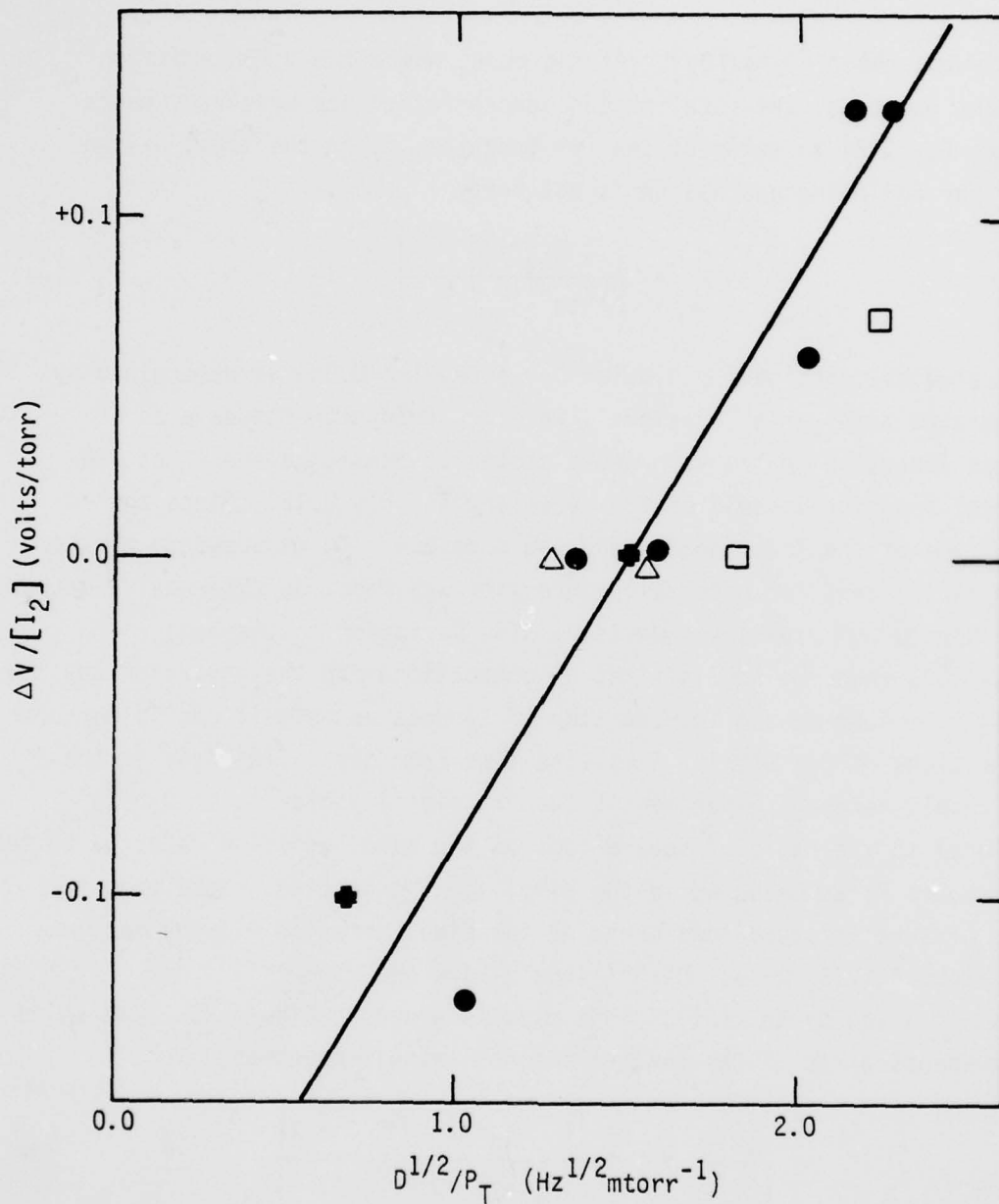


Figure 26. Normalized Variation of the 206.2 nm Signal vs. the Ratio of the Square Root of the Dimol Emission Rate to the Total Oxygen Pressure. The 206.2 nm signal strength is normalized to the total amount of molecular iodine added to the flow. The symbols, ●, ○, △, □, ■, represent increasing  $I_2$  partial pressures which are 0.7, 1.0, 1.4, 1.7, and 2.6 mtorr respectively. In all cases the  $I_2$  injector is 0.5 ms upstream from the point at which the double resonance experiments occur.

The proportionality constant,  $b$ , represents a calibration factor for the fractional yield of  $O_2^*$  at the point where the population inversion is tested. The value of  $b$  can be determined from the zero value of  $\Delta V$  (and hence  $\Delta N$ ), assuming  $f = 0.15$ , as the equilibrium condition requires. For these experiments  $b = 0.10 \text{ mtorr Hz}^{-1/2}$ . The gain,  $\alpha$ , can be calculated as follows:

$$\alpha = \sigma (3-4)\Delta N = \frac{\sigma (3-4) \left[ (2 K_{eq} + 1)f - 1 \right]}{\left[ (K_{eq}^{-1} - 1)f + 1 \right]} I_2 o \quad (35)$$

For a value of  $D^{1/2} p^{-1} = 2.0 \text{ Hz}^{1/2} \text{ mtorr}^{-1}$  (see Figure 26),  $f = 0.20$  and utilizing the value of  $\sigma$  presented earlier, the gain is calculated to be  $\sim 1 \times 10^{-4} \text{ cm}^{-1}$ . This value represents an upper estimate of the gain since total dissociation of molecular iodine is assumed.

The two methods of calculating the gain indicate that

$$10^{-5} \text{ cm}^{-1} < \alpha < 10^{-4} \text{ cm}^{-1} \quad (36)$$

Unfortunately the optical double resonance technique checks for the gain only at a specific point in the spatial gain profile. For evaluating the feasibility of this system to produce a laser, the gain profile must be determined in order to calculate the integrated gain which must exceed optical cavity losses before reaching laser threshold. Assuming that the pressure decreases by a factor of two along the laser path, and that quenching processes reduce the fractional yield of  $O_2^*$  along this path, the chances of producing lasing with the current  $O_2^*$  generator are remote.

#### D. $I(5^2P_{1/2})$ Fluorescence Experiments

In these experiments the PDL was not utilized. Instead, another diagnostic technique was employed. The  $I^*$  fluorescence was monitored by an intrinsic germanium detector along the direction of flow in the test cell.

The radiation was chopped and was dispersed by a 1/8 m monochromator (f/3.7 Oriel). Due to the sensitivity of the germanium detector, the slits were opened to only .5 mm, and the detector bias voltage reduced 30%. The chopper, monochromator and detector moved as a unit along the direction of flow, thus permitting the measurement of the I\* concentration profile. Two typical profiles are plotted in Figure 27, and the data are presented in Table 11.

TABLE 11. DATA FOR THE [I\*] TIME PROFILES

11.A Data Set for [I<sub>2</sub>] = 2.5 mtorr added to oxygen stream. The total oxygen pressure at the viewing port was 630 mtorr.

<u>[I*] (relative units)</u>	<u>% O<sub>2</sub>*</u>	<u>Distance from Injector (cm)</u>
14.7	22	5.5
15.9	22	8.5
15.5	24	15.5
15.3	25	26.5
12.0	25	36.5
10.5	31	46.5
9.6	31	51.5

11.B Data set for [I<sub>2</sub>] = 1.2 mtorr added to oxygen stream. The total oxygen pressure at the viewing port was 480 mtorr.

<u>[I*] (relative units)</u>	<u>% O<sub>2</sub>*</u>	<u>Distance from Injector (cm)</u>
13.5	50	5.5
13.0	50	8.5
12.0	45	14.5
11.5	51	26.5
10.5	52	39.5
8.4	45	53.5

An optical resonator was positioned around the O<sub>2</sub>\*-I<sub>2</sub> flowing test cell in order to check for lasing. From the optical double resonance, the estimated gain at best was  $1 \times 10^{-4} \text{ cm}^{-1}$ . If that gain were to be constant along the flow length of 65 cm, a net round trip gain of  $\sim 1.3\%$  would be realized. It must be noted however in light of the I\* profile experiments that the gain would be even lower, and the possibility of reaching threshold, doubtful. A 99.8% reflector (.2% absorption, 2 m radius of curvature) was

The proportionality constant,  $b$ , represents a calibration factor for the fractional yield of  $O_2^*$  at the point where the population inversion is tested. The value of  $b$  can be determined from the zero value of  $\Delta V$  (and hence  $\Delta N$ ), assuming  $f = 0.15$ , as the equilibrium condition requires. For these experiments  $b = 0.10 \text{ mtorr Hz}^{-\frac{1}{2}}$ . The gain,  $\alpha$ , can be calculated as follows:

$$\alpha = \sigma (3-4) \Delta N = \frac{\sigma (3-4) \left[ (2 K_{eq} + 1) f - 1 \right]}{\left[ (K_{eq} - 1) f + 1 \right]} I_2 o \quad (35)$$

For a value of  $D^{\frac{1}{2}} p^{-1} = 2.0 \text{ Hz}^{\frac{1}{2}} \text{ mtorr}^{-1}$  (see Figure 26),  $f = 0.20$  and utilizing the value of  $\sigma$  presented earlier, the gain is calculated to be  $\sim 1 \times 10^{-4} \text{ cm}^{-1}$ . This value represents an upper estimate of the gain since total dissociation of molecular iodine is assumed.

The two methods of calculating the gain indicate that

$$10^{-5} \text{ cm}^{-1} < \alpha < 10^{-4} \text{ cm}^{-1} \quad (36)$$

Unfortunately the optical double resonance technique checks for the gain only at a specific point in the spatial gain profile. For evaluating the feasibility of this system to produce a laser, the gain profile must be determined in order to calculate the integrated gain which must exceed optical cavity losses before reaching laser threshold. Assuming that the pressure decreases by a factor of two along the laser path, and that quenching processes reduce the fractional yield of  $O_2^*$  along this path, the chances of producing lasing with the current  $O_2^*$  generator are remote.

#### D. $I(5^2p_{1/2})$ Fluorescence Experiments

In these experiments the PDL was not utilized. Instead, another diagnostic technique was employed. The  $I^*$  fluorescence was monitored by an intrinsic germanium detector along the direction of flow in the test cell.

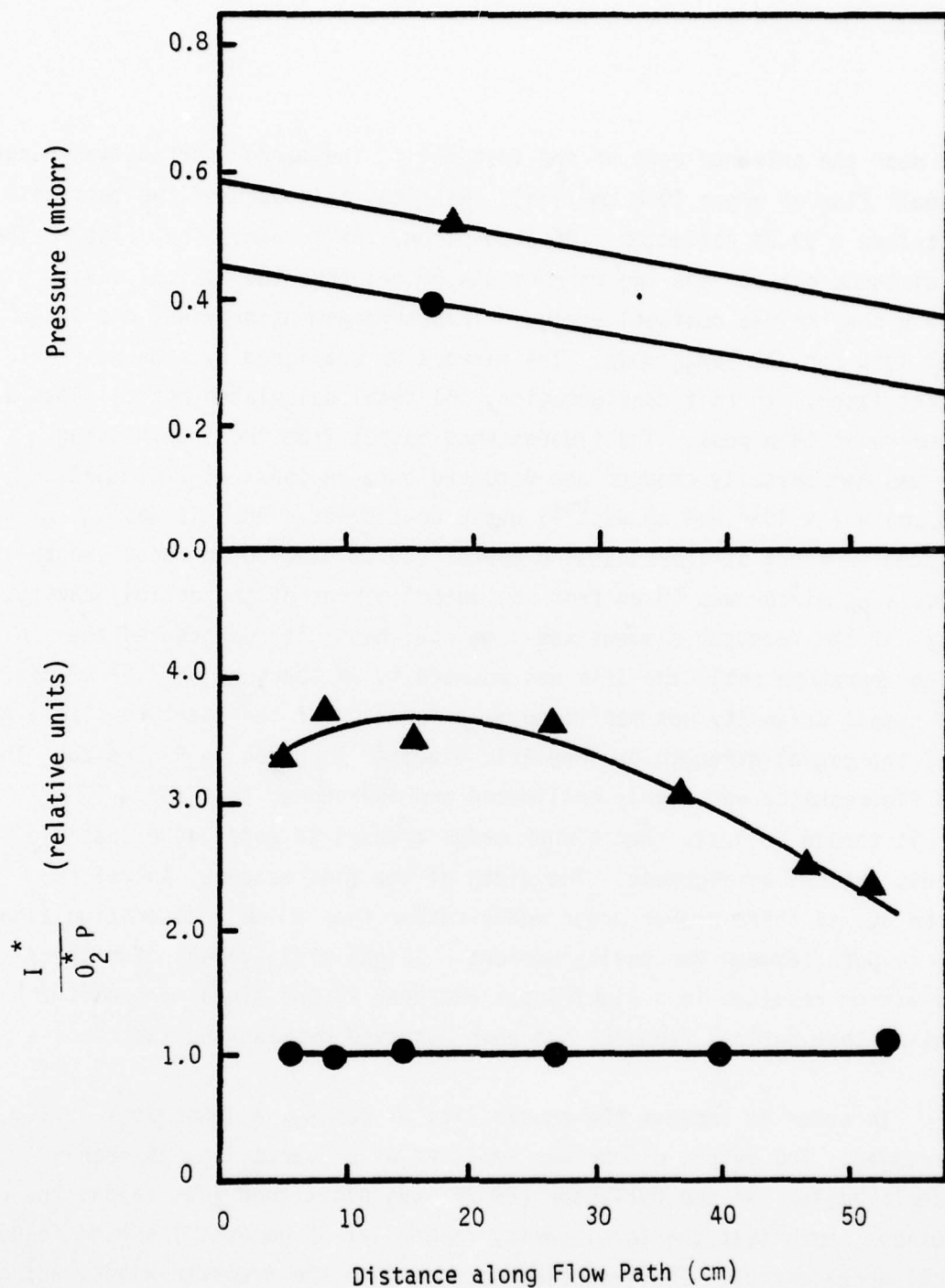


Figure 27. Variation of the Pressure and  $I^*$  Fluorescence Along the Flow Path in the Laser Cavity. The  $I^*$  fluorescence signal is normalized to the total pressure at each point along the flow path and to the  $O_2^*$  initially produced in the generator. This second normalization is necessary since the output of the generator was not constant during the course of the experiment. For the  $\blacktriangle$  data the initial partial pressure of  $I_2$  injected into the stream was 2.5 mtorr; for the  $\bullet$  data the  $I_2$  partial pressure was 1.2 mtorr.

placed near the entrance port of the test cell. The mirror surface was purged by a small flow of argon ( $0.2 \text{ cm}^3/\text{sec}$ ). Near the exit port of the test cell was attached a 99.3% reflector (.2% absorption, .5% transmission, flat). The total distance between the two mirrors was 85 cm; thus the optical cavity was that of a near folded confocal design. This arrangement provides the least optical loss for the  $\text{TEM}_{00}$  mode. The mirrors were aligned by a He:Ne alignment laser. In this configuration, the total calculated optical loss was 0.9% per round trip pass. The fluorescence output from the transmitting mirror was mechanically chopped and focussed onto an InAs (at 77K, SBRC,  $D^*(1.3 \mu\text{m}) = 1 \times 10^{12} \text{ Hz}^{1/2} \text{ cm watt}^{-1}$ ) detector element. An iris was positioned in front of the focussing mirror (50 mm dia; 30 cm focal length). The focussing mirror was 50 cm from the output mirror of the optical cavity. The size of the detector element was 1 mm dia, hence it represented the limiting aperture until the iris was reduced to an aperture of 1.67 cm dia. The  $I^*$  signal intensity was monitored as a function of the aperture size. A plot of the signal strength vs. the iris diameter is given in Figure 28. The output fluorescence was highly collimated and approached that for a  $\text{TEM}_{00}$  mode. It should be noted that higher order transverse modes were possible with this optical arrangement. The width of the fluorescence, therefore, could be due to these higher order modes rather than a small absorption along the 85 cm path between the cavity mirrors. Slight misalignment of either cavity mirror resulted in a significant decrease in the signal intensity indicating that optical feedback had been achieved between the two mirrors.

In order to improve the possibility of lasing, a lower loss cavity was arranged. The output mirror was replaced by a quartz flat at nearly Brewster's angle. An end reflector (99.9%) was positioned just beyond the flat window, such that the total cavity length was 95 cm (still a near folded confocal arrangement). The weak fluorescence from the Brewster window was mirrored into the cooled InAs detector. With this arrangement, the round trip loss of the parallel polarization (with respect to the plane of incidence formed by the optical axis and the window normal) was no more than 0.5%. The

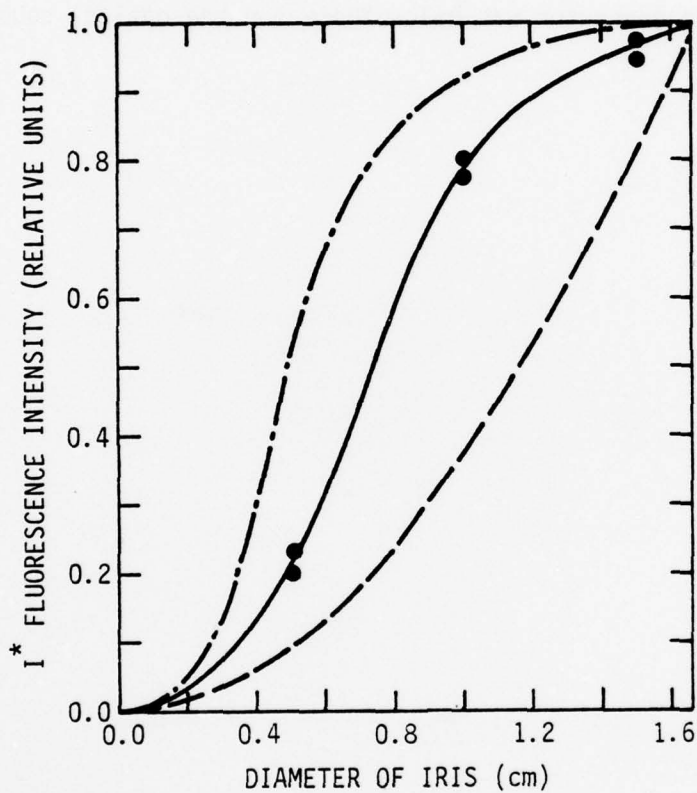


Figure 28.  $I^*$  Fluorescence vs. Iris Diameter. The limiting aperture up to 1.6 cm is the diameter of the iris. Above 1.6 cm the limiting aperture is the detector element size which is 1 mm diameter. The dashed line (---) is the intensity dependence for a radiating disc. The intermittent dashed line (- · -) is that for a calculated  $TEM_{00}$  distribution based upon the optical cavity geometry.

loss at the Brewster was checked by the He:Ne alignment laser, i.e., the reflected intensity of the parallel polarization vs. the total light reflections were compared. Under these conditions the net round trip gain of the  $O_2^*$  flowing system was less than 0.5%, and since no lasing was observed, the integrated gain was less than 0.5% also. For these experiments, the performance of the generator was below those for the optical double resonance experiments.

## SECTION V

### CONCLUSIONS

Although a population inversion between the spin-orbit states of atomic iodine has been produced by the present  $O_2^*$  generator, the generator has not produced lasing on the iodine transition. An increase of either the fractional yield and/or the molar flow rates from the current generator would increase the population inversion density for atomic iodine. The future success of the  $O_2^*$  generator, therefore, depends on whether or not the base-catalyzed CFS- $H_2O_2$  reaction can be scaled to producing greater molar flow rate without sacrificing yield. Based upon this work, we have not identified any fundamental barriers to improving the fractional yield of  $O_2^*$  or scaling to greater flow rates.

The limitation of the current  $O_2^*$  generator appears to be one of design rather than chemical reaction. Two rather obvious improvements can be made. During the course of this study, the Kenics mixer was of specific size. Increasing the flow rate of CFS and  $H_2O_2$  through this mixer region resulted in increased temperatures. At sufficiently high temperatures, a catastrophic disappearance of  $O_2^*$  was noted implying that the  $H_2O_2$  underwent autodecomposition. Heterogenous decomposition is known to take place at relatively low temperatures. Temperature control of the mixer coupled with passivation of the mixer surfaces to  $H_2O_2$  decomposition should aid in prevention of this problem. Secondly, the formation of salt deposits in the annular region of the reactor vessel proceeded without control over the amount of surface area generated and the degree by which the gas flow is restricted. Regulation of the salt deposits will be necessary for further reactor improvement.

A systematic variation of all design parameters will be difficult until a detailed study is made of the mechanism by which  $O_2^*$  is produced in

the base catalyzed CFS-H<sub>2</sub>O<sub>2</sub> reaction system. Furthermore, once the mechanism is well understood, alternative oxidizers and/or fuel, whose properties are compatible with O<sub>2</sub>\* production, could be investigated.

Quenching of O<sub>2</sub>\* by the salt surface seems to be minimal. The removal of molecular chlorine and other possible quenching gases appears to be solved. Temperature dependent wall quenching efficiencies should be determined for O<sub>2</sub>\* to optimize the fractional yield without sacrificing potential downstream quenching of I\*.

## REFERENCES

1. R. G. Derwent and B. A. Thrush, "The Radiative Lifetime of the Metastable Iodine Atom  $I(5^2P_{1/2})$ ," *Chem. Phys. Letts.* 9, 591 (1971).
2. R. F. Heidner III, J. G. Coffey, and C. E. Gardner, " $O_2(^1\Delta)$ -I Atom Energy Transfer Studies: C. W. Inversion on 1.315  $\mu\text{m}$  I-Atom Transition," Interim Report, TR-0078 (3610)-1, The Aerospace Corp., El Segundo, Calif, 1977.
3. R. M. Badger, A. C. Wright, and R. F. Whitlock, "Absolute Intensities of the Discrete and Continuous Absorption Bands of Oxygen Gas at 1.26 and 1.065  $\mu\text{m}$  and the Radiative Lifetime of the  $^1\Delta_g$  State of Oxygen," *J. Chem. Phys.* 43, 4345 (1965).
4. K. H. Becker, W. Groth, and U. Schurath, "The Quenching of Metastable  $O_2(^1\Delta_g)$  and  $O_2(^1\Sigma^+g)$  Molecules," *Chem. Phys. Letts.* 8, 259 (1971).
5. S. J. Arnold and E. A. Ogryzlo, "Some Reactions Forming  $O_2(^1\Sigma_g)$  in the Upper Atmosphere," *Can. J. Phys.* 45, 2053 (1974).
6. R. G. Derwent and B. A. Thrush, "Excitation of Iodine by Singlet Molecular Oxygen," *Disc. Faraday Soc.* 53, 162 (1972).
7. J. V. V. Kasper and G. C. Pimentel, "Atomic Iodine Photodissociation Laser," *Appl. Phys. Letts.* 5, 231 (1964).
8. H. Hohl and K. L. Kompa, "The Photochemical Iodine Laser," in Handbook of Chemical Lasers, R. W. F. Gross and J. F. Bott, eds., Wiley-Interscience, New York (1976).

- 9 A. E. Cahill and H. Taube, "Use of Heavy Oxygen in the Study of Reactions of Hydrogen Peroxide," J. Am. Chem. Soc. 74, 2312 (1952).
10. A. U. Khan, "Singlet Molecular Oxygen, A New Kind of Oxygen," J. Phys. Chem. 80, 2219 (1976).
11. P. B. Merkel and D. R. Kearns, "Radiationless Decay of Singlet Molecular Oxygen in Solution, J. Am. Chem. Soc. 94. 7244 (1972).
12. I. B. Goldberg, D. Pilipovich, and R. I. Wagner, "A Novel Singlet Molecular Oxygen Generator," patent pending (1977).
13. J. J. Deakin and D. Husain, "Electronic Excited Iodine Atoms,  $I(5^2P_{1/2})$ : A Kinetic Study of Some Chemical Reactions by Atomic Absorption Spectroscopy Using Time-Resolved Attenuation of Resonant Radiation at  $\lambda = 206.23$  nm  $I 5p^46S(2P_{3/2}) 5p^5(2P_{1/2})$ ," J. Photochem. 1, 353 (1973).
14. C. J. Schack and R. D. Wilson, U.S. Patent No. 3, 780, 165, Dec., 1973.
15. I. M. Kolthoff and R. Belcher, Volumetric Analysis Vol III, (trans. by N. H. Furman, New York, Interscience Publishers, 1957) p. 75.
16. L. Elias, E. A. Ogryzlo, and H. I. Schiff, "The Study of Electrically Discharged  $O_2$  by Means of an Isothermal Calorimetric Detector," Can. J. Chem. 37, 1680 (1959).
17. U. K. Kurzweg, A. M. Bass, and H. P. Broida, "Spectra and Afterglows and Discharges from Nitrogen-Oxygen Mixtures," J. Mol. Spectry. 1, 184 (1957).

18. L. W. Bader and E. A. Ogryzlo, "Reactions of  $O_2 (^1\Delta_g)$  and  $O_2 (^1\Sigma_g^+)$ ," Disc. Faraday Soc. 37, 46 (1964).
19. J. S. Arnold, R. J. Browne, and E. A. Ogryzlo, "The Red Emission Bands of Molecular Oxygen," Photochem. Photobio. 4, 963 (1965).
20. A. A. Westenberg, "Use of ESR for the Quantitative Determination of Gas Phase Atom and Radical Concentrations." Progr. Reaction Kinetics 7, 23 (1966).
21. L. W. Bader and E. A. Ogryzlo, "Halogen Atom Reaction. II. Luminescence from the Recombination of Chlorine Atoms," J. Chem. Phys. 41, 2926 (1964).
22. R. L. Powell, W. J. Hall, C. H. Hyink, Jr., L. L. Sparks, G. W. Burns, M. G. Scrogee, and H. H. Plumb, "Thermocouple Reference Table Based on the IPTS-68," Nat. Bur. Stand. (US), Monogr. 125, 13 (1974).
23. C. N. Satterfield and T. W. Stein, "Decomposition of Hydrogen Peroxide Vapor," J. Phys. Chem. 61, 537 (1957).
24. "Hydrogen Peroxide Handbook," Chemical and Material Sciences Department, Research Division, Rocketdyne, Canoga Park, Calif. p. 426 (1974).
25. T. P. J. Izod and R. P. Wayne, "The Formation Reaction, and Deactivation of  $O_2 (^1\Sigma^+g)$ ," Proc. Roy. Soc. A308, 81 (1978).
26. C. L. Lin and F. Kaufman, "Reactions of Metastable Nitrogen Atoms," J. Chem. Phys. 55, 3760 (1971).

27. S. J. Arnold, M. Kulo, and E. A. Ogryzlo, *Advan. Chem. Ser.* 77, 133 (1969).
28. R. B. Badachlape, P. Mamarchik, A. P. Convoy, G. P. Glass, and J. L. Margrove, "Preparation of Nonreactive Surfaces for Reaction-Rate Studies," *Int. J. Chem. Kinetics* 8, 23 (1976).
29. R. B. Kurzel and J. I. Steinfeld, "Energy Transfer Processes in Monochromatically Excited Iodine Molecules, III. Quenching and Multiquantum Transfer from  $v' = 43$ ," *J. Chem. Phys.* 53, 3293 (1970).
30. L. Gillespie and L. Fraser, "The Normal Vapor Pressure of Crystalline Iodine," *J. Am. Chem. Soc.* 58, 2260 (1936).
31. W. C. Hwang and J. V. Kasper, "Zeeman Effects in the Hyperfine Structure of Atomic Iodine Photodissociation Laser Emission," *Chem. Phys. Letts.* 13, 507 (1972).
32. C. Dymek and A. K. MacKnight, unpublished results (1975).
33. T. D. Padrick and R. E. Palmer, "Pressure Broadening of the Atomic Iodine  $5^2P_{1/2} - 5^2P_{3/2}$  Transition," *J. Chem. Phys.* 62, 3350 (1975).
34. G. A. Cappelle and H. P. Broida, "Lifetimes and Quenching Cross Sections of  $I_2 (B^3\pi_{0_u}^+)^*$ ," *J. Chem. Phys.* 58, 4211 (1973).
35. A. J. Arnold, Ph.D. Thesis, University of British Columbia, 1966.
36. R. H. Garstang, "Transition Probabilities for Forbidden Lines," *J. Res. NBS* 68, 61 (1964).

AD-A062 091

ROCKWELL INTERNATIONAL THOUSAND OAKS CALIF SCIENCE --ETC F/G 20/5  
A CHEMICAL SINGLET MOLECULAR OXYGEN GENERATOR.(U)  
JUL 78 A T PRITT, R D COOMBE, I B GOLDBERG F29601-76-C-0070

UNCLASSIFIED

AFWL-TR-77-265

NL

2 OF 2  
AD  
A062091



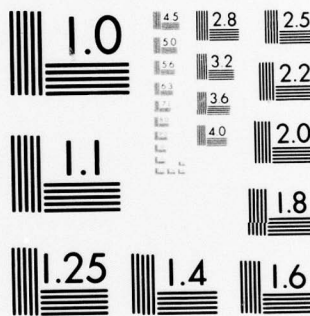
END

DATE

FILMED

3-79

DDC



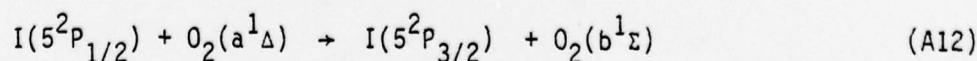
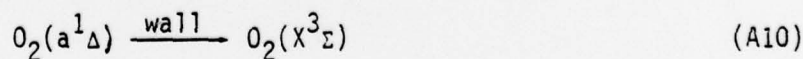
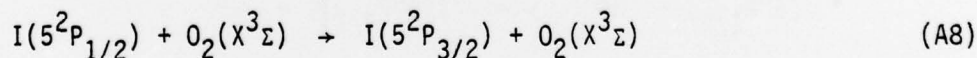
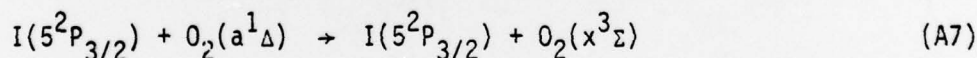
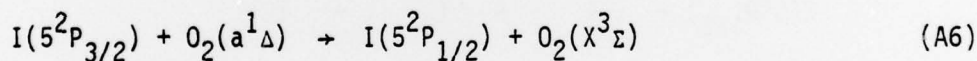
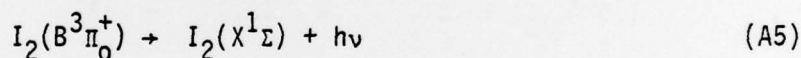
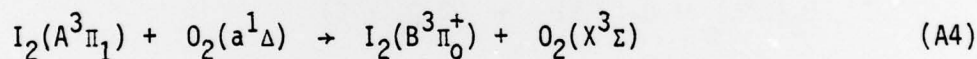
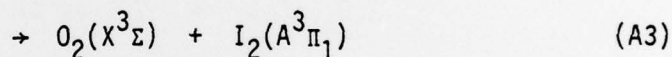
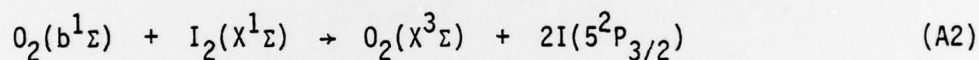
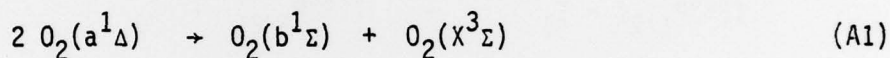
MICROCOPY RESOLUTION TEST CHART  
 NATIONAL BUREAU OF STANDARDS-1963-A

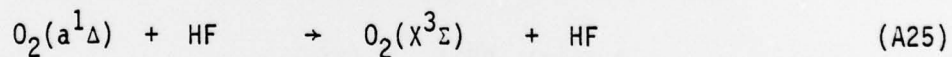
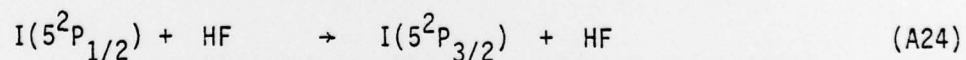
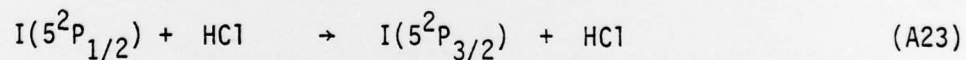
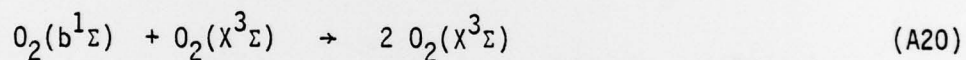
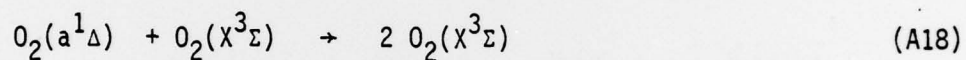
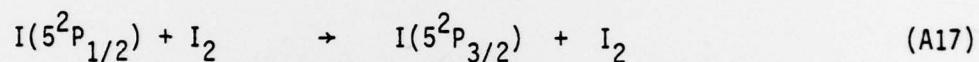
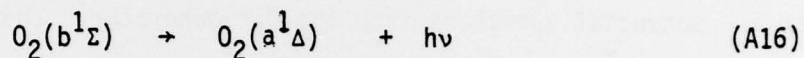
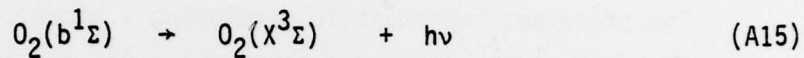
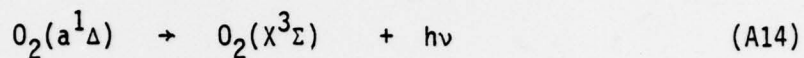
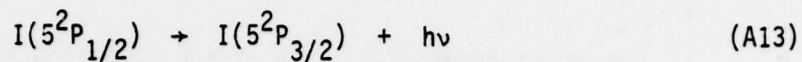
37. L. Wallace and D. M. Hunter, "Dayglow of the Oxygen A Band," J. Geophys. Res. 73, 4813 (1968).
38. J. F. Noxon, "Observation of the ( $b^1 - a^1 g$ ) Transition in  $O_2$ ," Can. J. Phys. 39, 1110 (1961).
39. D. H. Burde, R. A. McFarlane, and J. R. Wiesenfeld, "Studies of the Deactivation of Electronically Excited Iodine Atoms," IEEE J. Quantum Electron. QE-11, 709 (1975).
40. A. T. Pritt, Jr. and R. D. Coombe, " $I^*(5^2P_{1/2})$  Quenching by the Hydrogen Halides," J. Chem. Phys. 65, 2096 (1976).
41. A. T. Pritt, Jr. and R. D. Coombe, unpublished results, 1977.

## APPENDIX A

### IMPORTANT PROCESSES IN THE $O_2^*-I_2$ REACTION SYSTEM

The processes important in developing a kinetic code for the  $O_2^*-I_2$  reaction system are given here. Processes A21 - A25 are also included since these are potential quenchers from the  $O_2^*$  generator. The kinetic rate constants for these processes are given in Appendix B.





APPENDIX B

RATE CONSTANTS FOR THE  $O_2^*-I_2$  REACTION SYSTEM

<u>Process</u>	<u>Rate Constant</u>	<u>Reference</u>
(A1)	$2.0 \times 10^{-17} \text{ cm}^3 \text{ molec}^{-1} \text{ s}^{-1}$	5
(A2)	$1.6 \times 10^{-10} \text{ cm}^3 \text{ molec}^{-1} \text{ s}^{-1}$	6
(A3)	$6.6 \times 10^{-11} \text{ cm}^3 \text{ molec}^{-1} \text{ s}^{-1}$	6
(A4)	- - -	
(A5)		34
(A6)	$7.6(\pm 2.4) \times 10^{-11} \text{ cm}^3 \text{ molec}^{-1} \text{ s}^{-1}$	6
	Equilibrium Constant = 2.9 @ 300K	2
(A7)	$1.3 \times 10^{-13} \text{ cm}^3 \text{ molec}^{-1} \text{ s}^{-1}$	6
(A8)	$5.6 \times 10^{-14} \text{ cm}^3 \text{ molec}^{-1} \text{ s}^{-1}$	6
(A9)	$\sim 10^{-2}$ (Pyrex)	25
(A10)	$\sim 10^{-5}$ (Pyrex)	35
(A11)	$\sim 1$ (Pyrex)	2, 28
	$\sim 10^{-2} - 10^{-3}$ (Halocarbon Wax)	2
(A12)	$2.7(\pm 0.3) \times 10^{-14} \text{ cm}^3 \text{ molec}^{-1} \text{ s}^{-1}$	6
(A13)	$7.8 \text{ s}^{-1}$ (Calculation)	36
	$6.6 \text{ s}^{-1}$ (Experimental)	1
(A14)	$2.5 \times 10^{-4} \text{ s}^{-1}$	3
(A15)	$0.077 \text{ s}^{-1}$	37
(A16)	$2.5 \times 10^{-3} \text{ s}^{-1}$	38
(A17)	$3.6 \times 10^{-11} \text{ cm}^3 \text{ molec}^{-1} \text{ s}^{-1}$	39
(A18)	$1.5 \times 10^{-19} \text{ cm}^3 \text{ molec}^{-1} \text{ s}^{-1}$	4
(A19)	$3 \times 10^{-21} \text{ cm}^3 \text{ molec}^{-1} \text{ s}^{-1}$	35
(A20)	$1.5 \times 10^{-16} \text{ cm}^3 \text{ molec}^{-1} \text{ s}^{-1}$	4
(A21)	$1.7 \times 10^{-13} \text{ cm}^3 \text{ molec}^{-1} \text{ s}^{-1}$	13
(A22)	$1.6 \times 10^{-11} \text{ cm}^3 \text{ molec}^{-1} \text{ s}^{-1}$	13
(A23)	$6.5(\pm 0.9) \times 10^{-15} \text{ cm}^3 \text{ molec}^{-1} \text{ s}^{-1}$	40
(A24)	$3(\pm 1) \times 10^{-12} \text{ cm}^3 \text{ molec}^{-1} \text{ s}^{-1}$	40
(A25)	$< 5 \times 10^{-15} \text{ cm}^3 \text{ molec}^{-1} \text{ s}^{-1}$	41